NAVAL POSTGRADUATE SCHOOL

MONTEREY, CALIFORNIA

THESIS

THE IMPACTS OF GLOBAL SCALE CLIMATE VARIATIONS ON SOUTHWEST ASIA

by

Damon C. Vorhees

March 2006

Thesis Advisor:	Tom Murphree
Second Reader:	Karl Pfeiffer

THIS PAGE INTENTIONALLY LEFT BLANK

REPORT DOCUMENTATION PAGE			Form Approved OMB No. 0704-0188
Public reporting burden for this collection of information is estimated to average 1 hour per response, including the time for reviewing instruction, searching existing data sources, gathering and maintaining the data needed, and completing and reviewing the collection of information. Send comments regarding this burden estimate or any other aspect of this collection of information, including suggestions for reducing this burden, to Washington headquarters Services, Directorate for Information Operations and Reports, 1215 Jefferson Davis Highway, Suite 1204, Arlington, VA 22202-4302, and to the Office of Management and Budget, Paperwork Reduction Project (0704-0188) Washington DC 20503.			
1. AGENCY USE ONLY *(Leave blank)*	**2. REPORT DATE** March 2006	**3. REPORT TYPE AND DATES COVERED** Master's Thesis	
4. TITLE AND SUBTITLE: The Impacts of Global Scale Climate Variations on Southwest Asia		**5. FUNDING NUMBERS**	
6. AUTHOR(S) Vorhees, Damon C.			
7. PERFORMING ORGANIZATION NAME(S) AND ADDRESS(ES) Naval Postgraduate School Monterey, CA 93943-5000		**8. PERFORMING ORGANIZATION REPORT NUMBER**	
9. SPONSORING /MONITORING AGENCY NAME(S) AND ADDRESS(ES) N/A		**10. SPONSORING/MONITORING AGENCY REPORT NUMBER**	
11. SUPPLEMENTARY NOTES The views expressed in this thesis are those of the author and do not reflect the official policy or position of the Department of Defense or the U.S. Government.			
12a. DISTRIBUTION / AVAILABILITY STATEMENT Approved for public release; distribution is unlimited		**12b. DISTRIBUTION CODE**	

13. ABSTRACT (maximum 200 words)

We have examined the impacts of global scale intraseasonal and interannual climate variations on Southwest Asia (SWA). The variations of primary interest are El Niño-La Niña (ENLN), the Indian Ocean Zonal Mode (IOZM), the Madden-Julian Oscillation (MJO), and the North Atlantic Oscillation (NAO). The impacts of primary interest are on fall-winter precipitation and temperature in SWA. We identified upper and lower level circulation anomaly patterns directly linked to the climate variations and to anomalous precipitation and temperature in SWA. For the tropical climate variations, the mechanisms for these circulation anomalies involve equatorial Rossby-Kelvin wave dynamics, and related alterations of the tropical and subtropical circulation in and near SWA. Much of the impact on precipitation occurs through anomalous moisture advection from the Indian Ocean. The climate variations we studied are relatively predictable once initiated. Thus, there appears to be significant potential for improving climate forecasts for SWA. The DoD still relies on long-term means to create climatological planning products to the field. We feel that by incorporating the anomalies associated with the climate variations discussed here, the DoD could add significant value to its climatology products.

14. SUBJECT TERMS El Niño, La Niña, Indian Ocean Dipole, Indian Ocean Zonal Mode, Madden-Julian Oscillation, North Atlantic Oscillation, long term mean, climate, climate variations, Southwest Asia, teleconnections, smart climatology, climatological support, moisture advection			**15. NUMBER OF PAGES** 175
			16. PRICE CODE
17. SECURITY CLASSIFICATION OF REPORT Unclassified	**18. SECURITY CLASSIFICATION OF THIS PAGE** Unclassified	**19. SECURITY CLASSIFICATION OF ABSTRACT** Unclassified	**20. LIMITATION OF ABSTRACT** UL

NSN 7540-01-280-5500

Standard Form 298 (Rev. 2-89)
Prescribed by ANSI Std. 239-18

THIS PAGE INTENTIONALLY LEFT BLANK

Approved for public release; distribution is unlimited

THE IMPACTS OF GLOBAL SCALE CLIMATE VARIATIONS ON SOUTHWEST ASIA

Damon C. Vorhees
Captain, United States Air Force
B. S., The Pennsylvania State University, 2000

Submitted in partial fulfillment of the
requirements for the degree of

MASTER OF SCIENCE IN METEOROLOGY

from the

NAVAL POSTGRADUATE SCHOOL
March 2006

Author:

Damon C. Vorhees

Approved by:

Tom Murphree
Thesis Advisor

Karl Pfeiffer
Second Reader

Philip Durkee
Chairman, Department of Meteorology

THIS PAGE INTENTIONALLY LEFT BLANK

ABSTRACT

We have examined the impacts of global scale intraseasonal and interannual climate variations on Southwest Asia (SWA). The variations of primary interest are El Niño-La Niña (ENLN), the Indian Ocean Zonal Mode (IOZM), the Madden-Julian Oscillation (MJO), and the North Atlantic Oscillation (NAO). The impacts of primary interest are on fall-winter precipitation and temperature in SWA, and associated lower and upper level circulation anomalies in the eastern hemisphere. Our primary data sets are National Centers for Environmental Prediction (NCEP) reanalysis fields and indices of ENLN, IOZM, MJO, and NAO activity.

We have identified several upper and lower level circulation anomaly patterns that are directly linked to both the primary climate variations and to anomalous precipitation and temperature in SWA. The circulation anomalies associated with these SWA anomalies are similar for ENLN, IOZM, MJO, and NAO periods. For the tropical climate variations, the mechanisms for these circulation anomalies involve equatorial Rossby-Kelvin wave dynamics, and related alterations of the southwesterly and northeasterly monsoon flows, tropical easterly jet, and subtropical jet in northeast Africa and SWA, and the tropical Africa - Indian Ocean - western tropical Pacific region. Much of the impact on precipitation occurs through: (1) anomalous moisture advection over the tropical northwest Indian Ocean, and tropical and subtropical North Africa; and (2) anomalous moisture convergence over SWA.

ENLN, IOZM, MJO, and NAO occur at intraseasonal to interannual scales, and are relatively predictable once initiated. Thus, there appears to be significant potential for improving intraseasonal-interannual forecasts for SWA. The DoD still relies mainly on long-term means of quantities such as winds, cloud cover, and precipitation to create climatological planning products to the field. We feel that by incorporating the anomalies associated with the climate variations discussed here, the DoD could add significant value to its climatology products.

THIS PAGE INTENTIONALLY LEFT BLANK

TABLE OF CONTENTS

LIST OF ACRONYMS

ACMES	Advanced Climate Modeling and Simulations
AFCCC	Air Force Combat Climatology Center
AH	Azores High
BOM	Bureau of Meteorology
CDC	Climate Diagnostics Center
CFS	Coupled Forecast System
CPC	Climate Prediction Center
CRU	Climatic Research Unit
CSW	Central Southwest
DMI	Dipole Mode Index
EN	El Niño
ENLN	El Niño/La Niña
ENSO	El Niño-Southern Oscillation
EOF	Empirical Orthogonal Function
ESP	Environmental Security Plan
EWP	Empirical Wave Propagation
FNMOD	Fleet Numerical METOC Detachment
GFS	Global Forecast System
GPH	Geopotential Height
IOD	Indian Ocean Dipole
IOZM	Indian Ocean Zonal Mode
IPX	Indian Ocean Precipitation Extension
IRI	International Research Institute for Climate and Society
ISR	Intelligence, Surveillance, and Reconnaissance
JFM	January, February, and March
LN	La Niña
LTM	Long Term Mean
MC	Maritime Continent
MEI	Multivariate ENSO Index
MJO	Madden-Julian Oscillation
NAM	Northern Hemisphere Annular Mode
NAO	North Atlantic Oscillation
NCEP	National Centers for Environmental Prediction
NCAR	National Center for Atmospheric Research
NH	Northern Hemisphere
OCDS	Operational Climatic Data Summary
OLR	Outgoing Longwave Radiation
OND	October, November, and December
PJ	Polar Jet
PR	Precipitation Rate
PW	Precipitable Water
R-K	Rossby-Kelvin

RMM	Real-time Multivariate MJO
SAH	Saudi Arabian High
SJ	Somali Jet
SLP	Sea Level Pressure
SPWG	Seasonal Prediction Working Group
SST	Sea Surface Temperature
STJ	Subtropical Jet
SWA	Southwest Asia
TSCP	Theater Security Cooperation Plan
TEJ	Tropical Easterly Jet
WFHQ	Warfighting Headquarters
WP	Western Pacific

ACKNOWLEDGMENTS

Words cannot express the debt of gratitude owed to my advisors, Tom Murphree and Lt Col Karl Pfeiffer. Through thick and thin they have provided endless guidance, often dropping what they were doing to answer questions or provide feedback. Professor Murphree's climatology courses inspired my interest in military applications of climate. Lt Col Pfeiffer acquired the reanalysis data we relied on and spend countless hours helping us learn the in's and out's of the NCAR Graphics Command Language. Without his patience and insight, I would probably still be writing code.

Though all of my peers in the meteorology department have been extremely supportive, I would like to extend a special thanks to Major Mark LaJoie and Captain Adam Stepanek. In many instances, tackling our climate theses seemed like a team effort as we were constantly sharing ideas, successes, and failures.

Finally, it would also be remiss of me to not thank my parents. They also have provided support throughout my time at NPS and constantly challenge my own understanding of weather and climate by asking tough questions.

THIS PAGE INTENTIONALLY LEFT BLANK

I. INTRODUCTION

A. BACKGROUND

Numerous historians, generals, and strategists, from Sun Tzu through Tommy Franks have noted the impacts that weather and climate can have on military operations. Joint Publication 3-59, *Joint Doctrine, Tactics, Techniques, and Procedures for Meteorological and Oceanographic Operations* (Joint Staff 1999), emphasizes that

> Accurate, timely, and reliable meteorological and oceanographic (METOC) information can provide the commander with knowledge necessary to anticipate and exploit the best window of opportunity to plan, execute, support, and sustain specific operations.

As operations from EAGLE CLAW to DESERT STORM to IRAQI FREEDOM demonstrate, the weather in Southwest Asia (SWA) has played, and is likely to continue playing, a very important role over a wide spectrum of U.S. military operations.

One particular facet of weather that has gained increasing Department of Defense (DoD) interest over the past decade has been climatology — both climate analysis and climate forecasting. Being able to accurately assess current climate conditions and forecast the state of the atmosphere weeks to months into the future has important applications in SWA. These include, but are not limited to analyses and forecasts of:

- cloud cover, dust, and ceilings — important for takeoffs and landings and intelligence, surveillance and reconnaissance (ISR) operations
- temperature — important for troops, equipment, and various aviation platforms
- snowfall, snow cover, and snow melt — important in assessing trafficability and flooding potential
- flooding and drought — important for their widespread humanitarian impacts, and a myriad of impacts on infrastructure, logistics, and resources.

Knowing weeks to months ahead of time that there is an increased probability of above normal rainfall or snowfall, for example, could be extremely useful for planning purposes throughout a wide spectrum of operations—from ISR to logistics to humanitarian operations.

There are several instances from the past that illustrate the potential role of climate forecasting. Weather conditions during one period of Operation DESERT STORM in 1991 were among the worst observed in Iraq in the last 50 years and were twice as bad as the historical climatology for the region. Impacts on operations were widespread, from target and bomb damage assessment to scud hunting (D. Smarsh 2005, personal communication). A decade later, Operations ENDURING FREEDOM and IRAQI FREEDOM were also affected by long periods of adverse weather. DoD meteorologists failed to identify the conditions associated with several extended periods of anomalous weather, and as a result were unable to provide accurate long-lead forecasts to commanders (D. Smarsh 2005, personal communication).

Before we can accurately assess the current state of the climate and attempt to project into the future, we must have a thorough understanding of the long-term mean (LTM) conditions in the region of interest. Once we understand the LTM, we can compare the current state of the climate system to the LTM, as one part of the analysis of the present climate conditions. As far as SWA is concerned, the LTMs with respect to precipitation, winds, temperature, moisture, and other parameters are well-understood and documented in various publications. Noteworthy DoD publications include *The Persian Gulf Region—A Climatological Study* (Walters and Sjoberg 1988) and *SWANEA—A Climatological Study, Volumes 2 & 3.* (Vojtesak et al. 1991; Walters et al. 1991). Recently the Air Force Combat Climatology Center (AFCCC) published in-depth studies into the climates of Iran (Higdon 2004), Iraq (Walker 2005), and other countries in SWA.

The other pieces of the climatology puzzle, ones that have remained more elusive than establishing the LTMs, are climate analysis and forecasting.

Climate analysis, in broad terms, is diagnosing the current state of the climate system and noting departures from the LTM. The term *climate forecasting* will be used here to mean forecasting with lead times of one week or more, including intraseasonal (usually defined as 20-90 days) and interannual lead times. Over the last 10-20 years, researchers have demonstrated increasing skill in predicting the evolution of the climate over these timescales. One critical element in this increase in skill was the creation of reanalysis datasets as a result of a collaborative effort between the National Centers for Environmental Prediction (NCEP) and the National Center for Atmospheric Research (NCAR) (Kalnay et al. 1996; Kistler et al. 2001). The reanalysis datasets will be discussed in further detail in Chapter II.

Another factor that has led to an increase in skill in long-range forecasting is identifying and accounting for climate variations. In this paper *climate variations* will be used to refer to large-scale natural variability in the climate system (including its atmosphere, ocean, and land components). The climate variations that we have addressed in this study are El Niño (EN) and La Niña (LN) (essentially two opposing phases of the same oscillation, considered here together), the Indian Ocean Zonal Mode (IOZM) (also known as the Indian Ocean Dipole (IOD)), the Madden-Julian Oscillation (MJO), and the North Atlantic Oscillation (NAO).

Identifying the patterns associated with one or more of these particular variations, or oscillations, gives the forecaster an advantage in many instances, as they are quasi-periodic and are generally understood well enough to be of use when generating long-range forecasts (greater than one week). In principle, if forecasters issuing long-range forecasts for SWA identify one of the climate variations listed above early on its development, and understand the impacts that variation tends to have on SWA, then they can provide better climatological support for planning operations in SWA.

B. GEOGRAPHY AND LTM CLIMATE OF SWA

1. Geography

In order to understand the climate system in SWA, it is imperative to start with a brief discussion of the geography of the region. For this study, we defined SWA as the area from 30°-80°E and 10°-50°N (Fig. 1), but our focus was primarily on Iraq, Iran, Afghanistan, and northern Pakistan. Portions of the Arabian Peninsula were also included, where applicable.

The complex terrain of the region is one of the most important factors driving the weather and climate of SWA. Much of the region is arid or semiarid, and the precipitation distribution is largely governed by the orientation of the major mountain chains in the region — the Zagros and Alborz in Iran, and the Hindu Kush (and other chains) in Afghanistan and northern Pakistan (Barlow et al. 2005, Fig. 2). Most precipitation in SWA generally occurs during October to April, and is associated with extratropical cyclones that transit the region (Barlow et al. 2005). Storm tracks and the synoptic climatology of extratropical cyclones are discussed later in this chapter.

As SWA lies within a region of westerlies during the fall and winter (Krishnamurti 1961; Barlow et al. 2005), precipitation is heaviest on the west-facing, windward slopes of the mountainous terrain. The interior of Iran and the southwestern regions Afghanistan, which lie in the rain-shadow of the Zagros and Alborz mountains, feature some of the driest regions found anywhere in the world. Numerous salt flats dot the region, which is characterized by very few permanent rivers or lakes — the Helmand River in Afghanistan is usually the only river that flows year-round (Walters et al. 1991). Rodwell and Hoskins (1996) provide a very good discussion of other possible climatological mechanisms that may be responsible for the extremely arid conditions found in portions of SWA.

Further to the west lies the Fertile Crescent and the Tigris-Euphrates river basin — the largest fresh-water basin in the area. The Tigris and Euphrates both originate in Turkey, but are fed by numerous tributaries originating in the

highlands of Syria, Turkey, and the Zagros chain in Iran. The Fertile Crescent, one of the only portions of the area dominated by typical mid-latitude seasons, features numerous flood plains and is home to extensive agriculture and a wide variety of crops (Vojtesak et al. 1991).

While the terrain of SWA plays a critical role in precipitation distribution, the large bodies of water that border the region also play an important role in governing the climate. The Mediterranean Sea, Caspian Sea, and Arabian Sea have been identified in prior studies as the main moisture sources for synoptic-scale low pressure systems (Vojtesak et al. 1991; Walters et al. 1991; Barlow and Salstein 2005). The Black Sea and the Persian Gulf have been described as playing a similar role (Nazemosadat 1998). The Mediterranean and Caspian Seas are also the primary areas of cyclogenesis for two climatologically important low pressure systems that are responsible for a large portion of the rainfall in SWA during the fall and winter — the Cyprus Low and the Caspian Sea Low (see Walters et al. 1991 and Vojtesak et al. 1991 for further details on cyclogenesis in these regions). Other studies have shown that the Atlantic Ocean and the Pacific Ocean play an important role in governing the climate (Aizen et al. 2001, Nazemosadat and Cordery 2000; Nazemosadat and Ghasemi 2004; Hoerling and Kumar 2003; Ting and Sardeshmukh 1993). The Indian Ocean (IO) may also influence weather and climate in SWA (Barlow et al. 2005). The role of the IO will be discussed in much greater detail later in this chapter.

2. Long Term Mean Climate

The LTM climate (and geography) of the region are described well in Vojtesak et al. (1991), Walters et al. (1991), and Walters and Sjoberg (1988), all available from AFCCC. In addition, AFCCC has compiled numerous shorter studies that describe the LTM climate down to the country scale and below, in some cases to the city scale. The reader is referred to those works, as they do an excellent job of consolidating and presenting information from a wide variety of sources. A brief overview of the predominant conditions during the summer,

autumn, and winter, based on the above references is presented below. Understanding these LTM conditions is important for understanding how climate variations affect SWA.

a. Summer (July to September)

Many of the climatological features that affect SWA during autumn are initiated during the summer, so it is necessary to present a brief overview of the LTM summer conditions. During the summer months, features related to the Asian monsoon dominate much of the weather over SWA. In particular, tropical convection in the vicinity of the Maritime Continent is strongest during the summer. Matsuno (1966) and Gill (1980) found that in response to strong convection in the tropics, Rossby-Kelvin wave ridging is induced in the upper levels of the atmosphere. The mathematical details are beyond the scope of this paper, but Fig. 3a contains a schematic that depicts the general pattern of the ridging. Figure 4 also shows that during the summer in the Northern Hemisphere (NH) the Rossby-Kelvin wave response extends westward to SWA (this is especially visible in the wind field). Therefore, any changes in the strength of the convection in the tropics may result in changes to the upper level circulation over SWA.

At the low levels, a thermal trough stretches from western North Africa to Southeast Asia. A prominent feature of this trough is the Pakistani Heat Low. South of the trough, winds in the low levels tend to converge into the broad troughing and Pakistani Heat Low, resulting in large-scale southwesterly flow. This period is therefore known as the southwest monsoon period (Fig 5). North of the thermal trough, winds tend to be northwesterly in the low levels. The major low level wind feature during this season is the Somali Jet (SJ). The SJ is a product of the cross-equatorial outflow from the Mascarene High into the thermal trough over SWA, with topographic compression of the flow along the eastern flanks of the mountain ranges of east Africa. The SJ is usually found between 4,000 and 7,000 feet MSL and contains winds in excess of 20 kts. Aloft, the

Tropical Easterly Jet (TEJ) appears over southern Asia in response to the strong upper level anticyclone over the Tibetan Plateau.

With the exceptions of the mountainous terrain of Afghanistan, Pakistan (both influenced by the monsoon), and extreme northwestern Iran, precipitation is largely nonexistent during the summer months in SWA. This is due to the large-scale subsidence observed over the region, a feature Rodwell and Hoskins (1996) attribute to descent of the outflow from the Asian monsoon.

b. Autumn (October to December)

In autumn, as the days become shorter and solar insolation decreases, the thermal trough over SWA collapses and high pressure begins to build into interior portions of Asia. As a result the southwest monsoon and SJ weaken, and by October the low level winds over the Arabian Sea and northwestern IO begin to reverse direction and become offshore. This is visible in Fig. 6, which depicts the LTM 850-hPa geopotential heights (GPH) and winds for autumn. Aloft, the TEJ over southern Asia disappears as well, and the winds aloft are westerly north of 10°N by October (Fig. 7). As the Northern Hemisphere begins to cool, the polar jet (PJ) begins to dip southward into SWA, with more frequent excursions later in autumn. The PJ ushers in increased extratropical cyclonic activity during the autumn, with most areas in SWA beginning to receive their first autumn precipitation during October. SWA is located in within the subtropical belt of upper-level westerlies by this time, and these winds help steer any extratropical cyclones created or intensified by the PJ into SWA (Barlow et al. 2005; Vojtesak et al. 1991).

In the tropics, strong convection continues in the vicinity of the Maritime Continent, and the Rossby-Kelvin wave ridging is still apparent in Fig. 7. Therefore, even as SWA is starting to become increasingly influenced by the mid-latitudes, convection in the tropics can still impact the upper level circulation over SWA.

Figure 8 depicts the LTM for precipitation over SWA during the autumn months. As discussed earlier, the locations of receiving the largest

amounts of precipitation tend to be on the western side of the regions major mountain chains, with lesser amounts of precipitation over leeward and interior regions.

c. Winter (January to March)

During winter, the climate in the low levels is largely driven by the Asiatic High, also known as the Siberian High. Centered near western Mongolia, the high forms over central Asia as a result of intense cold generated by radiational cooling. It is a very strong and very shallow semipermanent feature that spans much of Asia. The high pressure over Asia tends to merge with high pressure centers over the Arabian Peninsula (Saudi Arabian High), Sahara Desert (Saharan High), and the eastern Atlantic Ocean (Azores High) to form a broad, continuous ridge of high pressure in the subtropics and midlatitudes. In response to the building high pressure over Asia, the offshore winds in Arabian Sea and northwestern IO continue to strengthen (Fig. 9).

While a relatively small feature, the Saudi Arabian High (SAH) plays an important role in the climate of SWA. According to Vojtesak et al. (1991), the SAH is “initiated and maintained by radiative surface cooling over the large desert surface.” It is an eastward extension of the Azores-Saharan High, but tends to “disappear” during frontal passages. Figure 10 shows the typical circulation patterns over northeast Africa and SWA in January. The westerly outflow on the northern side of the SAH steers Mediterranean low pressure systems into SWA. The westerly outflow is also responsible for feeding low level moisture from the Arabian Sea and Persian Gulf into SWA, thereby influencing the precipitation distribution and amounts generated by the low-pressure systems crossing SWA. Along with autumn, this is the primary rainfall period for most regions of SWA. Figure 11 shows the LTM for precipitation over SWA during winter.

In the tropics, the convection near the Maritime Continent shifts slightly eastward, with a corresponding shift in the Rossby-Kelvin wave ridging at 200 hPa (Fig. 12). In addition, the PJ is strongest and found at its southernmost

latitudes during the winter. Because of these two factors, the impacts of tropical convection on the upper level circulation in SWA may diminish from autumn to winter.

3. Extratropical Cyclones and Synoptic Climatology

As discussed earlier, in many regions of SWA most of the annual precipitation falls in the autumn and winter as the result of extratropical synoptic low pressure systems transiting the region. Figure 13 (from Higdon 2004) shows the LTM storm tracks for October-November and December-February, respectively. These storm tracks tend to frequent Turkey, the northern third of Iran, and northern Afghanistan (Vojtesak et al. 1991; Higdon 2004). Inland SWA is arid to semiarid, and the extratropical cyclones that move through (generally Cyprus and Caspian Sea Lows) are generally assumed to draw their moisture primarily from the Mediterranean, Black, and Caspian Seas. Barlow and Salstein (2005) have recently come to the conclusion, however, that the Persian Gulf and Arabian Sea "may be equally or more important [as moisture sources for Central-Southwest Asia], particularly for the Tigris-Euphrates basin." This is an important conclusion as it seems the roles of the Persian Gulf and Arabian Sea have been overlooked when studying the climatology of the region. Chapter III explores much further the roles they play in climate variations in SWA.

C. CLIMATE VARIATIONS AND THEIR IMPACT ON SWA

1. El Niño-La Niña

By far the most well-publicized and well-understood global-scale climate variations are El Nino and La Nina (ENLN) events. These are interannual events occurring in the tropical Pacific Ocean. EN events include unusually weak trade winds and high sea surface temperatures (SSTs, Fig. 14), and above normal levels of convective activity in the eastern and central Pacific. Concurrently, in the west Pacific there are lower than normal SSTs and decreased convective activity (Ford 2000). LN events are associated with an approximately opposite pattern of anomalies (e.g., lower than normal SSTs, Fig. 15) and convection in the eastern and central Pacific, with corresponding opposite conditions in the western Pacific). More details concerning the

evolution of global phenomena associated with ENLN events can be found in Philander (1990), Ropelewski and Halpert (1987, 1989, 1996), Kiladis and Diaz (1989), Halpert and Ropelewski (1992), Ford (2000), and Hildebrand (2001).

Numerous studies have demonstrated that the anomalous convection in the equatorial Pacific during ENLN periods leads to tropical and extratropical atmospheric circulation anomalies (e.g., Ford 2000). Part of the mechanism by which this is accomplished was first advanced by Matsuno (1966) and Gill (1980), who found that the forcing induced by anomalous convection can produce an equatorial Rossby-Kelvin wave response. Nitta (1987) and others showed that the Rossby wave portion of this response can extend into the extratropics, leading to global responses far from the location where the forcing was initiated (Fig. 16). Horel and Wallace (1981), and other studies, have documented a number of characteristic extratropical anomalies that occur during EN and LN events. Such linkages between widely separated areas of the globe are referred to as *teleconnections.*

ENLN, because of its worldwide impacts, is a relatively well-researched phenomenon. Investigations have been carried out using both statistical and deterministic models (Mason and Goddard 2001; Cane and Zebiak 1985; Cane et al. 1986; Latif et al. 1998; Neelin et al. 1998; Stockdale et al. 1998a,b; Evans et al. 2004; Tippett et al. 2003). Knowing what occurred during previous ENLN events can also give some indication of what is likely to happen during an upcoming event. Mason and Goddard (2001) asserted that “for many parts of the world this knowledge provides a better estimate of the probable future climate than the assumption that seasonal conditions will be the same as average.”

However, relatively little research into the effects of ENLN on SWA has been conducted, especially compared to the research done for the Americas, east Asia, and the Pacific. What direct research has been done has mainly come within the last five to ten years and has largely been focused on drought mitigation. In addition, there are few well agreed upon conclusions as to the effect of ENLN on SWA. Ropelewski and Halpert (1989), found that the impacts

of ENLN on the Middle East were “indeterminate.” Pagano et al. (2003) described the link between ENLN and precipitation in SWA as weak, indirect, and unstable. Pagano et al. (2003) postulate that one possible explanation for the lack of definitive impacts by EN on the region is its remoteness from both the Atlantic and Pacific Oceans, though they acknowledge that ENLN may have more influence in eastern SWA than western SWA.

Mason and Goddard (2001) investigated worldwide ENLN related climate impacts by calculating the observed percentage of times that seasonal precipitation has been in the upper, middle, and lower climatological terciles during ENLN extremes. ENLN extremes were determined from a three-month mean of the Nino3.4 index (a measure of EN conditions), and were used to determine the warmest (coldest) eight EN (LN) events between 1951 and 1996 (Mason and Goddard 2001). For the eight ENLN years and for each season (ignoring areas experiencing annual dry seasons), they tabulated the frequency at each grid point with which the observed precipitation anomalies were in each of the terciles listed above. This gave the authors an indication of the likelihood of observing a climate anomaly in each of the climatological categories during ENLN events.

Mason and Goddard (2001) identified impacts on precipitation during strong ENLN events in several regions of SWA, and in a couple of instances the relations seem to be particularly robust. For example, during autumn, northwest Iran was wetter than normal during at least five of the eight years and never drier than normal. On the other hand, during autumn LN periods the same regions were drier than normal in more than five of the eight years. Also, winter LN events often led to wet conditions in central and southern Iran and never led to drier than normal conditions. During the winter of the EN years they investigated, the Zagros Mountain in Iran never received above normal precipitation. Their results indicate that from autumn to winter there is a general reversal in anomalies. During autumn, EN periods often lead to above normal precipitation,

and LN conditions lead to drier than normal conditions over SWA; the opposite anomalies are observed during winter.

Within SWA, the majority of the research has been conducted by researchers in Iran, but they have focused solely on EN impacts in that country. A discussion of these impacts can be found in Nazemosadat and Cordery (2000), Nazemosadat and Ghasemi (2004), and Ghasemi (2003). A summary of their conclusions can be found in Pagano et al. (2003), and their results agree with those of Mason and Goddard (2001).

A pair of recent studies by Mariotti et al. (2002) and Mariotti et al. (2005) seem to offer the first definitive evidence and explanation of ENLN effects on SWA in general. In their 2002 study, Mariotti et al. used rainfall data from the Climatic Research Unit (CRU) and NCEP/NCAR reanalysis data, and found that during the boreal autumn, EN conditions in the Pacific generally lead to an increase in precipitation in the eastern Mediterranean and western Europe. During the winter, this relationship reversed, and the corresponding areas generally experienced a precipitation deficit. This particular study focused primarily on Europe and the Mediterranean, and only extended as far east as central Iran (approximately 55°E) and as far south as the Arabian Peninsula (approximately 25°N). But the relationships between EN and the portion of SWA that the authors analyzed are relatively strong (Fig. 17a,b).

In their concluding remarks Mariotti et al. (2002) noted importantly that the mechanisms by which the SST anomalies in the Pacific associated with ENLN exert their influence in the Europe-Mediterranean region are “poorly known.” The atmospheric reanalyses they constructed did show that during autumn “anomalous moisture coming from the Arabian ocean brings more rain to Middle East regions” (Mariotti et al. 2002). They failed, however, to take the next step and discuss whether the corresponding offshore moisture flux during winter is responsible for the reversal in precipitation patterns observed from autumn to winter. The seasonal regression of vertically integrated moisture flux and the

Nino3.4 index calculated by Mariotti et al. (2002) shows that anomalous circulation and onshore moisture flux in the vicinity of the Arabian Peninsula, Arabian Sea, and SWA during autumn of EN years was much stronger than the corresponding offshore flow during the winter (Fig. 17c,d). While it's not possible to draw any definitive conclusions concerning mechanisms by which EN influences the climate in SWA solely from their work, Mariotti et al. (2002) have proposed that anomalous circulation and moisture transport in the Arabian Sea may play an important role.

Using direct correlations of precipitation data and the Nino3.4 index Mariotti et al. (2005) found a region of positive correlation between autumn precipitation and the Nino3.4 index that stretched from Iraq and Iran eastward into Pakistan and Afghanistan, and up into Turkmenistan, Uzbekistan, Tajikistan, and Kyrgyzstan. To attempt to explain their observations, Mariotti et al. composited sea level pressure (SLP) and vertically integrated moisture flux from the NCEP reanalyses, (Fig. 18a,b). These two figures (one for periods of higher than average precipitation and another for below average precipitation in SWA) reveal some very intriguing relationships. In particular, note the SLP anomalies, and associated moisture flux anomalies, stretching from the Arabian Peninsula through the Indian Subcontinent into the Bay of Bengal. During periods of high precipitation (Fig. 18a) SWA lies at the downstream end of an anomalous moisture flux pathway coming out of the Arabian Sea and northwest Indian Ocean that joins, in the vicinity of the Red Sea, anomalous moisture flux from the southwest that originated over western and central Africa. During periods of below normal precipitation in SWA, Mariotti et al. (2005) found the opposite to be true — an anomalous offshore moisture flux over Iran and the Arabian Peninsula, with a cyclonic circulation anomaly in the Arabian Sea (Fig. 18b) It is interesting to note that Yang et al. (2002) also found a comparable pattern in the low level (850 hPa) winds for the winter (December through February) during EN periods, with an anticyclonic circulation in the Arabian Sea and onshore flow over the Arabian Peninsula and SWA during EN events..

Mariotti et al. (2005) concluded that there is a “robust statistical relationship” between ENSO and *autumn* rainfall in parts of southwest Europe, northern Africa and SWA. In addition, they found that, while there is a demonstrated connection between autumn precipitation anomalies in these areas and eastern Pacific SSTs, overall the connection with the Indo-Pacific variability is stronger. Referring specifically to SWA, they stated that “a more direct connection to the Indo-Pacific region is suggested by the upper air anomaly observed over southern Asia, possibly the Rossby wave response to enhanced heating on the Indian Ocean” (Mariotti et al. 2005).

Mariotti et al. (2005) also examined the global anomalies in GPH, streamfunction, and velocity potential during periods of above and below normal precipitation in SWA. To do this they composited 850-hPa and 200-hPa GPH fields during the two periods; their results are presented in Fig. 19 as standardized GPH anomalies. When heavier than normal precipitation occurred over SWA (and southwest Europe), an elongated area of ridging at 850 hPa tended to stretch from the Arabian Peninsula eastward to the western Pacific. It is largely confined to the Indian Ocean and nearby areas, staying south of 40°N. In the upper levels, at 200 hPa, an elongated area of troughing tended to occur from northeast Africa to the vicinity of Japan, with relative height minimums over the northwest Arabian Peninsula and southern China. The 200-hPa trough was centered at approximately 30°N, furthered north than the 850-hPa ridge. As can be seen in Fig. 19, when SWA rainfall was below normal, nearly opposite patterns tended to occur at upper and lower levels.

2. Indian Ocean Zonal Mode

The eastern portions of the Indian Ocean tend to be warmer (by approximately 1-2°C) than the western portions (Black et al. 2003). However, during the late 1990s, in seeking a mechanism to explain anomalous rainfall in tropical east Africa, Saji et al. (1999) identified an interannual mode of variability in SSTs across the Indian Ocean that creates an anomalous east-west temperature gradient, with positive (negative) SST anomalies in the western

(eastern) Indian Ocean. This mode came to be called the IOZM, or Indian Ocean Dipole, and is a phenomenon that occurs in the Indian Ocean basin but at times is intertwined with ENLN. Saji et al. (1999) concluded, however, that it is independent of ENLN. Because the reversal in signs of SST anomalies across the basin is "so striking," Saji et al. (1999) identify the dipole mode as a simple time series that describes the difference in SST *anomaly* between the tropical western Indian Ocean (50°E-70°E, 10°S-10°N) and the tropical south-eastern Indian Ocean (90°E-110°E, 10°S-Equator) (near the west coast of the island of Sumatra). A schematic of the IOZM is presented in Fig. 20.

The IOZM has been demonstrated to have a strong influence not only on the immediate regions neighboring East Africa and Indonesia (Saji et al. 1999; Behera et al. 2004), but also on the Indian summer monsoon (Behera et al. 1999; Ashok et al. 2001), East Asia, the Mediterranean, Australia and Brazil (Saji and Yamagata 2003). While there is evidence that the IOZM is independent of ENSO, the two are at times intimately related. Researchers interested in the relationship between SST and east African rainfall have proposed mechanisms by which ENLN and IOZM can work together to alter the climate of the Indian Ocean and surrounding areas. Black et al. (2003) suggested that under the right circumstances EN can trigger an IOZM event and the two can work together through the following sequence of events:

1. The EN must be sufficiently strong during the boreal summer to significantly perturb the convection and circulation in the vicinity of the Maritime Continent. This is most likely during the developing year (year 0) of and EN event.

2. The perturbation to the climate of the Maritime Continent should be sufficiently strong to generate a persistent change in the local Hadley circulation with enhanced southerly winds in the eastern Indian Ocean

3. The enhanced southerly winds must be long-lived and strong enough to cool the eastern Indian Ocean (via enhanced upwelling) during boreal summer and autumn such that the zonal gradient in SST across the Indian Ocean is reversed during autumn, leading to the development of the IOZM.

4. If the equatorial easterly wind anomalies of the IOZM over the Indian Ocean are strong enough to extend across the Indian Ocean, they can influence the climate of the western rim of the basin. Black et. al proposed the easterly wind anomalies reduce the transport of moisture away from east Africa, leading to increased rainfall.

Webster et al. (1999) proposed a similar series of events for explaining how the EN event of 1997-1998 influenced the climate throughout the Indian Ocean basin.

Unfortunately little research has been done to date to investigate the influence of the IOZM in SWA. On the other hand, though not directly addressed in their reports, one can infer from the results of Saji et al. (1999) and Black et al. (2003) that the IOZM might play a role in altering the climate in SWA.

3. Madden-Julian Oscillation

On interannual time scales, ENSO is the dominant mode of variability in the atmosphere, but at intraseasonal time scales (20-90 days) the MJO is the dominant mode of tropical intraseasonal variability and is most active in the boreal winter (Jones et al. 2004). Madden and Julian (1971) first identified the MJO as a 40-50 day “oscillation” that propagated from the west coast of equatorial Africa, through the Indian Ocean and Maritime Continent, out into the equatorial Pacific Ocean. The “oscillation” describes alternating regions of enhanced convective activity (the convective component) and enhanced subsidence (the subsidence component) (Fig. 21). Owing to its modification of convective activity in the tropics, fields of outgoing longwave radiation (OLR) are often used to identify the MJO; but it is also associated with wind anomalies in the lower and upper troposphere, the origins of which will be discussed below. The MJO patterns of convection, subsidence, and upper and lower level height and circulation anomalies propagates eastward along with the MJO at about five meters per second (Hendon and Salby 1994).

While the actual MJO is typically limited in its meridional extent to within a few degrees of the equator, the influence of MJOs can be felt throughout much of the extratropics. Sardeshmukh and Hoskins (1988) demonstrated that the

horizontal divergence above a region of tropical convective heating, which is analogous to the latent heat release by areas of tropical convection associated with the convective component of the MJO, can induce an extratropical wave train through Rossby wave dynamics. One important result Sardeshmukh and Hoskins (1988) demonstrated was that the upper level response to convection in the equatorial region was a pair of nearly symmetric *anticyclones* near the longitude of the forcing. The pair of anticyclones identified was very similar to the Rossby-Kelvin wave response found by Matsuno (1966) and Gill (1980) that exists in the LTM 200-hPa GPH-wind fields discussed earlier. In addition, these anticyclones stretched back to SWA in response to convection in the vicinity of the Maritime Continent. Sardeshmukh and Hoskins (1988) also note that

> The response to such changes is typically baroclinic in the tropics, with flow anomalies at upper levels having an opposite sense to those at lower levels, whereas in the middle-latitudes the anomalies exhibit an equivalent barotropic structure with the flow generally having the same sign at all levels.

In addition the authors demonstrated that the upper level response (and therefore lower level response) is independent of the longitude of the forcing — similar responses were found when the tropical convection was in the Indian Ocean, Maritime Continent and the central Pacific.

The extratropical wave trains generated by the MJO as it propagates through the Indian and Pacific Oceans impact numerous distant regions of the globe from Australia to California to South Africa (Jones et al. 2004; Stepanek 2006; Bond and Vecchi 2003; Whitaker and Weickmann 2001; Hendon and Liebmann 1990, Nogues-Paegle and Mo 1997). Understanding the teleconnections associated with the MJO is critical to medium-long range forecasting. Until very recently SWA had been largely ignored by researchers interested in examining the far-reaching impacts of the MJO. Barlow et al. (2005), however, showed that this was a significant oversight and that the MJO does play a role in modulating autumn-winter precipitation over SWA.

While Barlow et al. (2005) were the first authors to directly examine the influences of MJO on SWA, results from previous studies hinted at the relationships they were to find. Weickmann et al. (1985), found the relationship between OLR anomalies over SWA and OLR anomalies centered in the eastern Indian Ocean (from 80-120°W along the Equator) was exactly out-of-phase, suggesting that when there is anomalous convection (subsidence) and precipitation in the eastern Indian Ocean, SWA is more cloud-free (rainier) than usual. Hendon and Salby (1994), using wind, temperature, and OLR data from 1979-1989, traced the life cycle of the MJO as it traverses the Indian Ocean (from the east coast of Africa) and western Pacific Ocean. Their results indicated that as the MJO moved westward from Africa it induced circulation anomalies at both the lower and upper levels through a Rossby-Kelvin wave response. While the MJO produced impacts throughout the Indian Ocean basin as it crossed the Indian Ocean, there are two specific stages at which Hendon and Salby (1994) found it impacted SWA the most. The first of these stages was when the convective component of the MJO was leaving the east coast of Africa, with the corresponding subsidence component located near 120°E. At this stage Hendon and Salby (1994) found a prominent Rossby-Kelvin wave response in the 200-hPa circulation, with an elongated trough stretching from the eastern Mediterranean Sea to southeast Asia. This elongated trough is very similar to the troughing depicted by Mariotti et al. (2005) during periods of anomalously high precipitation over SWA (Fig. 19a). At the low levels (850 hPa and 1000 hPa) there was a large area of convergence centered over eastern SWA, and winds (regressed onto the OLR field) at these levels exhibited a marked anticyclonic onshore flow from the Arabian Sea into SWA — also similar to the pattern found in Mariotti et al. (2005) (Fig. 18a). As the convective component moved across the Indian Ocean, its influence on SWA diminished in the central Indian Ocean. There was still, however, weak onshore flow at 850 hPa and 1000 hPa. The second time at which the MJO showed significant influence on SWA was as the convective component approached 100°E and peaked in intensity. At

this time the Rossby-Kelvin wave response at 200 hPa was very prominent, with strong ridging over northeast Africa and SWA. At 850 hPa and 1000 hPa there was divergence centered over SWA; and the low level winds were offshore, with a cyclonic circulation in the Arabian Sea, similar to that found in Mariotti et al. (2005) (Fig. 18b). This same relationship held as the convective component moved eastward to 120°E, but the impact of the MJO on SWA diminished rapidly east of that longitude.

Wheeler and Hendon (2004) found very similar relationships between the components of the MJO and the low level circulation anomalies during the winter (December through February) as Hendon and Salby (1994). Wheeler and Hendon (2004, Fig. 22) showed a complete reversal in the 850-hPa wind vector anomalies as different components of the MJO passed through the eastern IO (especially near 100°E). When the convective component (their phases 2 through 5) was between 80°E and 120°E there was a northerly, offshore, 850-hPa wind anomaly south of 20°N (the northern limit of their domain) over SWA. When the subsidence component (their phases 6 through 1) was in this area, the wind anomaly reversed to be southerly and onshore (Wheeler and Hendon 2004). As their study focused on monitoring the MJO and predictability in the vicinity of Australia, they did not discuss the impacts of these wind anomalies on SWA.

Building on these results, Barlow et al. (2005) demonstrated that there was a 23% increase in daily precipitation relative to the mean when the subsidence component of the MJO was in the eastern Indian Ocean. When the convective component of the MJO was in the same region there was a corresponding decrease in daily precipitation. According to Barlow et al. (2005) this response is largely driven by Rossby-Kelvin wave dynamics, as was also noted by Hendon and Salby (1994). Barlow et al. (2005) also found that when the MJO rainfall anomalies (either convective or subsidence component) are in the eastern IO, the corresponding Northern Hemisphere upper level Rossby gyre extends over SWA. The MJO-induced wind anomalies can then affect SWA

through changes in both the upper level and lower level winds (and therefore moisture transport).

Figure 23 shows the difference Barlow et al. (2005) found in daily OLR and 200-hPa wind anomalies between when the subsidence and convective components of the MJO were in the eastern IO. It is important to note that when there were negative OLR anomalies (corresponding to increased convection and precipitation) in the eastern Pacific, SWA experienced positive OLR anomalies and decreased precipitation. The circulation anomalies depict the Rossby wave response mentioned above, with an anticyclonic anomaly located to the northwest of the convection. Barlow et al. also noted that the lower level circulation was opposite to that of the upper levels. This is in-line with the baroclinic response discussed by Gill (1980) and Sardeshmukh and Hoskins (1988). Barlow et al. (2005) also found that when the subsidence component of the MJO moved into the eastern IO, the OLR, precipitation, and circulation anomalies were opposite in sign. In addition, Barlow et al. (2005) listed the following two factors to explain the sensitivity of precipitation in SWA to the MJO:

1. The proximity of SWA to the most active region of the MJO (eastern IO), so that SWA is within the direct wind response to the MJO tropical convection anomalies when they are at their largest values

2. The vigorous wind response to tropical forcing in the same region (Ting and Sardeshmukh 1993)

Barlow et al. (2005) emphasized that because precipitation in SWA comes primarily from the infrequent passage of extratropical synoptic storms, the MJO can only affect local precipitation during the occasional passage of these storms — typically during the autumn and winter. Because a typical track for extratropical low pressure systems passes through southern Iran, Afghanistan, and Pakistan (Fig. 13), Barlow et al. (2005) were able to show, using autumn-winter rainfall data solely for Afghanistan, that the MJO can at times play a large role in modulating daily precipitation across much of SWA. The predictability of the MJO (Waliser et al. 2003; Wheeler and Hendon 2004) and the link between

the MJO and SWA precipitation suggests the potential for prediction of SWA precipitation (Barlow et al. 2005).

4. North Atlantic Oscillation

Halfway across the world from where the MJO, IOZM, and ENSO exert their influence, the most prominent and recurrent pattern of atmospheric variability in the middle and high latitudes of the Northern Hemisphere is the North Atlantic Oscillation (Hurrell et al. 2003; Trigo et al. 2002). The NAO corresponds to a large-scale alternation of mass in the North Atlantic between regions of subtropical high pressure (centered near the Azores) and subpolar-low pressure (south and east of Greenland—located near the climatological position of the Icelandic Low) (Lamb and Peppler 1987; Trigo et al. 2002) (Fig. 24). This oscillation accounts for one-third of the total variance of the SLP field over the North Atlantic, and is most pronounced during the winter months (Cullen and deMenocal 2000). A simple NAO index can be defined as the difference between the normalized mean winter SLP anomalies at locations representative of the relative strengths of the Azores High (AH) and Icelandic Low. During the positive phase of the NAO, the Azores High is stronger than normal, while the Icelandic Low is weaker than normal (Cullen and deMenocal 2000). The opposite anomalies are observed during the negative phase.

On the global scale, the NAO is thought to be the North Atlantic component of a hemispheric-scale meridional seesaw in SLP between polar and mid-latitudes known as the Northern Hemisphere Annular Mode (NAM) (Hurrell et al. 2003). The term “NAM” has come into favor recently to describe what has more commonly been called the Arctic Oscillation. There is still a great deal of debate, however, as to whether the NAO is in fact the North Atlantic component of the NAM (Hurrell et al. 2003; Wallace, 2000; Ambaum et al., 2001). For example, Thompson and Wallace (1998, 2000) argued that the NAO “reflects the modification of the annular mode by zonally-asymmetric forcings, such as topography and land-ocean temperature contrasts.” An in-depth discussion of this debate is beyond the scope of this study, however.

The details of North Atlantic winter storms have proven to be extremely difficult to forecast more than a few days ahead, and as a result it is reasonable to assume that long-lead prediction of the NAO would be equally or more difficult (Rodwell 2003). Recently, however, investigators have made progress in this realm on two different fronts—the ocean and the stratosphere. Rodwell (2003) demonstrated that the ocean may play an active role in determining the evolution of the NAO, as new statistical analyses have revealed SST patterns that precede specific phases of the NAO by up to nine months. This is possible because the extratropical ocean is able to preserve much of its thermal energy through much of the year (Kushnir et al. 2002). Tropical oceans may play a similar role on even longer time scales (Hoerling et al. 2001). On the other hand, Thompson et al. (2003) suggested that prospects for improved predictability of the NAO may lie in links through which changes in stratospheric wind patterns might exert some downward control on surface climate. Thompson et al. (2003) extended previous work by Perlwitz and Graf (1995) that established a statistical connection between the month-to-month variability of the Northern Hemisphere stratospheric polar vortex and the NAO (Hurrell et al. 2003).

Hand-in-hand with research into the predictability of the NAO has been investigation into the impacts of the NAO throughout the North Atlantic sector — North America, the North Atlantic ocean, and Europe. The positive phase of the NAO favors storm tracks that drive low-pressure systems further north than usual, into northern Europe (Fig. 24). As a result, positive phase periods feature warmer and wetter weather in this region (Hurrell 1995; Trigo et al. 2002). During the negative phase of the NAO, low-pressure systems crossing the Atlantic tend to take a more zonal path, often penetrating into the Mediterranean Sea, thereby linking the Middle East to climate variations in the North Atlantic. (Cullen and deMenocal 2000). For more specific details concerning the impacts of NAO on Europe and the North Atlantic, see Rogers (1990, 1997), Hurell and van Loon (1997), Hurrell et al. (2001), Hurrell (1995,1996), Trigo et al. (2002), and Serreze et al. (1997) .

Cullen and deMenocal (2000) and Cullen et al. (2002) were the first authors to look directly at the role the NAO plays in the climate of the Middle East, specifically in how it governs the streamflow of rivers in the region. They expected to find a relationship because the NAO "regulates Atlantic heat and moisture fluxes into the Mediterranean" through the influence it exerts on storm tracks (Cullen et al. 2002). As these winter cyclones are the dominant source of rainfall in the Middle East, NAO-related changes in North Atlantic heat and moisture transport can be expected to influence Middle Eastern climate (Cullen et al. 2002). Cullen and deMenocal (2000) calculated, standardized, and correlated winter (December through March) precipitation (403 stations) and temperature (211 stations) from the western Mediterranean Sea to the Middle East (as far east as 50°E) to the Hurrell (1995) NAO index. Temperature correlations during the winter were negative in the western portions of the Middle East (Iraq and western Iran) and ranged from -0.3 to -1.0. The correlations for stations further east — along the Caspian Sea and in the Caucasus Mountains — were weak or nonexistent (Cullen and deMenocal 2000). Correlations between the NAO and precipitation in the region were also negative during the winter, but only stations close to the Mediterranean showed correlations greater than 0.3. Correlations in Iraq, Iran, and the Caucasus were lower than 0.3. These results supported their hypothesis that by deflecting the Atlantic storm track further north, the positive phase of the NAO tends to deprive the eastern Mediterranean (but not necessarily SWA) of rainfall during the winter.

Trigo et al. (2002) also investigated the influence the NAO has on European climate during the winter (December through March), but unlike Cullen and deMenocal (2000) and Cullen et al. (2002), they used the NCEP/NCAR reanalysis data. The large scale influences they found support many of the conclusions already mentioned, but as SWA was on the periphery of their study area, it is worth mentioning a few of their findings that add to the picture constructed by Cullen and deMenocal (2000) and Cullen et al. (2002). During positive NAO periods (NAO > 1) both maximum (T_{max}) and minimum

temperatures (T_{min}) were below normal, with T_{max} being impacted more. As was expected, during negative NAO months, both T_{max} and T_{min} were higher than normal, but the temperature anomalies were greater than in the positive NAO case. A portion of the differences in T_{max} and T_{min} can likely be explained by the 10m wind anomalies Trigo et al. (2002) calculated. During high NAO months (when temperatures were lower than average), the 10 m wind anomaly is weak but northerly (offshore) throughout SWA. Winds in this regime would tend to advect cooler, continental air into SWA. The opposite pattern is observed during periods of negative NAO, with southerly winds advecting warmer air northward. Trigo et al. (2002) also examined anomalies of monthly cloud cover data obtained from the CRU at the University of East Anglia. They found that during negative NAO periods there was more cloud cover (by between 0.1 and 0.5 oktas) over SWA. Trigo et al. (2002) also suggested that the cloud cover anomalies are partly responsible for the temperature anomalies noted above through the modulation of short and long-wave radiation. The final two fields Trigo et al. (2002) investigated were precipitation rate (PR) and precipitable water (PW). They found the same general relationship as Cullen and deMenocal (2000), with a negative correlation between NAO and precipitation rate over the eastern Mediterranean and SWA during the winter. The anomaly was much stronger during the negative phase of the NAO, however, with areas of northeastern Iraq and northwestern Iran showing a marked increase in precipitation. PW anomalies showed the same pattern as PR, with the increase in PW over SWA being among the largest observed in the North Atlantic/Eurasia sector. Trigo et al. (2002) did not draw any connection between the 10 m wind anomalies and the PR and PW anomalies, but it is worth noting that during periods of higher than average PR and PW, winds over SWA were onshore from the Arabian Sea and Persian Gulf.

In addition to exploring ENLN, Marotti et al. (2005) investigated the role NAO has in influencing the climate of Europe and SWA during autumn. Upon correlating precipitation and the Hurrell (2003) NAO index for September through

November, they found a significant positive correlation, a reversal from the relationship Cullen and deMenocal (2000), Cullen et al. (2002), and Trigo et al. (2002) found for winter. As with their results for EN, Mariotti et al. (2005) were unable to explain their findings. The authors demonstrated, however, that during autumn the positive phases of both EN and NAO tend to lead to anomalously high precipitation in SWA. In addition Mariotti et al. (2005) also found an onshore component to the 850-hPa wind anomalies (see Fig 10a) during periods of above normal precipitation.

Principal component analysis performed by Mariotti et al. (2005) also confirmed that the leading mode of autumn rainfall variability for 1948-2000 is related significantly to the precipitation anomalies during positive phases of the NAO and EN. The prior studies on the relationships between the NAO and SWA are promising, but more work needs to be done in this "underdeveloped field" (Pagano et al. 2003) in order to understand the mechanisms by which the NAO influences precipitation in SWA.

5. Indian Ocean Precipitation and SST

Barlow et al. (2002), while investigating possible mechanisms that led to a severe drought in central-southwest (CSW) Asia from 1998-2001 (wet season precipitation was less than 55% of the average) documented a regional mode of climate variability that seems to profoundly influence the climate of SWA at times. (Additional details concerning this historical drought and its wide-ranging impacts can be found in Agrawala et al. (2001)). Composites Barlow et al. (2002) constructed of November-April 1998-2001 anomalies of precipitation, SST, and 200-hPa winds were similar to the LN signatures of these quantities, especially in the central and western Pacific (Barlow et al. 2002; Rasmusson and Carpenter 1982, Ropelewski and Halpert 1987, 1989; Horel and Wallace 1981). There were, however, other prominent features that were not usually associated with a LN event — above average precipitation in the eastern Indian Ocean (which they called the Indian Ocean Precipitation Extension or IPX), which extended from the western Pacific; exceptionally warm SSTs in the western Pacific (Hoerling et al.

2001); and most importantly, prolonged drought in SWA. The spatial pattern of SWA precipitation correlated to precipitation in the IPX region (calculated as precipitation covariance with IPX for 1979-1996) and the time-series (1979-2001) comparison of SWA precipitation and IPX precipitation both show an inverse relationship.

Barlow et al. (2002) explained the observed upper level circulation anomaly patterns in terms of the Rossby wave dynamics proposed by Matsuno (1966) and Gill (1980). In this model the deep tropical latent heat release associated with the IPX precipitation would produce two baroclinic Rossby wave packets (including upper level anticyclones), symmetric about the equator, westward of the heating, as shown in the upper panel of Fig. 3. The persistent anticyclonic anomalies would be consistent with the suppression of synoptic extratropical cyclone activity. These same mechanisms appeared when Barlow et al. (2005) examined the relationship between the MJO and precipitation in SWA and feature prominently in our results (chapter III).

The strength of the warm pool in the western Pacific during this period also seemed to play a role in the drought experienced in SWA (Barlow et al. 2002). Only La Niña events with a strong warm pool signal (see their study for further details on this signal) were associated with an extension of significant positive precipitation anomalies into the Indian Ocean (the IPX region) and negative precipitation anomalies over CSW Asia. The similarity between the rainfall pattern in the strong warm pool cases and the drought period rainfall was striking. The similarity between the enhanced warm pool-La Niña composite and climate anomalies of 1998-2001 suggested that the prolonged, westward-concentrated La Niña during this period was a major factor in the CSW Asia drought. The severity of the drought was speculated to be a result of the prolonged duration of the La Niña and the unusually warm SSTs in the west Pacific (from 1998-2001), which may have enhanced the regional dynamics.

D. EXISTING CLIMATE PRODUCTS FOR SWA

1. DoD Products

Within the DoD, AFCCC and the Fleet Numerical METOC Detachment (FNMOD), both in Asheville, North Carolina, provide the majority of the climatological support to warfighters. A review of the products offered by these two centers shows their products are constructed largely with LTMs of meteorological fields. The strengths of AFCCC and FNMOD lie in the collection, synthesizing, and visualization of LTM fields, in order to provide planning products for warfighters at all levels. Examples include atlases of ceilings, visibility, and icing; narratives describing the climate over the course of the year for numerous locations; and Operational Climatic Data Summaries (OCDS) — summaries of monthly and annual climate data for various cities and airfields. While it is critical to develop a conceptual picture of the LTMs, it is important to recognize that LTMs provide an incomplete picture. The climate variations discussed in the previous section all involve departures from LTMs and have been shown to strongly influence the weather and climate of SWA

While AFCCC provides a suite of high-quality products focused on LTM conditions, especially for SWA, it does not relate current climate conditions to these LTMs or attempt climate forecasting. AFCCC is currently exploring ways to correct this shortfall, and one effort that shows particular promise is the Seasonal Prediction Working Group (SPWG). The SPWG is investigating, and considering the possible adaptation of, the types of climate analyses and forecasts produced by several different civilian agencies (particularly the Climate Prediction Center (CPC) and the International Research Institute for Climate and Society at Columbia University (IRI)) and are issuing experimental forecasts of their own.

2. Non-DoD Products

While analysis of the current state and impacts of climate variations is still a relatively young field in the civilian community, there have been considerably more resources dedicated to these problems than in the DoD. A few of the major

players in this field are the Climate Prediction Center in Camp Springs, Maryland (www.cpc.ncep.noaa.gov, accessed 21 March 2006), the Climate Diagnostics Center (CDC) in Boulder, Colorado (http://www.cdc.noaa.gov/index.html, accessed 21 March 2006), International Research Institute for Climate and Society (http://iri.columbia.edu/, accessed 21 March 2006) , and the Australian Bureau of Meteorology (BOM) in Melbourne (http://www.bom.gov.au/, accessed 21 March 2006). The various products provided by each center will be discussed below. These are just a subset of the experimental and operational monitoring and prediction products that are available, but they will provide an overview on the state of climatology in the civilian sector.

a. Climate Prediction Center

CPC is the most authoritative source of climate monitoring and prediction for the United States. As far as analysis products are concerned, CPC provides various indices for many of the climate variations and teleconnections discussed above. For ENLN, CPC provides numerous resources for assessing the current state of the atmosphere and ocean including plots of SST (both surface and subsurface), OLR, and 850-hPa zonal winds. As the impacts of the IOZM on the US are largely unexplored, they do not include any resources for monitoring it. With regard to the NAO, the CPC provides both graphical and tabular products to monitor this teleconnection using an index based on the Rotated Principal Component Analysis technique developed by Barnston and Livezey (1987). Lastly, CPC provides daily updates of a MJO index (based on an extended empirical orthogonal function (EOF) applied to pentad 200-hPa velocity potential) and weekly discussions on the state of the MJO. None of these products discusses SWA specifically, as they are focused on global anomalies or anomalies that impact the US.

As its name implies, CPC also provides forecast products for some of the teleconnections discussed in the previous paragraph. CPC provides seasonal outlooks of precipitation and temperature to the public that incorporate the impacts of teleconnections. Their web page, however, contains forecast

products tailored to the meteorology community, including discussions of the rationale they used to create the seasonal forecasts. For ENLN, they generate forecasts of SST (and numerous other parameters) using the NCEP coupled forecast system (CFS) model (CFS03). CPC uses the Global Forecast System (GFS) model and an 11-member ensemble model to generate seven, ten, and fourteen day outlooks of the NAO. CPC uses the GFS/Empirical Wave Propagation (EWP) model and CFS model to generate one and two-week forecasts of 200-hPa velocity potential and 45-day forecasts of 850-hPa zonal winds, respectively, to forecast the MJO. Again, SWA is not specifically addressed as the majority of CPC's customers are concerned with impacts in the US.

b. Climate Diagnostics Center

According to their website, CDC "develops national capabilities to analyze, interpret, and forecast important climate variations on time scales ranging from a few weeks to centuries." They are especially focused on climate variations causing major floods and droughts in the US and on global-scale impacts of ENLN. None of their products (monitoring or prediction) focus specifically on SWA. CDC provides tools to monitor the current state of ENLN at http://www.cdc.noaa.gov/ENSO/ (accessed 21 March 2006) and for NAO and the MJO in their "Map Room" (http://www.cdc.noaa.gov/map/, accessed 21 March 2006).

CDC also offers a wealth of climate prediction tools for ENSO, NAO, and MJO at the two websites listed above. The NAO forecasts are for seven, ten, and fourteen days. For details concerning CDC's experimental MJO prediction methodologies see their webpage at http://www.cdc.noaa.gov/MJO/Predictions/ (accessed 21 March 2006).

c. International Research Institute for Climate and Society

IRI's mission is to "enhance society's capability to understand, anticipate and manage the impacts of seasonal climate fluctuations, in order to improve human welfare and the environment, especially in developing countries."

To accomplish this they provide numerous resources dedicated to monitoring, predicting, and investigating the impacts of climate variations. While it is impossible to discuss the full spectrum of resources here, this study will highlight a few of the most interesting and applicable products.

For monitoring the climate, IRI has constructed an entire web page (http://iridl.ldeo.columbia.edu/maproom/.ENSO/, accessed 21 March 2006) dedicated to aggregating from various sources current (and recent) values of numerous quantities often used to assess ENLN, including SST, Southern Oscillation Index, low level winds, and expert discussions. While the other teleconnections are not discussed specifically, IRI accounts for them when issuing their outlook discussions, discussed below. For SWA specifically, one can access temperature, precipitation, and atmospheric circulation anomalies for the last month and last three months at http://iridl.ldeo.columbia.edu/maproom/.Regional/ (accessed 21 March 2006).

As far as climate prediction is concerned, IRI issues probabilistic ENSO forecasts for the Nino3.4 region and seasonal climate forecasts of precipitation and temperature for both regional and global domains. For additional products and details, see their webpage at http://iri.columbia.edu/pred/productlist.html (accessed 21 March 2006). The seasonal climate forecasts (http://iri.columbia.edu/climate/forecast/net_asmt/, accessed 21 March 2006) are "net assessments of information from a variety of climate prediction tools, including dynamical models of the atmosphere, statistical models of climate variability related to sea surface temperature variability, and knowledge of the current state of the climate system." The forecasts are in the form of gridded maps showing the likelihood of a particular quantity falling within each of the three climatological terciles of "below-normal," "near-normal," and "above-normal," with an accompanying discussion detailing the rationale used. In addition to the Middle East being one of the subregions included in their seasonal forecasts, IRI also provides a seasonal "Climate Outlook for Southwestern Asia" (http://iri.columbia.edu/climate/forecast/cswasia/index.html,

accessed 21 March 2006) including a zoomed-in forecast of precipitation and temperature as outlined above and an additional forecast discussion. Clearly IRI is paving the way for climate monitoring and prediction in SWA, and a great deal can be learned from their methodologies.

d. Australian Bureau of Meteorology

While the BOM is understandably focused on the climate of Australia, it does provide several additional climate monitoring and forecasting tools. Perhaps the most important tool they provide is the MJO monitoring tool known as the Real-time Multivariate MJO Index (RMM). For further details concerning this index, please see Wheeler and Hendon (2004) and Chapter 2. The BOM also provides a webpage devoted to ENLN monitoring (http://www.bom.gov.au/climate/enso/, accessed 21 March 2006) and a climate monitoring bulletin (http://www.bom.gov.au/climate/current/cmb/, accessed 21 March 2006) that includes maps of various climate parameters such as circulation and OLR. Unfortunately the only maps that include SWA are global, so there is less detail than one would ideally like.

The BOM's climate prediction efforts are largely focused on Australia, but they do provide computer model forecasts (from the Predictive Ocean Atmosphere Model for Australia) of various ENSO parameters. In addition, The Bureau of Research Meteorology Centre provides MJO-related forecasts of OLR anomalies out to 20 days. These can be found at http://www.bom.gov.au/bmrc/clfor/cfstaff/matw/maproom/OLR_modes/index.htm (accessed 21 March 2006).

3. The Need to Update DoD Climatology Products

As can be seen from the above two sections there is an enormous disparity between efforts within the DoD and efforts within the civilian community to incorporate climate variations into climate monitoring and prediction. To bridge this gap in capability between the two sectors there are several areas in which the DoD needs to focus its resources.

First, and most importantly, the DoD needs to incorporate recent and current research when generating climatology products. AFCCC devotes an enormous amount of time and computer resources to calculating LTMs and tailoring the output to customers' needs. The resulting maps, tables, and narratives are employed by a wide variety of users, from the tactical to the strategic level. A review of the wide-spectrum of products offered by AFCCC, however, found none that addressed how climate variations could impact the LTM climate. Though it may be easy to dictate that the DoD needs to incorporate more scientific research, there are numerous obstacles to actually accomplishing this. Climate variations themselves are a very complex topic, and within the community of climate monitoring and prediction there are numerous conflicts and contradictions between studies. Sifting through the research already accomplished and staying abreast of current research would be a very time-consuming.

Hand-in-hand with incorporating additional research is acquiring, analyzing, and incorporating new data. Only within the last decade have the NCEP/NCAR reanalysis datasets (Kalnay et al. 1996; Kistler et al. 2001) been created and made available to the public. While AFCCC has launched its own mesoscale reanalysis effort via Advanced Climate Modeling and Simulations (ACMES), resource and time constraints led AFCCC to limit the model runs to only 10 years. This is a significant limitation in dealing with the time-scales of interest in climatology; and the approximately 50-year, though coarser resolution, NCEP/NCAR reanalysis dataset is preferred. Constructing its own reanalysis dataset is very time-consuming and would require significant amounts of resources from AFCCC, but significant progress in incorporating climate variations into military planning is possible using the NCEP/NCAR dataset. This dataset is ready to be directly exploited by the DoD. This study, and those by Ford (200), Hildebrand (2001), Feldmeier (2005), LaJoie (2006), and Stepanek (2006) are examples of how to do so.

The additional research and data discussed above can be incorporated into existing AFCCC products and used to generate new products through the paradigm of "smart climatology." Murphree (2005a) defines smart climatology to be "climatology that includes LTMs, but also accounts for higher order statistics than the LTMs and modern developments in climate science and operational climatology." This approach would address on-going and forecasted climate variations *in addition to* LTMs. Murphree (2005a) notes that "modern [smart] climatology provides a more comprehensive view of the climate system and is much better suited than traditional climatology for supporting combatant commanders." Forecasters should apply smart climatology methods to adapt existing climatology products and create new products for use by the warfighter at all different levels of operations.

C. MOTIVATION

The overarching objective of this study is to take the first step in shifting DoD climate products for SWA from their traditional LTM focus to a more up-to-date and valuable smart climatology focus. Within this objective, the goals of this study are three-fold:

1. Review existing climate variations and examine their impacts on SWA.

2. Examine forecasting applications of climate variations. To accomplish this we focused on two specific topics

    a. How do climate variations alter atmospheric circulations in and near SWA?
    b. What are the mechanisms by which these altered circulations contribute to fall-winter precipitation anomalies in SWA?

3. Explore the impacts of climate variations on military operations and interests. One question we seek to answer is to what degree the impacts of climate anomalies could be mitigated by identifying the anomalies ahead of time and accounting for them during planning.

To fit within time constraints, this study focuses on climate variations and their relationships to circulation, temperature, and, especially, precipitation patterns and anomalies. Note that precipitation fields can also be used to study cloud and moisture fields, in addition to incorporating many other variables (e.g.,

vertical motion, stability, etc.). Precipitation forecasting is also crucial to predicting flooding and drought. Because the populations in large portions of SWA lead a pastoral lifestyle, the potential impact of flooding and drought can be enormous (Agrawala et al. 2001). For this reason mitigating the impacts of climate-driven natural disasters can potentially play a large role within the scope of humanitarian operations conducted by DoD in this part of the world.

Our hypotheses are that:

1. The upper and lower circulation anomaly patterns associated with ENLN, IOZM, MJO, and NAO are directly linked to *both* the primary climate variations that affect SWA and anomalous precipitation in the region.
2. Much of the impact on precipitation occurs through: (1) anomalous moisture advection over the tropical northwest Indian Ocean, and tropical and subtropical North Africa; and (2) anomalous moisture convergence over SWA.
3. ENLN, IOZM, MJO, and NAO occur at intraseasonal to interannual scales, and are relatively predictable once initiated. Thus, knowledge of these climate variations and their impacts on SWA should improve intraseasonal-interannual forecasts for SWA.

Chapter II presents our data and methods. Our results our detailed in Chapter III, and Chapter IV contains a summary of our results, discussions, conclusions, and suggestions for future research.

II. DATA AND METHODS

A. DATA

The primary data source for this study was the NCEP/NCAR reanalysis data set (Kalnay et. al. 1996; Kistler et al. 2001), acquired from the Climate Diagnostics Center via their website at http://www.cdc.noaa.gov (accessed 21 March 2006). The reanalysis process uses a fixed, state-of-the-art global data assimilation system to collect and analyze land surface, ship, rawinsonde, pibal, aircraft, satellite, and other observational data to produce a record of global atmospheric fields at 2.5° latitude x 2.5° longitude resolution for a variety of variables (Kalnay et al. 1996). These renanalysis fields were available for most variables from 1948 through the present as of the time of this writing. As is inevitable for a project of such an immense scope, researchers have come across some questionable and erroneous data, and known problems in the dataset are documented at http://www.cdc.noaa.gov/cdc/reanalysis/problems.shtml (accessed 21 March 2006). Monthly and daily mean fields were used. To avoid potentially inconsistent data, we sought to limit our use of reanalysis data as much as possible to the era of meteorological satellites, so as a rule, we usually limited ourselves to using post-1970 data.

Because the majority of the precipitation in SWA falls between October and March, we chose to limit our study to these six months. Outside of this period, precipitation in SWA is very sparse, and often falls in the form of convective showers, which often are difficult to predict. We split the six-month period of investigation further into autumn (October-December) and winter (November-March) and analyzed those seasons separately when assessing the impacts of ENLN and the NAO on SWA. Our investigation of the IOZM and MJO was confined to October-March, as well, but we worked with the daily reanalysis data for these cases.

B. CLIMATE INDICES

1. El Niño-La Niña

Because ENLN phenomena have been researched so extensively, there are several different methods used by researchers to classify ENLN events and quantify their strength. One of the most comprehensive measures of ENLN is the Multivariate ENSO Index (MEI) introduced by Wolter and Timlin (1993), and because of the broad range of parameters it includes, we chose this index for our study. This index monitors the six main observed variables over the tropical Pacific — SLP, zonal surface wind, meridional surface wind, SST, surface air temperature, and total cloudiness fraction of the sky. The MEI is computed for each of twelve sliding bi-monthly seasons (e.g., Dec/Jan, Jan/Feb….Nov/Dec). Positive (negative) values of the MEI represent El Niño (La Niña) events. More information on the MEI can be found at: http://www.cdc.noaa.gov/people/klaus.wolter/MEI/index.html (accessed 21 March 2006).

Similar to Ford (2000) and Hildebrand (2001), we selected 15 years between 1960 and 2000 from their Table 2 to investigate with respect to ENLN. Because of the limited number of LN autumn and winter periods after 1970, we included two years from the late 1960's. Table 1 (next page) lists the years we used the El Niño and La Niña events identified for this study. Using the classification process of Ford (2000), we identified eight strong EN and eight strong LN periods (magnitude of the MEI > 1.0). When analyzing EN and LN years, we looked at autumn of the first year of the event and the subsequent winter.

2. Indian Ocean Zonal Mode

The primary means for measuring the IOZM is the Dipole Mode Index (DMI), as defined by Saji et al. (1999). It is simply the difference in SST *anomaly* between the tropical western Indian Ocean (50°E-70°E, 10°S-10°N) and the

First Year of EN Event		First Year of LN Event	
1972	1991	1964	1984
1976	1992	1966	1988
1977	1993	1967	1995
1978	1994	1970	1996
1979	1997	1971	1998
1982	2002	1973	1999
1986	2003	1974	2000
1987		1975	

Table 1. List of ENLN Years Selected for Compositing in this Study

tropical southeastern Indian Ocean (90°E-110°E, 10°S-Equator). Running tallies of this index are available on several different timescales, from weekly to monthly and longer. Because it offers a weekly measurement of the IOZM, we chose to use the DMI compiled by Kevin Vranes and available at http://www.ldeo.columbia.edu/~kvranes/research/DMI/ (accessed 21 March 2006). The index available there is slightly different than the one originally used by Saji et al. (1999) in that it uses a weekly rather than a monthly sampling and the Integrated Ocean Services System data set, rather than the Global Sea Ice and Sea Surface Temperature version 2.3b data set used by Saji et al (1999). Both indices measure SST anomalies in identical areas, just using different data sets. The weekly index of the DMI is available from the website above for the period November 1981 through June 2001.

We set a DMI threshold of 1.0 to determine what periods to include in our IOZM composites. The seven days following the day on which the weekly index is given were incorporated into the composites we created. Saji et al. (1999) noted that dipole mode events usually peak in October, and the DMI index data support this conclusion. Because the vast majority of strong (DMI magnitude > 1.0) dipole mode events tend to occur in the autumn and involve the positive

phase of the IOZM (cool water off the coast of the coast of Sumatra), we investigated only the impacts of the positive phase of the IOZM on SWA during the autumn. This left us with 135 days to composite. Using the threshold of 1.0, there are not enough days when the DMI > 1.0 during the winter, or when the DMI < -1.0 in either season to allow for a meaningful study.

As noted in Chapter I, at times, EN and the IOZM can be interconnected. Saji et al. (1999) and Black et al. (2003) both demonstrate, however, that the two climate variations are not directly related. For example Saji et al. (1999) found a correlation of less than 0.35 between the Nino3 index and the DMI. Nevertheless, strong positive phases of the IOZM do tend to occur during the autumn of EN years, perhaps through the processes suggested by Black et al. (2003) outlined in Chapter I. This is still an area of ongoing research. It therefore is essential to note that all of the days we used to create our composites of conditions during the positive phase of the IOZM also occurred during the autumn of strong EN years (MEI > 1.0). In identifying the IOZM we used daily data, instead of the monthly data we used for ENLN. In addition, there were fewer years included in our IOZM composites. Because of these disparities in the data sets and the low correlation between the two climate variations, we expected our results for ENLN to be similar to but different from those for the IOZM.

3. Madden-Julian Oscillation

It has only been during the last few years that methods to quantify the strength and location of the MJO in real-time have been introduced. The fundamental problem of real-time MJO-monitoring is extracting the frequency-limited signal without the use of a bandpass filter (Wheeler and Hendon 2004). Bandpass filters, typically used to identify MJO episodes after-the-fact, require information beyond the end of the time series, i.e., from the future. Researchers at the Australian Bureau of Meteorology overcame this limitation by projecting daily data onto spatial patterns characteristic of the MJO of selected meteorological variables. The details of their techniques are beyond the scope of

this paper, but in essence they projected combinations of daily meteorological fields onto two EOFs associated with the MJO. For a more detailed discussion of EOF analysis see Wilks (2006). The fields they chose to combine were OLR, 850-hPa zonal wind, and 200-hPa zonal wind, each averaged over the latitudes of 15°S-15°N (Wheeler and Hendon 2004). The real-time projection of the data onto the two EOF fields yields two MJO indices—the Real-time Multivariate MJO series 1 (RMM1) and series 2 (RMM2).

In order to diagnose the state of the MJO, the RMM indices are combined into a two-dimensional phase space. Points representing sequential days are then joined by a line. Often sequential days trace a counter-clockwise around the "origin," signifying the eastward propagation of the MJO across the Indian Ocean into the western Pacific (Wheeler and Hendon 2004). An example of the RMM phase space appears in Fig. 25. In order to further diagnose the state of the MJO and to facilitate compositing, the phase space is divided into eight numbered phases that are associated with the location of the convective component of the MJO. As the enhanced convection moves off the east coast of Africa and transits the Indian Ocean into the western Pacific, it moves from phase 1 through phase 8. Wheeler and Hendon (2004) noted that the nominal time between each of the numbered phases is six days, but it can vary from event to event. The composites of the observed anomaly fields (OLR, 850-hPa zonal wind, and 850-hPa meridional wind) for each phase are depicted in Fig. 22 for December-February.

Daily values of the RMM1 and RMM2 indices are available in near real-time from June 1, 1974 through the present from the Australian Bureau of Meteorology at http://www.bom.gov.au/bmrc/clfor/cfstaff/matw/maproom/RMM/ (accessed 21 March 2006). A gauge of the strength of the MJO at any given time is obtained by taking the square root of ($RMM1^2$ + $RMM2^2$), referred to here as the *magnitude* of the MJO. Using the data available we selected periods of time for which the magnitude of the MJO was > 1.5 for at least seven consecutive

days during the October-March timeframe. If a particular MJO started in March and lasted into April, the days in April were included, as well.

The location of the enhanced convection or subsidence associated with the MJO is of paramount importance when investigating impacts on SWA. Hendon and Salby (1994) and Barlow et al. (2005) found that the impacts of the MJO on SWA are often strongest when the convective or subsidence component is in the eastern Indian Ocean. For this reason, we chose to classify the phases in Fig. 22 into two groups — one when the convective component was in the eastern IO, and the other when subsidence component was in the eastern IO. Using these guidelines, Wheeler and Hendon's phases 2-5 were grouped together to represent enhanced convection in the eastern IO; and phases 6, 7, 8, and 1 were grouped to represent enhanced subsidence in the eastern IO. Using this algorithm, we identified 483 days between June 1, 1974 and December 31, 2005 when enhanced convection was in the eastern IO, and 555 days when enhanced subsidence was in the eastern IO.

4. North Atlantic Oscillation

Like ENLN, the NAO has been researched extensively, and there have been a number of different methods devised to quantify the positive and negative phases of the oscillation (see Chapter I). Because the NAO essentially measures the oscillation of mass between the subtropical Azores High and subpolar-low (Icelandic Low), most of these methods involve measuring SLP differences between a point associated with the Azores High (either in the Azores Islands or in mainland Portugal) and a point in Iceland. This is a particularly effective means of measurement as SLP records from these locations frequently extend far enough back in time to facilitate creation of a historical record of the NAO over at least the last century.

Because it is more rigorous than a simple SLP-difference between two locations, we chose to use the NAO index calculated and compiled by CPC for our study. CPC maintains a monthly index of the NAO dating back to January 1950 and a daily index that stretches back 120 days. The monthly index we used

can be found at http://www.cpc.ncep.noaa.gov/products/precip/CWlink/pna/norm.nao.monthly.b5001.current.ascii.table (accessed 21 March 2006). The method CPC uses to calculate the daily and monthly index is based on the RPCA technique presented in Barnston and Livezey (1987). This technique, like that used to create the RMM indices for the MJO, uses EOF analysis; and, as a result, the details are beyond the scope of this paper.

To investigate the impacts of the NAO on SWA during the autumn and winter, we selected periods of positive and negative phases of the NAO to composite. The three-month periods we chose were autumns (Oct-Dec) and winters (Jan-Mar) when the average value of the NAO index (simply the arithmetic mean of the NAO index for the three months) was greater than 0.5 (for the positive phase) or less than -0.5 (for the negative phase). Even though CPC maintains monthly values of the NAO back to 1950, we confined this study to years from 1960 onwards in order to use the most reliable reanalysis data. For each phase of the NAO, we selected eight autumns and ten winters between 1960 and 2005 when the average magnitude of the NAO was greater than 0.5. There were more years used in the winter composites because the magnitude of the NAO tends to peak in the January-March timeframe, resulting in generally higher values of the index during the winter. The years selected for this investigation can be found in Table 2 (next page). A comparison of Tables 1 and 2 reveals that many of the NAO events were also ENLN events. This is particularly the case during the autumn, where all the years after 1960 that met the criteria listed above also were also ENLN years. Owing to the greater number of years that met our criteria during winter we were able to select an even mix of years for each phase of the NAO — four years that were EN years, four years that were LN years, and two years that were neither. Unlike the methods used to investigate ENLN, described earlier, the winter periods we chose did not necessarily follow the autumn periods. This is because the NAO

shows much greater month-to-month variability, while ENSO tends to stay in the same phase over the course of the autumn and winter.

Years Used to Composite for NAO			
Autumn (OND)		**Winter (JFM)**	
(NAO > 0.5)	**(NAO < - 0.5)**	**(NAO > 0.5)**	**(NAO < - 0.5)**
1972	1968	1984	1960
1974	1970	1988	1963
1982	1973	1989	1964
1986	1976	1990	1965
1978	1995	1992	1966
1993	1996	1993	1969
1994	1997	1994	1970
1999	2005	1995	1971
		1997	1977
		2000	1984

Table 2. Autumn and Winter Time Periods Selected for NAO Composites

C. METHODS

1. Composite Anomalies

We constructed composite anomalies of a variety of meteorological fields to highlight the impacts ENLN, IOZM, MJO, and NAO had on SWA. The anomalies were calculated as the difference between the actual values for a period and the LTM value for that period. For example, 200-hPa geopotential height anomalies for autumn of EN years were calculated by subtracting the LTM autumn 200-hPa from the mean 200-hPa GPH calculated for the selected EN years. By subtracting the LTM from the average anomalies during the selected years, we created composite anomalies to highlight phenomena attendant to the events.

Monthly means from the NCEP/NCAR reanalysis data were used to investigate ENLN and the NAO, and the long-term monthly and seasonal means were calculated for the 35-year period from 1960-2005. Daily data from the NCEP/NCAR reanalysis were used to study the MJO and IOZM, and the LTM for these cases was calculated for 1975-2005.

2. Moisture Advection

One of the quantities we investigated was moisture advection anomalies at 850 hPa. We chose advection at 850 hPa because we felt it was most representative of the low-level moisture advection in an area of such complex terrain. In order to do this we calculated the LTM and composite mean moisture advection at each point using the following equation

$$\text{Moisture advection} = -\vec{\mathbf{v}} \bullet \nabla q$$

Where on the right hand side of the equation, the first term is the vector wind at 850 hPa and the second term is the gradient of the specific humidity at 850 hPa. To calculate the composite moisture advection anomalies, the LTM mean moisture advection was subtracted from the composite mean moisture advection. For example, to calculate the October-December moisture advection anomaly during EN, we subtracted the October-December LTM moisture advection from the October-December EN composite mean moisture advection.

THIS PAGE INTENTIONALLY LEFT BLANK

III. RESULTS AND DISCUSSION

A. OVERVIEW OF OUR RESULTS

In this section we give a brief overview of the results of our analyses. The subsequent sections of this chapter describe our results in detail.

As described in Chapter I, prior studies have indicated that climate in SWA is tied to the climate in the tropics through the upper and lower level responses to convection in the eastern Indian Ocean, Maritime Continent, and western Pacific Ocean. A major component of the link between these two regions is the upper level response to tropical convection. In the LTM autumn and winter 200-hPa GPH-wind field (Figs. 7 and 12) there is a clear Rossby-Kelvin (R-K) wave structure visible over the Maritime Continent (MC) and western Pacific (WP) that is associated with the convection found there throughout the year. SWA falls under the influence of the northern lobe of this R-K wave response. Thus, changes in convection in the vicinity of the MC and WP, through Rossby-Kelvin wave dynamics, can lead to changes in the upper level circulation over SWA. Previous research (Sardeshmukh and Hoskins 1988) indicates that in the tropics the upper and lower level circulations (including Rossby-Kelvin waves) have opposite sign. This link between the two levels is very important, as it has implications for the low level circulation over SWA as well.

Our results indicate that onshore and offshore flow anomalies in the northwestern IO and Arabian Sea play a critical role in governing precipitation anomalies in SWA. In addition, we found that the mechanism connecting flow anomalies and precipitation anomalies is anomalous moisture transport. Because precipitation in SWA occurs mainly during the passage of extratropical synoptic low pressure systems that transit the region during autumn and winter, changes in the low level moisture available to these systems may have a profound impact on SWA precipitation.

An analogous situation occurs in the eastern U. S. and the Gulf of Mexico. If the low level flow over the Gulf of Mexico is anomalously southerly (northerly), then extratropical synoptic low pressure systems moving through the US will receive anomalously high (low) levels of moisture from the Gulf, leading to anomalously high (low) precipitation from the systems (cf. Carlson 1991). (Such anomalies have been observed over the Midwest and other regions of the eastern U.S (Trenberth and Guillemot 1995). While low level moisture transport in the Midwest and Plains regions in the U.S. is influenced by the low level jet, the offshore monsoon winds play an important role in governing low level moisture transport in SWA is during autumn and winter.

It has also been suggested by prior research that the North Atlantic Oscillation may influence the climate in SWA. In fact, it appears similar moisture transport anomalies to those associated with climate variations that originate in the tropics are also observed in conjunction with the NAO — especially during the winter.

This summary of our results is based on detailed analyses of the chain of events that takes place over the tropical Indian and Pacific Oceans and SWA that leads to low level moisture advection anomalies over SWA. These analyses involved examination of a variety of fields. Upper and lower level GPH and winds, specific humidity, moisture advection, precipitation, OLR, and temperature anomalies were all investigated and are presented in the following sections for ENLN, the IOZM, the MJO, and the NAO.

B. TROPICAL TELECONNECTIONS

1. El Niño/La Niña

a. October – December (OND)

During the autumn, as an EN event builds in the central Pacific, the strongest convection shifts from the MC eastward towards the dateline, where higher than normal SSTs are observed (Fig. 14a). As a result the LTM zonal-flow at 200 hPa (Fig. 7), especially the subtropical jet over southern Asia, is severely disrupted during EN periods. In fact, the western portion of the Rossby-

Kelvin wave structure associated with this anomalously strong convection can be seen in the EN 200-hPa GPH-wind composite anomalies in Fig. 26. As a result of the below-normal SSTs in the Maritime Continent-western Pacific (MC-WP) often observed during autumn of an EN event, convection in this region is typically suppressed. Converging winds at 200 hPa over the MC-WP in the EN composite anomalies are one signature of the below normal convection. The decrease in convection induces an additional R-K wave response, analogous to that observed in the central Pacific to the increased convection. Over the MC-WP, the response to the decrease in convection is *below-normal* upper level heights, however. The northern and southern lobes of this R-K wave response are evident in the elongated troughing and cyclonic winds in the 200-hPa GPH-wind composite anomalies over southern China and Australia. The origin of the troughing over the Middle East is less clear; it may be part of the aforementioned response to events in the tropics or part of a wave train propagating westward from the Atlantic Ocean and Europe. It is also important to note that the elongated troughing visible over southern Asia (from the Middle East to China) is very similar to that observed by Mariotti et al. (2005) for periods of above-normal precipitation in SWA.

As the upper and lower levels of the atmosphere are inextricably linked, there is a corresponding response in the low levels. Sardeshmukh and Hoskins (1988) noted that in the tropics the response at the low levels is often the opposite of that observed in the upper levels. The corresponding EN composite anomalies for 850-hPa GPH-winds are shown in Fig. 27, and a circulation opposite to that in the upper levels is evident. Over southern Asia, there is a clear R-K wave response in the anticyclonic 850-hPa GPH-wind anomaly below the cyclonic 200-hPa GPH-wind anomaly field. Over southern Asia and the northern IO, 850-hPa GPH is above normal, and the wind anomalies are anticyclonic. The southern lobe of the low level R-K wave response is visible to the northwest of Australia. Further to the east, over the

MC-WP, where there is anomalous convergence at 200 hPa, there is now anomalous divergence in the 850-hPa wind field, corresponding to the anomalous subsidence.

The anomalous flow around the low level R-K wave anticyclone over southern Asia is especially important to our study. In Fig. 27, SWA lies in an area where anomalous southeasterly winds around this anticyclone converge with anomalous southwesterly winds associated with troughing over northeast Africa and the Middle East. The result is a distinctly *onshore* anomalous flow in the low levels over most of SWA; on the other hand, parts of northern Iraq, Iran, and the Caspian Sea experience anomalous northerly flow. It must be emphasized that the anomalous onshore flow does not represent a reversal in the LTM offshore winds observed over SWA during autumn. Rather, it is an indication that during the autumn of an EN event, it is likely that there is an increase in the number of days with onshore flow that are interspersed among the days with offshore flow (Murphree 2005b). As a result, the average magnitude of the offshore winds during the autumn appears lower during the autumn of EN periods, thus the onshore anomaly.

If, as proposed above, there is an increase in days with onshore flow over SWA during the autumn of EN years, we would expect this to be borne out in the anomaly fields of other meteorological fields. In fact, this is exactly what we observe. Figures 28 and 29 depict the specific humidity (SH) and moisture advection anomalies during the autumn of EN years. Figure 28 shows a distinct increase in SH over most of SWA, especially the Arabian Peninsula, Iran, Afghanistan, and Pakistan. The moisture advection anomalies also highlight the moist flow out of the Arabian Sea into these areas that accompanies the southerly wind anomalies.

Recent research (Barlow and Salstein 2005) has suggested that the Arabian Sea and northwest IO may be a larger moisture source than previously thought for the extratropical cyclones that move through SWA during the autumn and winter. If this is the case, with the above-normal moisture

advection into SWA and the widespread higher-than-usual SH anomalies shown, an increase in precipitation would be expected during the autumn of an EN event. Indeed, Fig. 30 shows that during the autumn time period, the precipitation rate is above normal throughout SWA. Comparing the composite precipitation anomalies for this case and the LTM precipitation (Fig. 8) reveals that several areas receive between 20-50% more precipitation than normal during EN autumns. This is especially true in the mountainous regions that receive significant precipitation from low-pressure systems transiting the region.

The increase in onshore flow also modifies the low level temperature advection over SWA. SSTs, and therefore surface temperatures (whenever "surface" temperatures are discussed here we will be referring to 2 m temperatures available from the NCEP/NCAR reanalysis data) are significantly higher over the Arabian Sea and northwest IO than over SWA during autumn (see Fig. 31 for LTM surface temperatures). As a result of these positive surface temperature anomalies and the increase in southerly flow, warm air advection northward into SWA occurs more often. Figure 32 shows that the southern and eastern portions of SWA are warmer during EN years as a result. To the north (around the Caspian Sea and northern SWA), where it was noted that the 850-hPa wind anomalies during EN autumns are northerly, the corresponding temperature anomalies are below normal. This makes sense as temperatures to the north, over the interior of Asia, are lower, and the northerly winds bring this cooler air down into SWA more frequently. Finally, hand-in-hand with the above normal precipitation observed during the autumn is anomalously low OLR throughout much of SWA (Fig. 33). This is indicative of increased cloud-cover and is consistent with the above-normal precipitation anomalies.

Compared to other climate variations, the impacts of EN on SWA have probably garnered the most attention, particularly during autumn. Our results for autumn are very similar to those found by Mariotti et al. (2002) and Mariotti et al. (2005). These investigators also noted a tendency toward increased precipitation over most of SWA in autumn during EN, and hinted that

increased moisture flux from the Arabian Sea may be responsible. In addition to confirming the general results and implications of these prior studies, our results also show that, owing to the anomalous southerly flow, SWA is generally warmer during the autumn of EN periods.

In contrast to EN, during LN periods the SSTs in the western Pacific are above average (Fig. 15a), and the anomalous convection in the Pacific Ocean is over and near the Maritime Continent. In response to the increase in convection near the MC-WP region, the 200-hPa GPH-wind anomalies during autumn of LN periods are almost the opposite of those observed during EN periods (Fig. 34). The shift in convection toward the MC-WP is evident in the anomalously divergent winds at 200 hPa over this region that replace the anomalously convergent winds observed in the EN case; and anomalous R-K wave cyclones over the central Pacific replace the anomalous anticyclones at 200 hPa. In addition, the anomalous troughing over southern Asia and Australia that is the R-K wave response to decreased convection over the MC-WP during EN, has been replaced by anomalous R-K wave ridging in the same regions. The ridging in southern Asia stretches westward back to the Mediterranean Sea. This pattern of ridging over southern Asia and troughing over the lower-latitudes in the IO is similar to the 200-hPa pattern Marrioti et al. (2005) observed during periods of below normal precipitation in SWA.

At 850 hPa, troughing and cyclonic wind anomalies over southern Asia and Australia replace the ridging observed there during EN periods (Fig. 35). In addition, the anomalous wind field reveals convergence into the increased convection in the vicinity of the MC. The anomalous cyclonic winds around the 850-hPa trough over southern Asia and the Indian subcontinent now lead to a strengthening of the offshore northeasterly winds over SWA. This offshore flow is enhanced over the western extremes of SWA by ridging over the eastern Mediterranean. It is likely, therefore, that during the autumn of LN periods there are more days than normal with offshore flow over SWA.

The increased frequency of winds from the cold, dry interior of Asia leads to cooler, drier conditions over SWA during autumn LN periods. Figures 36 and 37 show the anomalous winds overlaid with anomalous specific humidity at 850 hPa and the 850-hPa moisture advection anomalies, and the drying effect on SWA is quite clear. Compared to the LTM, the specific humidity over portions of SWA are anywhere from five to ten percent lower than normal during LN autumns. This represents a significant drying compared to normal.

The cumulative effect of the increase in cool, dry flow from the continent is apparent in Figs. 38 and 39, which depict the precipitation rate and temperature anomalies for autumn during LN events. Though there are pockets of above-normal precipitation rate (especially around Turkey), the precipitation rate as a whole is generally below normal throughout SWA. The temperature anomalies are an even better reflection of the increase in northerly winds, as all of SWA is cooler than normal, up to 1°C cooler over parts of the Arabian Peninsula. The anomalous OLR (Fig. 40) during LN periods clearly depicts the increase in convection in the vicinity of the MC and the trend towards drying and less precipitation over SWA.

As was the case for EN during the autumn, the results we found fit well with those found by Mariotti et al. (2002) and Mariotti et al. (2005). These researchers also noted the direct correlation between SST in the central Pacific and precipitation anomalies over SWA during autumn. Outside of the moisture flux anomalies detailed earlier, they did not explore any mechanisms that explained this relationship. Not only have we offered a possible mechanism—the Rossby-Kelvin wave response to anomalous convection in the tropics altering moisture transport into SWA — we have also found that SWA is cooler in association with the offshore flow anomalies during autumn LN periods.

b. January – March (JFM)

During winter, the center of anomalously low convective activity over the MC-WP, associated with the anomalously low SST and convection during an EN event, shifts to the south and east. The effects of this shift are

evident in Fig. 41, which shows the composite anomaly of 200-hPa GPH-winds during the winter of EN events. Compared to the corresponding figure for EN autumns, the anomalous trough over southern Asia (especially China) has contracted, weakened, and shifted to the east and south (compare Figs. 26 and 41). These changes, combined with the southward shift of the subtropical jet (STJ) axis (see Fig. 12 for JFM LTM GPH-winds) over southern Asia, leads to profound changes over SWA compared with the autumn EN events. In particular, at 200 hPa over SWA, anomalous low heights are replaced by anomalous high heights (compare Figs. 26 and 41)..

The changes in the upper level anomalies are reflected in the lower levels. The 850-hPa GPH-wind anomalies during the winter are significantly weaker than they are during the autumn (compare Figs. 27 and 42). Two factors now combine to produce anomalous offshore flow throughout much of SWA during the winter of EN events. The low level anomalous anticyclone over southern Asia and the Indian Subcontinent that leads to anomalous onshore flow into SWA during EN autumns is considerably contracted, weaker, and shifted to the southeast, and the trough over the Middle East that enhances the southerly flow anomaly in the autumn has been replaced by ridging.

The increase in offshore flow has the expected impact on low level moisture over SWA. Figures 43 and 44 show the widespread drying over SWA during the winter. While the magnitude of the specific humidity anomalies is not as strong as those during the autumn, the offshore wind anomaly does have a substantial impact on low level moisture available to the extratropical synoptic low-pressure systems that frequent SWA during the winter. In conjunction with the anomalous flow reversing from onshore to offshore as autumn transitions to winter, the anomalous precipitation and temperature patterns reverse, as well. Figures 45 and 46 reveal that the warm and wet anomalies over SWA during the autumn of EN years are replaced by cool and dry anomalies during the winter. In addition, the OLR anomalies reveal that SWA is, in general, more cloud-free during this time period (Fig. 47). Mariotti et al. (2002) found the same general

patterns, but were unable to explain their findings. We have proposed the southeastward shift from autumn to winter in the negative tropical convection anomaly region over the MC-WP, combined with the southward shift of the STJ and extratropical westerlies, as a possible explanation for the transition in SWA during EN events from anomalously warm and wet conditions in SWA in autumn to anomalously cool and dry conditions in winter. In addition, in the winter EN case, SSTs in the eastern IO are warmer than they are during autumn EN events (Fig.14b). The higher SSTs in the winter case may lead to a regeneration of convection in the eastern IO, further enhancing the southeastward shift in tropical convection anomalies and reducing or reversing the impacts of EN over SWA.

During LN, the positive convection anomaly over the MC-WP shifts east and south as autumn transitions to winter. This causes the anomalous ridge over southern Asia during autumn to contract, weaken, and shift to the east and south (compare Figs. 34 and 48).

As was found for the EN winter case, the weakening of the upper level response over southern Asia has a significant impact on the climate of SWA. As in that case, the weakening and eastward-shift of the R-K wave response to the convection is evident in the low levels, as well. Figure 49 shows that the 850 hPa cyclones that are over the Bay of Bengal and MC in the autumn LN case weaken significantly and drift eastward. The strong cyclonic flow over the Indian Subcontinent and Bay of Bengal has all but disappeared. This leads to a weakening of the offshore flow anomaly over eastern SWA. It is important to note, however, that the anomalous wind in the low levels are still offshore, but weaker than in the autumn LN case. Another notable feature in the 850-hPa anomaly field is the slight weakening of the Saudi Arabian High. This is evident in the anomalous cyclonic flow observed over the Arabian Peninsula in Fig. 49. Again, it is critical to point out that the LTM high pressure observed over the Arabian Peninsula is not replaced by a cyclone, but that it is likely that there are more days when low pressure dominates the peninsula — perhaps a result of more frequent low-pressure systems passing through the region. The cyclonic

wind anomaly induces a southerly flow anomaly over portions of SWA that border the Persian Gulf and northern Arabian Sea and a northerly flow anomaly over regions to the northwest — Iraq, western Saudi Arabia, and western Iran, especially.

These low level wind anomalies have a significant impact on the low level moisture field. As a result of the somewhat complicated flow anomalies observed during the winter, the low level specific humidity (Fig. 50) and moisture advection (Fig. 51) anomalies are not as striking as in the other cases. Despite the weakening of the low level northerly flow over eastern portions of SWA (close to India) the overall trend during the winter is for LN years to be slightly drier than normal — a continuation of the autumn pattern.

Like the anomalous moisture field, the anomalous precipitation pattern is complicated for the LN winter case. Figure 52 shows that precipitation anomalies vary widely throughout SWA, with the specific area's location relative to the anomalous wind being a critical factor. For instance, the areas of higher terrain in Iran and Afghanistan that are downstream of the southerly wind anomaly on the eastern flank of the Saudi Arabian High receive notably more precipitation during LN winters. On the other hand, most of the western regions of the Arabian Peninsula (on the western flank of the Saudi Arabian High) are slightly drier than normal. The anomalous temperature during this timeframe, shown in Fig. 53, is evidence of how significant an effect the northerly wind anomaly can have. While the precipitation anomaly shown in Fig. 52 did not depict any areas experiencing significantly below normal precipitation, most of SWA is decidedly cooler during the winter of LN years — similar to the autumn pattern (Fig. 53). The eastern flank of the Saudi Arabian High, where winds were southerly more often than average, is the only region that is slightly warmer than usual during the winter. OLR anomalies indicate that there is an increase in cloud cover over most of SWA (Fig. 54).

2. Indian Ocean Zonal Mean (October – December)

Owing to the data constraints and thresholds set, we only investigated the impacts of IOZM on SWA during the autumn and only when the IOZM was in the positive phase. We also chose this time period because the IOZM peaks during the boreal autumn (Saji et al. 1999), so autumn has a greater potential than winter for showing the impacts of the IOZM. Because of the below normal SSTs in the eastern Indian Ocean during positive IOZM events (Fig. 55), seasonal convection in the region is suppressed. This is similar to the situation during EN events. A comparison of Fig. 14a and Fig. 55 shows that during positive IOZM periods the SST anomalies in the eastern IO are between 0.6-0.8°C cooler than in the autumn EN case. Because the SST anomaly (and therefore the convection) pattern in the eastern Indian Ocean is similar, but stronger, to that during an EN period, the anomaly fields during positive IOZM events in the autumn often similar but stronger than those during EN events.

A comparison of the 200-hPa GPH-wind anomalies during positive IOZM periods (Fig. 56) and during EN periods (Fig. 26) reveals many of the same features, but the anomalies are much stronger in the case of the IOZM. In Fig. 56 there are three Rossby-Kelvin wave response patterns evident throughout the tropical Indian and Pacific Oceans. From west to east, the first is the R-K wave pattern in the ridging in the western Indian Ocean that reflects the increased convection associated with the higher than normal SSTs in the western Indian Ocean (a signature of the IOZM), off the east coast of Africa. For more on the R-K wave response in the western IO and its impacts on the Horn of Africa, see Lajoie (2006). There is also a very well-defined R-K wave trough over the Maritime Continent, associated with the decrease in SSTs and convection over the eastern Indian Ocean and MC. The Northern Hemisphere response in this case stretches from the MC, northwestward to the Middle East and Africa. Finally, the tail-end of the R-K wave ridging associated with the increase in SSTs and convection over the central Pacific is visible at the eastern fringes of the figure. This was also visible in Fig. 26 (EN autumn case). As the IOZM has little

influence on the central Pacific, the R-K wave response in this composite anomaly is evidence that EN and IOZM are often reinforcing phenomena.

The second R-K wave pattern discussed above is the one of interest to this study. The elongated troughing stretching from the MC across southern Asia (and mirrored in the Southern Hemisphere) present during positive events is similar to that observed during the EN autumn events, but is now much more pronounced. In addition, the resulting wind anomalies are almost twice as strong. At 850 hPa the R-K wave response, like the upper levels, is also considerably stronger (Fig. 57). Many of the same features are present — e. g., the anticyclonic R-K wave response over southern Asia and the northern IO and the troughing over the eastern Mediterranean — but they are considerably enhanced. As a result of the stronger ridge and deeper trough, the onshore flow anomaly, discussed earlier for the EN case, is also stronger. The onshore anomaly is particularly strong across the Arabian Peninsula into Iran and Afghanistan. From this, it can be interpreted that during periods when the DMI magnitude > 1.0, there are even more days when the low level winds are onshore from the Arabian Sea into SWA. The increase in onshore flow leads to even stronger positive specific humidity anomalies over SWA (Fig. 58). The SH anomaly at 850 hPa is quite striking during the positive IOZM case, with SH in some areas on the Arabian Peninsula and in Iran and Afghanistan running 10-20% higher than average.

The substantial increases in low level moisture lead to a corresponding increase in cloud cover and precipitation as well (Figs. 59 and 60). A large region stretching from northeast Africa, across SWA, into India is much cloudier than usual, with widespread OLR anomalies of -20 W/m^2. A significant increase in OLR, corresponding to a decrease in convection, is observed over much of the eastern Indian Ocean and MC, as well. The greatest precipitation increases are in the mountainous areas of western Iran, Afghanistan, and Pakistan. In these regions, precipitation is between 50-100% higher than normal, with even higher values locally. Finally, accompanying the strong onshore flow anomalies is a

distinct warming over SWA. Temperature anomalies are shown in Fig. 61, and areas that experience the strongest southerly flow anomalies are much warmer than usual — e.g., Saudi Arabia, southeastern Iran, and southwestern Afghanistan. The 1-2°C increase in these regions represents conditions that are significantly warmer than usual.

We are not aware of any research that directly investigates the impacts of the IOZM on SWA, so we do not have a basis with which to compare our results. As the SST and other anomaly patterns observed during the positive phase of the IOZM during the autumn are similar to those observed during EN (but much stronger), intuitively our results are consistent with what is known about both climate variations. The IOZM impact on SWA is clearly an area worthy of further exploration.

3. Madden – Julian Oscillation

The third and final climate variation that originates in the tropics that was investigated in this study was the Madden-Julian Oscillation (MJO). Our initial investigations of the differences between autumn and winter in MJO activity and patterns showed relatively few differences. For this reason, we chose not to break down our MJO analyses into autumn and winter periods, as was done for ENLN and the IOZM. Instead, we only looked at the impacts on SWA when enhanced convection or subsidence associated with the MJO was located in the eastern IO during October-March. Chapter II details the methods we used to construct our composites. Again, we must note that to investigate the impacts of the MJO when enhanced convection is in the eastern IO, we composited days from Wheeler and Hendon's (2004) phases 2-5. Their phases 6, 7, 8, and 1 were composited for the analyses of enhanced subsidence in the eastern IO.

a. MJO Convective Component in the Eastern IO

This case is analogous to the case discussed above for LN during the autumn. Barlow et al. (2005) showed that when the MJO convective component moves into the eastern IO, there is a corresponding decrease in precipitation in SWA. They attributed this to the fact that SWA lies beneath the

upper level Rossby-Kelvin wave response to the enhanced convection, thus altering the upper level circulation pattern over SWA. Figure 62 shows the composite 200-hPa GPH-wind anomalies we constructed for the case of enhanced convection in the eastern IO. The R-K wave response is quite prominent in the form of an anomalous ridge stretching from the MC back to SWA in the Northern Hemisphere, with a corresponding ridge in the Southern Hemisphere. In addition the divergent upper level winds over the eastern IO associated with the increased convection there are evident in the composite anomaly. The upper level anomaly pattern described here is very similar to that found by Hendon and Salby (1984) and discussed in Chapter I. Barlow et al. (2005) also noted the R-K wave response is stronger in the Northern Hemisphere, owing to the stronger upper level winds north of the Equator during boreal autumn and winter.

The corresponding R-K wave response at 850 hPa shows up quite well in Fig. 63. The R-K wave trough and cyclonic flow at 850 hPa centered over India is in roughly the same position as in the autumn LN case. The cyclonic flow over India, in combination with weak anticyclonic flow around weak ridging over the eastern Mediterranean, acts to produce an offshore flow anomaly throughout most of SWA — again, similar to the autumn LN case. The resulting specific humidity anomaly (Fig. 64) shows that the result of this offshore flow is significant drying over SWA. With the offshore wind and drying anomalies observed over SWA bearing a resemblance to those observed during autumn of LN events, it is not a surprise that the precipitation anomalies are also similar. Figures 65, 66, and 67 show that SWA, in general, receives less precipitation, is cooler, and is more cloud-free than normal during periods when there is enhanced convection in the eastern IO.

Our results are quite similar to those found by Barlow et al. (2005), as they also found that when the MJO convective component was in the eastern IO, SWA tends to be drier than normal. Our results indicate that, in addition, SWA is significantly cooler, as well. Barlow et al. (2005) did not analyze the low

level response; however, our results indicate that the low level R-K wave response is a critical factor in altering the moisture transport anomalies over SWA. These moisture transport anomalies, in turn, are responsible for the observed precipitation anomalies.

b. MJO Subsidence Component in the Eastern IO

If enhanced convection in the eastern IO is analogous to the autumn LN case, then enhanced subsidence in the eastern IO corresponds to EN events during the autumn. It is worth noting that during the EN case, decreased convection is observed over the MC; by definition this is also the case during the MJO when enhanced subsidence is located over the eastern IO and MC. The 200-hPa GPH-wind anomalies illustrate this similarity (Fig. 68). Note the convergence in the upper level anomalous winds over the MC in both Figs. 68 and 26. As was the case with anomalous convection over the eastern IO, the upper level R-K wave response over southern Asia (and in the Southern Hemisphere) is quite prominent when the subsidence component of the MJO is in the eastern IO. The 200-hPa R-K wave response over southern Asia results in an elongated trough stretching from Southeast Asia eastward to northeast Africa and the Middle East. Comparing this to the 200-hPa GPH-wind anomalies in the same region for the EN autumn case (Fig. 26) reveals the striking similarity in responses over southern Asia to decreased convection in the eastern IO. Hendon and Salby (1984) also found the same patterns in the upper-level anomaly fields when the convective component of the MJO was in the eastern IO.

The similarities do not stop upon moving to the lower levels, as can be seen in Fig. 69. Where there are twin anticyclones paired about the equator in the autumn EN case (Fig. 27) we find similar anticyclonic anomalies in this case, as well. In fact the anticyclones are in nearly the same location as the cyclones are for the case of enhanced convection in the eastern IO. The strong anticyclonic anomaly over India plays a similar role to the one it plays during the autumn EN case; it directs onshore flow into SWA. In this case, owing to the

orientation of the anticyclone over India, the onshore flow is more southeasterly and is directed towards the Arabian Peninsula, Iraq, and eastern portions of SWA.

The specific humidity anomalies reflect the onshore flow, with almost all of SWA experiencing higher than normal SH (Fig. 70). This SH anomaly pattern is strikingly similar to the SH pattern during EN autumn cases, providing further evidence to the link between the two cases. With the increase in SH over the region, there is a concurrent increase in cloud-cover and precipitation (Figs. 71 and 72), as there is in the autumn EN case (Fig. 31). In addition, as is the case with EN during the autumn, all of SWA is warmer than average — up to a 1°C in some places (Fig. 73).

Barlow et al. (2005) found a 23% increase in precipitation over SWA when the subsidence component of the MJO was in the eastern IO, and this seems plausible given the precipitation anomalies we found. For this case, our anomalies indicate that the onshore moisture flow anomaly seems to be directed over the Arabian Peninsula into eastern SWA, but this is not necessarily always the case. It is important to remember that this is only the *average* anomaly, and that for any individual MJO event the onshore flow anomalies may come from one of many directions.

C. EXTRATROPICAL TELECONNECTIONS

We have shown that SWA's location relative to the Indian Ocean and Maritime Continent plays a major role in determining what global-scale climate variations have a significant impact there. Because SWA falls within the broad area affected by the Rossby-Kelvin wave response to tropical convection in the vicinity of the MC, climate variations that originate in the tropics that alter this R-K wave response play a prominent role. That is not to say SWA is exclusively affected by climate variations originating in the tropics. Indeed, as SWA lies at the crossroads between the European-North Atlantic sector and the tropics, climate variations from the North Atlantic may impact SWA through several mechanisms. For example, since a significant number of the extratropical

cyclones that affect SWA form in the eastern Mediterranean Sea (Cyprus Lows) and Black Sea, climate variations that impact these two cyclogenesis regions will also impact SWA. Also, circulation anomalies induced by climate variations in the North Atlantic may extend all the way to SWA, altering moisture transport in the same fashion as climate variations originating to the east of SWA

Prior research (detailed in Chapter I) indicates that the primary extratropical climate variation that exerts an influence on SWA is probably the NAO. However, there has been little research done to investigate the impacts of the NAO on SWA, especially on Iran, Afghanistan, and Pakistan. As outlined in Chapter I, it is not clear whether the influence of the NAO extends as far west as these areas. The goal of this study is to examine the impacts and the mechanisms by which the NAO affects the climate in SWA. To do this, we followed the same outline we did for ENLN, IOZM, and the MJO. Because the magnitude of the NAO tends to peak in the winter, we will examine autumn and winter separately.

Before we present our results for the NAO, it must be emphasized that during autumn the extratropics and tropics are in essence competing for influence over SWA. During autumn, the axis of the STJ lies over SWA, and the region is especially susceptible to the influence of enhanced or suppressed convection in the tropics (which is still strong in the Northern Hemisphere), especially during early autumn. Later in autumn, extratropical phenomena begin to affect the region more frequently. The frequency tends to peak in January (Walters et al. 1991). For these reasons, we expected the influence of the NAO on SWA during autumn to be somewhat harder to detect than it is in the winter.

1. October – December (OND)

A comparison of the composite anomalies of 200-hPa GPH-winds and 850-hPa GPH-winds, shown in Figs. 74 and 75, highlights an important difference between climate variations that occur within the extratropics (e.g., within the extratropical westerlies) and those that occur in the tropics. In the case of the NAO, with an extratropical regime over SWA, the anomalies have an

equivalent barotropic structure, such that the anomalies are qualitatively the same in the upper and lower levels. This is evident in the ridging observed at both 200 and 850 hPa over the Mediterranean Sea and southern Europe, which represents the eastward extension of the anomalously strong Azores High. Further to the west, anomalous troughing is found at both levels over SWA.

The role these two different circulation anomalies (ridging over the Mediterranean and troughing over SWA) play in low level moisture transport over SWA is somewhat complicated. One would expect the northerly wind anomalies around the eastern Mediterranean to lead to drying over western SWA, and the southerly wind anomalies around the trough to lead to an increase in SH over eastern SWA. This is what is observed, but the anomalies are not as dramatic as they were for ENLN, IOZM, and the MJO. The specific humidity (Fig. 76) and moisture advection (Fig. 77) anomalies for this case depict an approximate east-west split in moisture transport patterns. This same geographic split is manifested in the OLR (Fig. 78) and precipitation (Fig. 79) anomalies, as well. East of approximately 50°E, areas receive less precipitation during the autumn under the influence of the positive phase of the NAO; to the west of this longitude, areas receive slightly more precipitation than average. The anomalous OLR field is more complicated, but in general, there is a rough east-west split in cloud cover. The temperature anomalies in this case are quite strong, with most regions actually being cooler (Fig. 80). Warm anomalies are observed over the northern Arabian Sea and southern Afghanistan and Pakistan, along the main axis of the anomalous southerly flow.

The case for the negative phase of the NAO during the autumn is even more complicated than the case for the positive phase. As is expected, however, an equivalent barotropic structure is observed in the GPH-wind anomalies at 200 hPa (Fig. 81) and 850 hPa (Fig. 82), but with the signs of the anomalies having reversed from the positive NAO case. The Mediterranean Sea and southern Europe are dominated at both levels by strong troughing and cyclonic wind anomalies, with ridging now extending southward from Asia into portions of

Iraq, Iran, and the Arabian Peninsula. The Saudi Arabian High weakens, as well (similar to the case for LN during the winter), creating southerly wind anomalies along the southern coasts of Iran, Afghanistan, and Pakistan.

The SH (Fig. 83) and moisture advection (Fig. 84) anomalies have grown more complicated than in the positive NAO case. Where the troughing associated with the weakening of the Azores High dominates (eastern shore of the Mediterranean Sea), there does seem to be a coherent increase in moisture associated with the southerly wind anomaly. There is also an increase in moisture advection and SH along the northeastern tip of the Arabian Peninsula and the northern reaches of the Arabian Sea, which is driven by the weakening of the Saudi Arabian High. Further to the north, where anomalous northern winds from the interior of the continent impinge on SWA, conditions are drier during the negative NAO phase.

The patterns observed in the moisture advection and SH anomalies are also observed in the precipitation (Fig. 85), temperature (Fig. 86), and OLR (Fig. 87) anomalies. As expected, areas that have higher (lower) SH than usual receive more (less) precipitation and are cloudier (more cloud-free) than average. Like the moisture and precipitation anomalies, the temperature anomalies are somewhat muddled. Where the anomalous winds are strong, there are coherent temperature anomalies. This is especially true over the northeastern portions of SWA, where there are cool anomalies as a result of the anomalous northerly winds. Eastern Turkey, the Caucasus, and northwestern Iran, which are on the fringes of the strong southerly wind anomalies, are significantly warmer.

Unfortunately, owing to the complexity of the anomaly fields during the autumn, directly applying our results to operational forecasting may prove to be difficult. In general during autumn we see a weakly positive correlation (especially in OLR) between precipitation in SWA and the NAO index, but there is considerable local variation within SWA. The general positive correlation we found is consistent with the results of Mariotti et al. (2005). On the other hand, the temperature anomalies are more coherent and, in general, show an inverse

relationship to the NAO. One notable exception is the cool anomaly over extreme eastern SWA during the negative phase of the NAO. As we will see, for the winter the signals are much clearer.

2. January – March (JFM)

In winter the NAO typically strengthens, the extratropics gain more influence in the region, and the impacts of the NAO on SWA become much clearer. Examining the positive phase first, the strengthening of the NAO is clearly evident in the 200-hPa (Fig. 88) and 850-hPa GPH-wind (Fig. 89) anomaly fields. At 200 hPa there is a very strong ridge over southern Asia and the northern Indian Ocean. This is similar to the ridging pattern Mariotti et al. (2005) found during periods of below normal precipitation in SWA. From the two anomaly fields it is apparent that the Azores High has strengthened substantially and its influence now stretches as far east as the Caspian Sea.

As a result of the strengthening and eastward extension of the Azores High, the anomalous low level winds are now northerly for much of SWA; and the low-level SH (Fig. 90) and moisture advection (Fig. 91) anomaly patterns reveal notable drying throughout SWA. The dry pattern over SWA quite clearly translates to the precipitation (Fig. 92) and temperature (Fig. 93) anomalies. Figures 92 and 93 reveal just how far-reaching an effect the NAO has on portions of the eastern Mediterranean and SWA. The entire region is significantly drier than usual, from the Mediterranean eastward to the Himalayas. The northerly flow anomalies also have a striking effect on temperatures throughout SWA. Figure 93 shows that all areas south of approximately 40°N are much cooler than average during positive NAO periods. On the other hand, areas north of this latitude are much warmer than usual.

The anomalies are also quite prominent when the negative phase of the NAO is in control during the winter. As one would expect, however, the signs of the anomalies are reversed. In this case there is deep troughing at 200 hPa (Fig. 94) and 850-hPa (Fig. 95) from the Mediterranean into Turkey and the Caspian Sea region. Again, note the elongated trough in the 200-hPa GPH field;

this is similar to the pattern Mariotti et al. (2005) associated with increased precipitation in southeast Europe and SWA. In the negative NAO case there are broad southerly flow anomalies associated with the deep, expansive troughing situated over southern Europe.

As indicated by the specific humidity (Fig. 96) and moisture advection (Fig. 97) anomalies, the southerly flow anomalies lead to increases in low level moisture throughout much of SWA — portions of interior Afghanistan and Pakistan are drier than normal, however. These moisture anomalies are reflected in the precipitation (Fig. 98), temperature (Fig. 99) and OLR (Fig. 100) anomalies, as well. The higher terrain of western Iran and the Caucasus receives much more precipitation than normal during the negative phase of the NAO. The anomalous drying in Pakistan and Afghanistan is reflected in the precipitation and OLR anomalies. As was the case for the positive phase of the NAO, the temperature anomalies for the negative phase are striking. For, this case, however, almost all of southeastern Europe and SWA is significantly warmer than average.

The results we found for the winter fall in line with those of Cullen and deMenocal (2000), Cullen et al. (2002), and Trigo et al. (2002). These researchers also found a negative correlation between precipitation and the NAO during the winter. Our results indicate a stronger correlation than Cullen and deMenocal (2000), however. While they were unable to find a strong relationship between the NAO and precipitation east of Iraq, our results indicate the relationship extends further east into Iran, Afghanistan, and Pakistan, especially for the case of the positive NAO. For the case of the negative phase of the NAO, things become less clear, as an apparent strengthening of the Saudi Arabian High leads to offshore flow anomalies in the areas bordering the northern Arabian Sea. The NAO-temperature relationships we found were very strong, however. We found a striking negative correlation between the NAO and temperature anomalies over SWA during the winter. Despite the local variations in the precipitation anomalies, the inverse NAO-temperature relationship holds

from the eastern Mediterranean to the Himalayas and as far south as the Horn of Africa. Research into the potential predictability of the NAO is ongoing, and because of the impacts the NAO has on SWA (especially during the winter) any long-range forecasting system for SWA should incorporate NAO prediction efforts.

D. SUPERPOSITION OF TELECONNECTIONS

There is one important caveat to the results and discussions presented so far in this chapter — we have tried to isolate each climate variation to discuss its individual impacts on SWA. In reality, rarely will one climate variation act alone on SWA. Because the climate variations we have investigated operate on timescales that stretch from weeks to months (e.g., MJO) to a year (e.g., ENLN), there is a distinct possibility that one or more variations may act concurrently. As the overlapping of variations can significantly muddy the waters, we have chosen to leave to a future study any investigation into the effects various combinations of climate variations can have on SWA. For an example of the interaction of the NAO and ENLN and their combined effects on the eastern U.S. and Europe see Rogers (1984). For an example of the interaction between the MJO and ENLN, and the impacts this can have on the west coast of the U.S. see Stepanek (2006).

As alluded to on several occasions, these climate variations not only interact with each other, but also modulate synoptic-scale low pressure systems. Barlow et al. (2005) emphasize that the circulation anomalies associated with the MJO will have little impact on SWA if there is no synoptic activity in the region. Specifically, they note, “the influence is only realized during the brief periods of precipitation associated with each storm and is extraneous the rest of the time.” This may be an oversimplification, but it is an important point to consider. Barlow et al. (2005) failed to note, however, that the circulations induced by distant climate variations may alter the synoptic pattern enough to create conditions favorable or unfavorable for midlatitudes synoptic activity, e. g. prolonged upper level troughing over SWA may provide enough favorable dynamics to encourage

cyclogenesis. The interplay between the synoptic-scale weather and climate variations certainly bears further research.

E. SUMMARY OF RESULTS

The results presented here suggest that using known climate variations to improve mid-long range forecasting for SWA is certainly feasible and merits further research. Climate variations originating in both the tropics and the extratropics were shown to have significant impacts on SWA, primarily through their ability to alter low level circulations and moisture transport in the region. Climate variations originating in the tropics exert their influence through Rossby-Kelvin wave dynamics induced by anomalies in convection in the eastern Indian Ocean, Maritime Continent, and western Pacific Ocean.

The impacts of the three climate variations of tropical origin that we investigated on SWA are heavily tied to their influence on convection in the tropics. When decreased convection was found in the eastern IO, MC, and western Pacific Ocean, the Rossby-Kelvin wave response led to increased onshore flow anomalies in SWA. This is true for EN and the positive phase of the IOZM in the autumn and also to phases 6, 7, 8, and 1 (according to Wheeler and Hendon 2004) of the MJO. The onshore flow anomaly observed in these cases leads to increased specific humidity throughout SWA, increased cloud-cover and precip, and warmer temperatures. When enhanced convection was located in the eastern IO, MC, and western Pacific the opposite anomalies are observed in SWA. This is the case for LN during the autumn and phases 2-5 of the MJO, and lower specific humidity is observed throughout SWA, along with a decrease in cloud cover and precipitation, and cooler temperatures. During the winter the impacts of ENLN are less clear as SWA comes under increasing influence from the mid-latitudes. Therefore, during winter operational forecasts for SWA may need to rely heavier on extratropical teleconnections. In addition, it was shown that between autumn and winter the SST anomalies in the eastern IO change from negative to positive for the EN case. For LN, the SST anomalies in the eastern IO are negative for both seasons, but are more intense during the

winter. The impacts SST anomalies have on convection and the resulting upper level circulation needs to be accounted for, as well.

The method by which the NAO alters low level moisture transport in SWA is very different. Moisture transport is driven by oscillations in the strength of the Azores High. During the winter, especially, this semi-permanent features stretches as far east as the Caspian Sea and can significantly influence the weather over SWA. When the Azores High strengthens (positive NAO) the anomalous anticyclonic flow brings an increase in northerly winds to SWA and cooler, drier weather prevails. This was evident in the specific humidity, precipitation, OLR, and temperature anomalies during the positive phase of the NAO during the winter. When the Azores High weakens relative to its LTM, there is anomalous cyclonic flow over the Mediterranean and the Middle East. As a result of this increase in southerly flow, increased moisture from the eastern Mediterranean Sea, Persian Gulf, and Arabian Sea is advected into SWA. This results in widespread increases in specific humidity, OLR, and precipitation, as well as a significant warming throughout SWA. During the fall, the impacts of the NAO on SWA are less clear, and there are significant local variations in moisture and precipitation anomalies. For this reason, the utility of the NAO as a forecasting tool during the autumn is questionable, but further research may uncover other relationships that provide more useful operational results.

The relationship uncovered here between convection, moisture transport anomalies, and precipitation in SWA is summarized in Fig. 101. These two schematics present simplified “recipes” for inducing above and below-average precipitation anomalies over SWA and could provide the basis for a forecasting system for SWA. Table 3 (next page) presents a preliminary analysis of the results we have found. Future work will undoubtedly clarify some of the relationships we found and address those that we were unable to in this study (i.e., negative phase of the IOZM).

	Autumn		Winter	
	Precipitation Anomaly	Temperature Anomaly	Precipitation Anomaly	Temperature Anomaly
El Niño	Wet	Warm: South and East Cool: North and West	Dry	Varied
La Niña	Dry	Cool	Wet	Cool
Positive Phase IOZM	Wet	Warm	Inconclusive	Inconclusive
Negative Phase IOZM	Inconclusive	Inconclusive	Inconclusive	Inconclusive
MJO Conv. Comp. in E. IO	Dry	Cool	Dry	Cool
MJO Sub. Comp. in E. IO	West: Wet East: Dry	Warm	West: Wet East: Dry	Warm
Positive Phase NAO	Dry	Cool	Dry	Very Cool
Negative Phase NAO	Varied	Varied	Wet	Very Warm

Table 3. Preliminary assessment of general precipitation and temperature anomaly patterns for SWA during the climate variations that were investigated.

F. MILITARY APPLICATIONS

1. Need for Climate Prediction/Seasonal Forecasting

Now that we know potential impacts of climate variations on SWA, how do we apply this knowledge to military operations? Because of the timescales involved when dealing with climate variations, the arena in which the results presented here can be best exploited is likely that of operational to strategic-level planning, particularly by staffs at the combatant command headquarters. The concepts of "strategic forecasts" and "strategic weather" as defined by Demmert et al. (2005) and Lanicci (2003), respectively, highlight that weather and climate forecasts at the strategic level can be critical to the attainment of military and political objectives. Another area involving the impact of climate variations that could be addressed at the strategic level is environmental security; this will be discussed in more detail later in this section.

An indication of the importance of the need for weather and climate forecasts at the operational and strategic levels are the requests received by AFCCC for these types of products. AFCCC has been asked, on numerous occasions, to provide regional weather forecasts in the 15-day to 9-month timeframe, such as 15-30 outlooks for the Pacific theater of operations, snowfall and drought forecasts for Afghanistan, long-range temperature outlooks to prepare for likely snowmelt runoff and flooding, and seasonal outlooks for European Command's area of operations (A. Gravier 2005, personal communication). AFCCC currently does not have the resources to produce these types of forecasts, and as a result, often is forced to fall back on LTM products.

The requirement for seasonal prediction is also included in the Centralized Aerospace Weather Capability Operational Requirements Document, but this document also recognizes that the capability does not exist within the DoD. Having recognized this shortcoming, AFCCC has recently embarked upon an experimental effort, the Seasonal Prediction Working Group, to assess the feasibility of producing climate analysis and prediction products. As this effort is

still ongoing, we do not have any conclusions to present; but the results seen so far are promising. A prototype product from the SPWG is presented in Fig. 102, however.

2. Operational Impacts of Climate Variations

The winter of 2004-2005 was particularly severe in parts of SWA — Iran, Afghanistan, and Pakistan, especially. This time period, therefore, affords us a timely opportunity to investigate the wide spectrum of impacts climate variations can have on military operations in SWA. Preliminary research points to the MJO as having the most impact on SWA that winter, as there was not a strong EN or LN event in the Pacific during this time. The majority of the extreme rain and snowfall, and subsequent flooding, was reported from February through March, and indeed during that time period a strong MJO event moved through the Indian Ocean into the Pacific. Associated with this was strong, persistent subsidence in the eastern IO for the first half of the period, followed by strong, persistent convection in the eastern IO during the second half. Our research indicates that this course of events would likely lead to a period of increased precipitation followed by cooler, drier weather. This is similar to what was observed, with many areas reporting very heavy rain and snow early on, resulting in flooding over the next several weeks. An in-depth study of the meteorological mechanisms (no doubt there were several operating concurrently) is beyond the scope of this study, however.

Regardless of the specific meteorological factors that led to such a harsh winter, the 2004/05 winter provides numerous valuable examples of impacts sustained periods of harsh weather can have on military operations, especially in such an unforgiving setting as Afghanistan and Pakistan. For example, because of the remoteness of many communities, the U. S. military was repeatedly called upon to deliver supplies and aid (North 2006; BBC News 2006; Synovitz 2006). The U. S. military also worked with various other agencies to mitigate the effects of dam breaks and flooding, especially in Afghanistan and Pakistan (J. B. Desjardins 2005, personal communication). In fact Synovitz (2006) noted that

the thermal imaging equipment on A-10 aircraft was used to help locate Afghan nationals missing during the flooding. For situations such as the winter of 2004-2005, seasonal forecasting (using known impacts of climate variations) could allow commanders to account for the possibility that air assets (especially helicopters and cargo aircraft) and other resources (time, money, and personnel) may be need to be devoted to relief/recovery operations. If the severe weather during February and March 2005 could be traced back to a particularly strong MJO event in the eastern IO, commanders could potentially be given several weeks notice of an *increased likelihood* of heavy rain and snow, and subsequent snowmelt and flooding.

Outside of the various humanitarian impacts, prolonged periods of harsh weather can affect military operations. For example, ISR could potentially be degraded by periods of increased cloudiness or other visibility restrictions (e.g., blowing dust or sand). Flooding or extreme snowfall may force troops to seek alternate means of transportation, or force commanders to bring additional resources into the theater to facilitate removal of excessive rain or snow.

This study is only a first-step towards accounting for the regional impacts of climate variations and focuses solely on one region. Considerable follow-on work still needs to be done to investigate the impacts of climate variations in SWA and other theaters of operation. Another area in need of follow-on work is determining how to best provide the results of ongoing research to forecasters in the field and on various staff. They do not have the time to sift through volumes of research, so it is important that they have access to forecast products that incorporate climate analysis and forecasting, once they are deemed suitable for operations. Since climate analysis and forecasting are still in their infancy within the DoD, there are several possible ways this could be accomplished, and all bear further exploration. These include, but are not limited to, applying products (several of which were discussed in Chapter I) from the civilian community (e.g., from CDC, CPC, and IRI) to military operations; incorporating the impacts of climate variations into existing products; and creating new forecasting products

that account for climate variations. Chapter I showed that many existing civilian products do not sufficiently address military concerns (only IRI does forecasts for SWA), but a thorough discussion of the merits and potential problems in working in conjunction with the civilian community is beyond the scope of this study.

On the other hand, there are several potential products that AFCCC currently issues that could be enhanced to include climate variations. These include the AFCCC narratives, climograms, and Operational Climatic Data Summaries (OCDS). We feel the creation of the Seasonal Prediction Working Group is a big step in the right direction, and products like the prototype presented in Fig. 102 could be generated for a variety of different situations — e.g., autumn EN in SWA, impact of MJO-enhanced convection off the east coast of Africa on operations in the Horn of Africa. The weather cell in the Air Force Operations Group at the Pentagon maintains briefings that detail potential seasonal impacts on operations using simple "stoplight" charts. These briefings, however, are constructed solely using long-term means. These briefings should be updated to account for climate variations and could serve as a template for a variety of briefings for different scenarios. A prototype of a possible "stoplight" chart is shown in Fig. 103. In this figure the right-hand side of the chart (the impact anomalies) depicts the impact that a climate variation or combination of climate variations is expected to have on the LTM. For example, in Fig. 104, the trend for all the parameters during periods when the subsidence component of the MJO is in the eastern IO is towards worse conditions than the LTM – this is indicated by the red shading of the parameters. The actual parameters (ceiling, visibility, etc.) are not in the "red" category, they are just worse than the LTM. This is only an example prototype, but it shows one possible method of incorporating climate variations into simple briefing charts.

3. Environmental Security

At the national scale, Demmert et al. (2005) state that "environmental issues can have a major impact on regional instability and conflict," and this sentiment is also echoed by Lanicci (2003). That environmental issues (including

climate-related phenomena such as floods, drought, and “global warming”) can have an impact on regional security is a major tenet of the field of environmental security. While there is still a great deal of debate within the military and political community as to exactly what is encompassed by the term “environmental security” (Smith 2001), we will work under the broad notion that environmental issues can have a further destabilizing effect on areas that are already suffering from ethnic, religious, economic, or other forms of tension. This particular interpretation of “environmental security” is discussed in much more detail in Homer-Dixon (1999).

Recently, the DoD has begun to recognize the potential role of environmental security, and King (2000) and Demmert et al. (2005) suggest that, because it is a regional issue, environmental security planning be incorporated into the strategic planning process. Specifically, they point to the Theater Security Cooperation Plan (TSCP) as the likely vehicle for addressing environmental security concerns. To support the TSCP process, Demmert et al. (2005) introduce the concept of an Environmental Security Plan (ESP), which would serve as a regional analog to the Weather Support Plan used at the base level. A planning document such as this that identifies potential environmental threats to regional security could incorporate specific regional impacts of climate variations, such as those identified in this study. In addition, Demmert et al. (2005) recommend that the Air Force weather community involve staff officers at the Warfighting Headquarters (WFHQ) and combatant command levels in the development of ESPs. Armed with the knowledge of the regional impacts of climate variations, these staff officers would be vital components of the TSCP program.

IV. SUMMARY AND CONCLUSIONS

A. SUMMARY

This study investigated the impacts of global-scale climate variations on SWA. In addition to diagnosing the meteorological mechanisms by which climate variations influence the climate in SWA, we have explored two other related issues. First, we have provided a review of existing climate variations and presented an up-to-date glimpse into the current state of research into the impacts these climate variations on SWA. This literature survey was sorely needed by the DoD. We have also explored possible impacts these climate variations have on military operations and possible avenues to be explored to use this knowledge to mitigate the effects of climate anomalies.

Using the NCEP/NCAR reanalysis data and climate indices associated with ENLN, IOZM, MJO, and the NAO we examined the impacts these climate variations have on SWA during the autumn and winter (October-March). We chose this time period because extratropical low-pressure systems that transit SWA during autumn and winter are responsible for a large majority of the annual precipitation to the region. We have identified several new relationships between the ENLN, MJO, and the NAO and anomalous conditions in SWA, as well as several new mechanisms to explain those anomalies. We have examined for the first time the relationships between the IOZM and SWA. We identified many new parallels between the mechanisms and impacts on SWA of these climate variations. We found that these climate variations, in addition to their impacts on precipitation, which have concomitant impacts on cloud and moisture fields, can have significant impacts on temperature in SWA. These impacts are presented in the following section.

B. IMPACTS ON SWA

We found that ENLN, IOZM, MJO, and the NAO have the following impacts on SWA:

1. ENLN

a) During the autumn (October – December) of EN events there is an increase in low-level (850-hPa) moisture, precipitation, and cloud cover in SWA. Temperature anomalies exhibit a northwest/southeast split. Areas to the northwest are cooler than normal, while the southeast is warmer than average.

b) During autumn of LN events, the opposite anomalies are usually observed. In general, SWA is drier than average, with a decrease in both low-level moisture and precipitation. OLR anomalies indicate that during LN autumns, there are likely to me more cloud-free periods in SWA. Also, as a result of the northerly wind anomalies over most of the region, most of SWA is cooler than average.

c) During the winter (January – March) of EN events, SWA is generally cooler and drier than normal — the opposite of what is observed during autumn. In addition it is slightly less-cloudy than usual over most of SWA.

d) Because of the complicated low-level wind anomalies patterns during winter LN events, the resulting precipitation and moisture anomalies show more small-scale variation than in any other ENLN case. In contrast, the temperature anomaly in this case is much more consistent, with SWA being cooler than average.

2. IOZM

a) Owing to the dataset we used and the thresholds we set, the only meaningful investigation we could carry out with respect to the IOZM was for the positive phase of the IOZM during the autumn. The anomalies we found were very similar to those observed during the autumn EN case, but significantly stronger. In particular, low-level moisture and precipitation show impressive increases relative to average, with well-above average cloud-cover, as well. Temperatures in most areas are higher than usual.

3. MJO

a) Because our preliminary work indicated that the impacts of the MJO on SWA are more dependent on the location of anomalous convection and subsidence and showed little sensitivity relative to the season (during autumn and winter), we feel our results are valid for both autumn and winter.

b) When the convective component of the MJO is in the eastern Indian Ocean, there is a decrease in low-level moisture and precipitation in SWA. OLR anomalies indicate that cloud-cover is reduced, as well. Temperatures are below normal throughout SWA.

c) When the subsidence component of the MJO is in the eastern Indian Ocean, there is an increase in low-level moisture, precipitation, and cloud cover. Temperatures are above normal throughout SWA.

4. NAO

a) During the autumn the impact of the NAO on SWA is weaker than it is during the winter. For both the positive and negative phases of the NAO, there are numerous small-scale variations in the moisture and precipitation anomaly fields. In general, SWA is cooler than average during autumn for the positive phase of the NAO and warmer during the negative phase.

b) During winter the impacts of the NAO are much more defined. For the positive phase, there is a decrease in low-level moisture, precipitation, and cloud cover through SWA. In addition, SWA is much cooler than average.

c) For the negative phase of the NAO during winter, the opposite is observed; there is an increase in low-level moisture, precipitation, and cloud cover. Temperatures are generally much higher than average

C. MECHANISMS BY WHICH CLIMATE VARIATIONS IMPACT SWA

In addition to investigating what impacts the climate variations had on SWA, we also sought to examine the mechanisms involved. There are two different chains of events, depending on whether the climate variation originates in the tropics or extratropics, but the end state is the same. We concluded that the primary means by which these climate variations impact SWA is through inducing anomalous circulations over SWA, thereby altering the low-level wind flow and resultant moisture and heat transports. By altering the amount of low-level moisture that is available to the low-pressure systems crossing the region, climate variations can impact long-term precipitation trends. Closer to home, an analogous situation was found for the Midwest and the Gulf of Mexico (Trenberth and Guillemot 1995).

For ENLN, IOZM, and MJO the following chain of events is proposed to summarize the impacts they have on SWA:

1. Large-scale changes in the location and intensity of tropical convection in the eastern IO, MC, and western Pacific produce a Rossby-Kelvin wave response in the upper-levels of the atmosphere.

2. In the tropics a response is also generated in the lower-levels that is opposite to that observed in the upper-level.

3. Because of SWA's location relative to the tropics, it is affected by the northwest extension of the Rossby-Kelvin wave response in the Northern Hemisphere at both the upper and lower-levels.

4. The circulation anomalies associated with the Rossby-Kelvin wave response alter moisture and heat transport into SWA.

The following proposed chain of events for the NAO is much simpler:

1. The Azores High strengthens (weakens) and extends as far as the eastern Mediterranean Sea.

2. The increase in northerly (southerly) winds leads to a decrease (increase) in onshore flow and moisture advection.

D. IMPLICATIONS FOR FORECASTING AND MILITARY OPERATIONS

The results we have presented so far lay the groundwork for further investigation into mid-range and long-range forecasting in SWA. This is an area of research ripe for exploration, especially by the DoD, for several reasons. As was highlighted in Chapter I, SWA remains a very volatile region with a long history of instability; and there does not appear to be any significant change on the horizon. In addition, many areas lack modern infrastructure, and millions of people throughout SWA lead a relatively rural lifestyle, rendering them susceptible to the vagaries of the climate. Chap III outlined several components of the DoD that could potentially benefit from improvements in mid-long range forecasting, using climate analyses and forecasts. These include operational and strategic-level planning and environmental security. Demmert et al. (2005) note, however, that both AFCCC and the Air Force Weather Agency (AFWA), "will need to improve their capabilities and methods for providing long-range weather and climate support for the environmental security mission."

E. RECOMMENDATIONS FOR FURTHER RESEARCH

Owing to time constraints, there were many potentially fruitful areas that we were unable to explore. As this is a relatively new field, especially within the DoD, there are plenty of important results yet to be developed.

What strikes us as the most promising area is the implementation of a forecast tool or product that incorporates our results and results from future work. The experimental work done so far by the SPWG points to examples of the types of products that could be created. We provided a few suggestions at the end of Chapter III, but there are certainly other potential applications. In the meantime we recommend that future work done at NPS be done hand-in-hand with AFCCC, particularly the SPWG.

We also strongly recommend that this study serve as a template for a future study on the impacts of climate variations on SWA during the other half of

the year. While we note that most of the precipitation falls during autumn and winter, there may be discernible impacts on precipitation and temperature during the spring and summer. In addition, it would be worthwhile to explore the impacts climate variations have on other quantities such as the frequency of dust storms, which would be pertinent for all seasons.

Two other important areas we were unable to explore are how the various climate variations interact with each other and what impacts the various combinations and permutations of climate variations have on SWA. For instance, what can we expect with a strong MJO moving through the Indian Ocean during an EN event. We noted when the same periods were used to explore EN and NAO, but we didn't seek out such cases. Along the same lines, it would be useful to explore the sensitivity of the response in SWA to the strength of the climate variations, alone or combined. Does SWA experience the same effects during a weak EN as it does during a strong EN?

We were also forced to make compromises in some of our methods. Future studies could address some of the areas we were unable to explore to our satisfaction. In particular we have noted the following areas:

1. Use different combinations of months for each season (e.g., use September, October, and December for autumn; or December, January, February for winter). In addition, further research could look at two or four months at a time, instead of three.

2. Use more advanced statistical methods such as principle component analysis (PCA), empirical orthogonal functions (EOF), or clustering.

3. Conduct statistical significance testing to confirm that the results we found can not be attributed to chance.

4. Use different thresholds when deciding which days/months to incorporate into the composites. For example, use an RMM magnitude of 1.0 instead of 1.5 or incorporate all the days when the RMM is > 1.5,

instead of only those days when convection or subsidence in the eastern IO persisted for seven or more days.

5. Conduct a more thorough analysis of the IOZM. Because SWA borders the Indian Ocean, any climate variation originating in the IO should impact SWA. To do this it may be necessary to use a different index than we used or lower the threshold. This is especially true for the negative phase of the IOZM.

6. Even though our preliminary analysis indicated that the impact of the MJO on SWA varies little between autumn and winter, this could be explored further. Changing thresholds or compositing methods may reveal a relationship between MJO enhanced convection (or subsidence) and its impacts on SWA that varies by season.

7. Use a compositing approach to examine in more detail the temporal evolution of the impacts of the climate variations on SWA, for example, the week by week evolution of the impacts of the MJO as it propagates across the IO and Pacific. This would help improve the foundation for intraseasonal forecasting for SWA.

The results we have presented here are undoubtedly only the tip of the iceberg, and there is a wealth of opportunity for further research. The weather community's inability to diagnose and forecast climate anomalies hurt the military during Operations DESERT STORM and ENDURING FREEDOM (D. Smarsh 2005, personal communication). We hope this study will serve as a jumping-off point for future work that will help us avoid repeating the mistakes of the past.

THIS PAGE INTENTIONALLY LEFT BLANK

LIST OF REFERENCES

Aizen, E. M., V. B. Aizen, J. M. Melack, T. Nakamura, and T. Ohta, 2001: Precipitation and atmospheric circulation patterns at mid-latitudes of Asia. *Int. J. Climatol*., **21**, 535-556.

Agrawala, S., M. Barlow, H. Cullen, and B. Lyon, 2001: The drought and humanitarian crisis in central and southwest Asia: A climate perspective. IRI Special Report No. 01-11, 20pp.[Available at http://iri.columbia.edu/outreach/publication/irireport/SWAsia/index.html.] Accessed March 2006

Air Force Combat Climatology Center, cited 2006. [Accessed online at http://www.afccc.af.mil]. Accessed March 2006.

Ambaum, M. H. P., and B. J. Hoskins, 2002: The NAO troposphere-stratosphere connection*. J. Climate*, **15**, 1969-1978.

Ashok, K., Z. Guan, and T. Yamagata, 2001: Impact of the Indian Ocean Dipole on the relationship between the Indian monsoon rainfall and ENSO. *Geophys. Res. Lett.*, **28**, 4499-4502.

Australian Bureau of Meteorology, cited 2006. [Accessed online at http://www.bom.gov.au/]. Accessed March 2006

Australian Bureau of Meteorology, cited 2006. "ENSO Wrap-up." [Accessed online at http://www.bom.gov.au/climate/enso/]. Accessed March 2006

Australian Bureau of Meteorology, cited 2006. "Monitoring of and Prediction of Modes of Coherent Tropical Variability." [Accessed online at http://www.bom.gov.au/bmrc/clfor/cfstaff/matw/maproom/OLR_modes/index.htm] Accessed March 2006

Barlow, M., and D. A. Salstein, 2005: Hydrological extremes in Central-Southwest Asia. *5th International Scientific Conf. on the Global Energy and Water Cycle*, Orange County, CA, USA, June 20-24, 2005. [Available at http://www.gewex.org/5thConfposterT2-3_Barlow.pdf]. Accessed March 2006

Barlow, M., H. Cullen, and B. Lyon, 2002: Drought in central and southwest Asia: La Niña, warm pool, and Indian Ocean precipitation. *J. Climate*, **15**, 697-700.

Barlow, M., M. Wheeler, B. Lyon, and H. Cullen, 2005: Modulation of daily precipitation over southwest Asia by the Madden-Julian Oscillation. *Mon. Wea. Rev,* **133**, 3579-3594.

Barnston, A. G., and R. E. Livezey, 1987: Classification, seasonality and persistence of low-frequency atmospheric circulation patterns. *Mon. Wea. Rev*., **115**, 1083-1126.

BBC News, cited 2006: UN warns of floods in Afghanistan. *BBC News Online,* February 24, 2005. [Accessed online at http://news.bbc.co.uk/2/hi/south_asia/4293163.stm.] Accessed March 2006

Behera, S. K., S. Krishnan, and T. Yamagata, 1999: Anomalous air-sea coupling in the southern tropical Indian Ocean during the boreal summer of 1994. *Geophys. Res. Lett*., **26**, 3001-3004.

Black, E., J. Slingo, and K. Sperber, 2003: An observational study of the relationship between excessively strong short rains in coastal east Africa and Indian Ocean SST. *Mon. Wea. Rev*., **131**, 74-94.

Bond, N. A., and G. A. Vecchi, 2003: The Influence of the Madden–Julian Oscillation on precipitation in Oregon and Washington. *Wea. Forecasting*, **18**, 600–613.

Cane, M. A., and S. E. Zebiak, 1985: A theory for El Nino and the Southern Oscillation. *Science*, **228**, 1085-1087.

Cane, M. A., S. E. Zebiak, and S. C. Dolan, 1986: Experimental forecasts of El Nino. *Nature*, **321**, 827-832.

Carlson, T. N., 1991: *Mid-latitude weather systems*. Routledge, 507pp.

Climate Diagnostics Center(CDC), cited 2006. [Accessed online at http://www.cdc.noaa.gov/index.html]. Accessed March 2006

Climate Diagnostics Center, cited 2006. "CDC Map Room." [Accessed online at http://www.cdc.noaa.gov/map/]. Accessed March 2006

Climate Diagnostics Center, cited 2006. "El Nino/Southern Oscillation." [Accessed online at http://www.cdc.noaa.gov/ENSO/]. Accessed March 2006

Climate Diagnostics Center, cited 2006. "MJO Experimental Prediction Project." [Accessed online at http://www.cdc.noaa.gov/MJO/Predictions/]. Accessed March 2006.

Climate Prediction Center (CPC), cited 2006. [Accessed online at http://www.cpc.ncep.noaa.gov]. Accessed March 2006

Climate Prediction Center (CPC), cited 2006. Monthly Mean NAO Index since 1950. [Accessed online at http://www.cpc.ncep.noaa.gov/products/precip/CWlink/pna/norm.nao.monthly.b5001.current.ascii.table.] Accessed March 2006

Cullen, H. M. and P. B. deMenocal, 2000: North Atlantic influence on Tigris-Euphrates streamflow. *Int. J. Climatol*., **20**, 853-863.

Cullen, H. M., A. Kaplan, and P. B. deMenocal, 2002: Impact of the North Atlantic Oscillation on Middle Eastern climate and streamflow. *Clim. Change*., **55**, 315-338.

Demmert, P., R. Whiton, K. Klein, and F. Zawada, 2005: Value of weather services to the combatant commands, Vol I—Main report and appendices A & B. Air Force Weather Agency Technical Note AFWA TN-05/001, 161pp.

Evans, J. P., R. B. Smith, and R. J. Oglesby, 2004: Middle East climate simulation and dominant precipitation processes. *Int. J. Climatol*., **24**, 1671-1694.

Feldmeier, J. W., 2005: Climatic variations of the California Current System: Application of smart climatology to the coastal ocean, M. S. thesis, Dept of Oceanography, Naval Postgraduate School, 168pp.

Ford, B. W., 2000: El Nino and La Nina Effects on Tropical Cyclones: The mechanisms. M. S. thesis, Dept of Meteorology, Naval Postgraduate School, 190pp.

Ghasemi, A.R., 2003: Meteorological drought in Iran and its association with the El Nino-Southern Oscillation and the Caspian Sea surface temperature. M. S. thesis, Dept. of Arid Region Management, University of Shiraz, 120pp.

Gill, A. E., 1980: Some simple solutions for heat induced tropical circulation. *Quart. J. Roy. Meteor. Soc*., **106**, 447-462.

Halpert, M. S., and C. F. Ropelewski, 1992: Surface temperature patterns associated with the Southern Oscillation. *J. Climate*, **5**, 577-593.

Hendon, H. H., and B. Liebmann, 1990: The Intraseasonal (30–50 day) Oscillation of the Australian summer monsoon. *J. Atmos. Sci.,* **47**, 2909–2924.

Hendon, H. H., and M. L. Salby, 1994: The life cycle of the Madden-Julian Oscillation. *J. Atmos. Sci*., **51**, 2225-2237.

Higdon, M., 2004: Iran—A full-year study. AFCCC/CCD-04/018, Air Force Combat Climatology Center, 48pp.

Hildebrand, P. E., 2001: El Nino and La Nina Events and North Atlantic tropical cyclones. M. S. thesis, Dept of Meteorology, Naval Postgraduate School, 98pp.

Hoerling, M. and A. Kumar, 2003: The perfect ocean for drought. *Science*, **299**, 691-694.

Hoerling, M. P., J. S. Whitaker, A. Kumar, and W. Wang, 2001: The midlatitude warming during 1998-2000. *Geo. Res. Letters*, **28**, 755-758.

Homer-Dixon, T., 1999: *Environment, Scarcity, and Violence*. Princeton University Press, 253pp.

Horel, J. D., and J. M. Wallace, 1981: Planetary-scale atmospheric phenomena associated with the Southern Oscillation. *Mon. Wea. Rev*., **109**, 813-829.

Hoskins, B. J., and D. J. Karoly. 1981: The Steady Linear Response of a Spherical Atmosphere to Thermal and Orographic Forcing. *J. Atmos. Sci,* **38**, 1179–1196.

Hurrell, J. W., 1995: Decadal trends in the North Atlantic Oscillation: regional temperatures and precipitation. *Science*, **269**, 676-679.

Hurrell, J. W., 1996: Influence of variations in extratropical wintertime teleconnections on Northern Hemisphere temperature. *Geophys. Res. Lett*., **23**, 665-668.

Hurrell, J. W., and H. van Loon, 1997: Decadal variations in climate associated with the North Atlantic Oscillation. *Climatic Change*, **36**, 301-326.

Hurrell, J. W., M. P. Hoerling, and C. K. Folland, 2001: Climatic variability over the North Atlantic. *Meteorology at the Millenium*. R. Pearce, Ed., Academic Press, 143-151.

Hurrell, J. W., Y. Kushnir, G. Ottersen, and M. Visbeck, 2003: An overview of the North Atlantic Oscillation. *The North Atlantic Oscillation: Climatic Significance and Environmental Impact. Geophys. Monogr.*, No. 134, Amer. Geophys. Union, 1-34.

Indian Ocean Dipole Homepage, cited 2006. [Accessed online at http://www.jamstec.go.jp/frsgc/research/d1/iod/IOD1.html] Accessed March 2006.

International Research Institute for Climate and Society (IRI), cited 2006. [Accessed online at http://iri.columbia.edu/]. Accessed March 2006

International Research Institute for Climate and Society, cited 2006. "Climate Outlook for Southwestern Asia." [Accessed online at http://iri.columbia.edu/climate/forecast/cswasia/index.html]. Accessed March 2006

International Research Institute for Climate and Society, cited 2006. "IRI Forecast Products." [Accessed online at http://iri.columbia.edu/pred/productlist.html]. Accessed March 2006

International Research Institute for Climate and Society, cited 2006. "IRI Map Room." [Accessed online at http://iridl.ldeo.columbia.edu/maproom/.ENSO/]. Accessed March 2006

International Research Institute for Climate and Society, cited 2006."IRI Map Room—Regional Monitoring." [Accessed online at http://iridl.ldeo.columbia.edu/maproom/.Regional/]. Accessed March 2006

International Research Institute for Climate and Society, cited 2006. "IRI Net Assessment Forecasts." [Accessed online at http://iri.columbia.edu/climate/forecast/net_asmt/]. Accessed March 2006

Joint Staff, 1999. *Joint Publication 3-59: Joint Doctrine Tactics, Techniques, and Procedures for Meteorological and Oceanographic Support.* U.S. Joint Chiefs of Staff, 23 Mar 99.

Jones, C., 2000: Occurrence of extreme precipitation events in California and relationships with the Madden-Julian Oscillation. *J. Climate*, **13**, 3576-3587.

Jones, C., D. E. Waliser, K. M. Lau, W. Stern, 2004: Global occurrences of extreme precipitation and the Madden-Julian Oscillation: Observations and predictability. *J. Climate*, 17, 4575-4589.

Kalnay, E., and Coauthors, 1996: The NCEP/NCAR 40-year reanalysis project. *Bull. Amer. Meteor. Soc*. **77**, 437-471.

Kiladis, G. N. and H. F. Diaz, 1989: Global climatic anomalies associated with extremes in the Southern Oscillation. *J. Climate*, **2**, 1069-1090.

King, W. C., 2000: Understanding international environmental security: A strategic military perspective. AEPI-IFP-1100A, 122pp. [Available from U. S. Army Environmental Policy Institute, 101 Marietta St., Suite 3120, Atlanta, GA 30303.]

Kistler, R., and Coauthors, 2001: The NCEP/NCAR 50-year reanalysis: monthly means CD-ROM and documentation. *Bull. Amer. Meteor. Soc*. **82**, 247-267.

Krishnamurti, T., 1961: The subtropical jet stream of winter. *J. Meteor*., **18**, 172-191.

Kushnir, Y., W. A. Robinson, I. Blade, N. M. J. Hall, S. Peng, and R. T. Sutton, 2002: Atmospheric GCM response to extratropical SST anomalies: Synthesis and evaluation. *J. Climate*, **15**, 2233-2256.

LaJoie, M., 2006: The impact of climate variations on military operations in the Horn of Africa. M. S. Thesis, Dept. of Meteorology, Naval Postgraduate School, 135pp.

Lamb, P. J. and R. A. Peppler, 1987: North Atlantic Oscillation: Concept and an Application. *Bull. Amer. Meteor. Soc.*, **68**, 1218-1225.

Lanicci, J., 2003: Weather operations in the transformation era. Air War College, Maxwell Paper No. 29, 30pp.

Latif, M., and Coauthors, 1998: A review of the predictability and prediction of ENSO. *J. Geophys. Res*., **103**, 14 375-14 393.

Madden, R. A., and P. R. Julian, 1971: Description of a 40-50 day oscillation in the zonal wind in the tropical Pacific. *J. Atmos. Sci*., **28**, 702-708.

Madden, R. A., and P. R. Julian, 1994: Observations of the 40-50-day tropical oscillation—a review. *Mon. Wea. Rev*., **122**, 814-837.

Mariotti, A., N. Zeng, and K.-M. Lau, 2002: Euro-Mediterranean rainfall and ENSO—a seasonally varying relationship. *Geophys. Res. Lett*., **29**, 59-1-4.

Mariotti, A., J. Ballabrera-Poy, and N. Zeng, 2005: Tropical influence on Euro-Asian autumn rainfall variability. *Climate Dyn*., **24**, 511-521.

Mason, S. J., and L. Goddard, 2001: Probabilistic precipitation anomalies associated with ENSO. *Bull. Amer. Meteor. Soc*., **82**, 619-638.

Matsuno, T., 1966: Quasi-geostrophic motions in the equatorial area. *J. Meteor. Soc*. *Japan*, **44**, 25-42.

Murphree, T., 2005a: *MR3610 Course Module 22: Smart Climatology: Concepts and Products.* Department of Meteorology, Naval Postgraduate School, Monterey, California, 46 pp.

Murphree, T., 2005b: *MR3610 Course Module 5: Introduction to Climate Science.* Department of Meteorology, Naval Postgraduate School, Monterey, California, 45 pp.

Murphree, T., 2005c: *MR3610 Course Module 18: Madden-Julian Oscillations, Part 1*. Department of Meteorology, Naval Postgraduate School, Monterey, California, 23pp.

Nazemosadat, M. J., 1998: Persian Gulf sea surface temperature as a drought diagnostic for southern Iran. *Drought Network News*, Vol. 10, No. 3, International Drought Information Center and the National Drought Mitigation Center, 10-12.

Nazemosadat, M. J. and I. Cordery, 2000: On the relationship between ENSO and autumn rainfall in Iran. *Int. J. Climatol.*, **20**, 47-61.

Nazemosadat, M. J. and A. R. Ghasemi, 2004: Quantifying the ENSO-related shifts in the intensity and probability of drought and wet periods in Iran*, J. Climate*, **17**, 4005-4018.

Neelin, J. D., D. S. Battisti, A. C. Hirst, F. F. Jin, Y. Wakata, T. Yamagata, and S. E. Zebiak, 1998: ENSO theory. *J. Geophys. Res*., **103**, 14 261-14 290.

Nitta, T., 1987: Convective activities in the tropical western Pacific and their impact on the Northern Hemisphere summer circulation, *J. Meteor. Soc. Japan*, **65**, 373-390.

North, A., cited 2006: Snow paralyzes Afghan villages, *BBC News Online*, February 22, 2005. [Accessed online at http://news.bbc.co.uk/2/hi/south_asia/4286233.stm.] Accessed March 2006

Pagano, T.C., S. Mahani, M. J. Nazemosadat, and S. Sorooshian, 2003: Review of Middle Eastern hydroclimatology and seasonal teleconnections. *Iran. J. Sci. Tech.*, **27**, 95-109.

Perlwitz, J., and H.-F. Graf, 1995: The statistical connection between tropospheric and stratospheric circulation of the Northern Hemisphere in winter. *J. Climate*, **8**, 2281-2295.

Philander, G. S., 1990: *El Nino, La Nina, and the Southern Oscillation*. Academic Press, 293pp.

Rasmusson, E. M., and T. H. Carpenter, 1982: Variations in tropical sea surface temperature and surface wind fields associated with the Southern Oscillation/El Nino. *Mon. Wea. Rev*., **110**, 354-384.

Rodwell, M., 2003: On the predictability of North Atlantic climate. *The North Atlantic Oscillation: Climatic Significance and Environmental Impact. Geophys. Monogr.*, No. 134, Amer. Geophys. Union, 173-192.

Rodwell, M., and B. J. Hoskins, 1996: Monsoons and the dynamics of deserts. *Q. J. R. Meteorological Soc.*, **122**, 1385-1404.

Rogers, J. C., 1984: The Association between the North Atlantic Oscillation and the Southern Oscillation in the Northern Hemisphere. *Mon. Wea. Rev*., **112**, 1999-2015.

Rogers, J. C., 1990: Patterns of low-frequency monthly sea level pressure variability (1899-1986) and associated wave cyclone frequency. *J. Climate*, **3**, 1364-1379.

Rogers, J. C., 1997: North Atlantic storm track variability and its association to the North Atlantic Oscillation and climate variability of northern Europe. *J. Climate*, **10**, 1635-1645.

Ropelewski, C. F. and M. S. Halpert, 1987: Global and regional scale precipitation patterns associated with the El Nino/Southern Oscillation. *Mon. Wea. Rev*., **115**, 1606-1626.

Ropelewski, C. F. and M. S. Halpert, 1989: Precipitation patterns associated with the high index phase of the Southern Oscillation. *J. Climate*, **2**, 268-284.

Ropelewski, C. F. and M. S. Halpert, 1996: Quantifying Southern Oscillation-precipitation realationships. *J. Climate*, **9**, 1043-1059.

Saji, N. H. and T. Yamagata, 2003: Possible impacts of the Indian Ocean Dipole mode events on global climate. *Clim. Res*., **25**, 151-169.

Saji, N. H., B. N. Goswami, P. N. Vinayachandran, and T. Yamagata, 1999: A dipole mode in the tropical Indian Ocean. *Nature*, **401**, 360-363.

Sardeshmukh, P. D., and B. J. Hoskins, 1988: The generation of global rotational flow by steady idealized tropical divergence. *J. Atmos. Sci*., **45**, 1228-1251.

Serreze, M. C., F. Carse, R. G. Barry, and J. C. Rogers, 1997: Icelandic low activity: climatological features, linkages with the NAO, and relationships with recent changes in the Northern Hemisphere circulation. *J. Climate*, **10**, 453-464.

Smith, H. A., 2001: Facing Environmental Security. *Journal of Military and Stategic Studies*., Winter 2000/Spring 2001. [Available online at http://www.jmss.org/2001/article3.html.] Accessed March 2006

Stepanek, A., 2006: North Pacific-North American circulation and precipitation anomalies associated with the Madden-Julian Oscillation. M. S. Thesis, Dept. of Meteorology, Naval Postgraduate School, 143pp.

Stockdale, T. N., D. L. T. Anderson, J. O. S. Alves, and M. A. Balmaseda, 1998a: Global seasonal rainfall forecasts using a coulpled ocean-atmosphere model. *Nature*, **392**, 370-373.

Stockdale, T. N., A. J. Busalacchi, D. E. Harrison, and R. Seager, 1998b: Ocean modeling for ENSO. *J. Geophys. Res*., **103**, 14 325-14 355.

Synovitz, R., cited 2006: Afghanistan: Death toll from floods appears lower than feared. *Radio Free Europe Radio Liberty*, March 22, 2005. [Accessed online at http://www.rferl.org/featuresarticle/2005/03/48adae1e-904a-4395-af42-2fef213c7b94.html.] Accessed March 2006

Thompson, D. W. J., and J. M. Wallace, 1998: The Arctic Oscillation signature in the wintertime geopotential height and temperature fields. *Geophys. Res. Lett*., **25**, 1297-1300.

Thompson, D. W. J., and J. M. Wallace, 2000: Annular modes in the extratropical circulation, Part I: Month-to-month variability. *J. Climate*, **13**, 1000-1016.

Thompson, D. W. J., S. Lee, and M. P. Baldwin, 2003: Atmospheric processes governing the Northern Hemisphere Annular Mode/North Atlantic Oscillation. *The North Atlantic Oscillation: Climatic Significance and Environmental Impact. Geophys. Monogr.*, No. 134, Amer. Geophys. Union, 81-112.

Ting, M. T., and P. D. Sardeshmukh, 1993: Factors determining the extratropical response to equatorial diabatic heating anomalies. *J. Atmos. Sci*., **50**, 907-918.

Tippett, M. K., M. Barlow, and B. Lyon, 2003: Statistical Correction of Central Southwest Asia Winter Precipitation Simulations. *Int. J. Climatol*., **23**, 1421-1433.

Trenberth, K. E., and C. J. Guillemot, 1995: Physical processes involved in the 1988 drought and 1993 floods in North America. *J. Climate*, **9**, 1288-1298.

Trigo, R. M., T. J. Osborn, J. M. Corte-Real, 2002: The North Atlantic Oscillation influence on Europe: climate impacts and associated physical mechanisms. *Clim. Res.*, **20**, 9-17.

Vojtesak, M. J., K. P. Martin, G. Myles, and M. T. Gilford, 1991: SWANEA (Southwest Asia-Northeast Africa)—A climatological study, Vol II—The Middle East peninsula. USAFETAC TN-91/002, USAF Environmental Technical Applications Center, 246pp.

Vranes, K., cited 2006. The Indian Ocean Dipole Index. [Accessed online at http://www.ldeo.columbia.edu/~kvranes/research/DMI/.] Accessed March 2006

Waliser, D. E., K. M. Lau, W. Stern, and C. Jones, 2003: Potential predictability of the Madden-Julian Oscillation. *Bull. Amer. Meteor. Soc*., **84**, 33-50.

Wallace, J. M., 2000: North Atlantic Oscillation / Annular Mode: Two paradigms – one phenomenon. *Quart. J. Roy. Meteor. Soc*., **126**, 791-805.

Wallace, J. M. and D. S. Gutzler, 1981: Teleconnections in the geopotential height field during the Northern Hemisphere winter. *Mon. Wea. Rev*., **109**, 784-812.

Walters, K. R., and W. F. Sjoberg, 1988: The Persian Gulf region—A climatological study. USAFETAC TN-88/002, USAF Environmental Technical Applications Center, 62pp.

Walters, K. R., M. J. Vojtesak, K. P. Martin, G. Myles, M. T. Gilford, and K. M. Traxler, 1991: SWANEA (Southwest Asia-Northeast Africa)—A climatological study, Vol III—The Near East mountains. USAFETAC TN-91/003, USAF Environmental Technical Applications Center, 266pp.

Webster, P. J., A. M. Moore, J. P. Loschnigg, and R. R. Leben, 1999: Coupled ocean-atmosphere dynamics in the Indian Ocean during 1997-98. *Nature*, **401**, 356-360.

Weickmann, K. M., G. R. Lussky, and J. E. Kutzbach, 1985: Intraseasonal (30-60 day) fluctuations of outgoing longwave radiation and 250-mb streamfunction during northern winter. *Mon. Wea. Rev*., **113**, 941-961.

Wheeler, M. C., and H. H. Hendon, 2004: An all-season real-time multivariate MJO index: Development of an index for monitoring and prediction. *Mon. Wea. Rev.*, **132**, 1917-1932.

Wilks, D. S., 2006: *Statistical Methods in the Atmospheric Sciences*, Second Edition. Academic Press, 627pp.

Wolter, K., and M. S. Timlin, 1993: Monitoring ENSO in COADS with a seasonally adjusted principal component index. *Proc. of the 17th Climate*

Diagnostics Workshop, Norman, OK, NOAA/N MC/CAC, NSSL, Oklahoma Clim. Survey, CIMMS and the School of Meteor., Univ. of Oklahoma, 52-57.

Yang, S., K.-M. Lau, and K.-M. Kim, 2002: Variations of the East Asian Jet Stream and Asian-Pacific-American Winter Climate Anomalies. *J. Climate*, **15**, 306-325.

THIS PAGE INTENTIONALLY LEFT BLANK

BIBLIOGRAPHY

Abdullah, M. A. and M. A. Al-Mazroui, 1998: Climatological study of the southwestern region of Saudi Arabia. I. Rainfall analysis. *Clim. Res.*, **9**, 213-223.

Alijani, B., 2002: Variations in 500 hPa flow patterns over Iran and surrounding areas and their relationship with the climate of Iran. *Theor. Appl. Climatol.*, **72**, 41-54.

Alijani, B., and J. R. Harman, 1985: Synoptic climatology of precipitation in Iran. *Ann. Assoc. Amer. Geogr*. , **75**, 404-416.

Bitan, A., and H. Sa'aroni, 1992: The Horizontal and vertical extension of the Persian Gulf pressure trough. *Int. J. Climatol*., **12**, 733-747.

Chang, C.-P., and K. M. Lau, 1982: Short-term planetary-scale interactions over the tropics and midlatitudes during northern winter. Part I: Contrasts between active and inactive periods. *Mon. Wea. Rev*., **110**, 933-946.

Dayan, U. and R. Abramski, 1983: Heavy rain in the Middle East related to unusual jet stream properties. *Bull. Amer. Met. Soc.,* **64**, 1138-1140.

Desai, B. N. 1967: The summer atmospheric circulation over the Arabian Sea. *J. Atmos. Sci.*, **24**, 216-220.

Goddard, L. S. J. Mason, S. E. Zebiak, C. F. Ropelewski, R. Basher, and M. A. Cane, 2001: Current approaches to seasonal-to-interannual climate predictions. *Int. J. Climatol.*, **21**, 1111-1152.

Halpern, D., and P. M. Woiceshyn, 2001: Somali jet in the Arabian Sea, El Nino, and India rainfall. *J. Climate*, **14**, 434-441.

Hamilton. K., 1988: A detailed examination of the extratropical response to tropical El Nino/Southern Oscillation events. *J. Climatol*., **8**, 67-86.

Hoerling, M. P., J. W. Hurrell, and T. Xu, 2001: Tropical origins for recent North Atlantic climate change. *Science*, **292**, 90-92.

Karamouz, F. M., S. Torabi, and S. Araghinejad, 2004: Analysis of hydrologic and agricultural droughts in central part of Iran. *J. Hydrol. Eng*., **9**, 402-414.

Liu, M., D. L. Westphal, T.R. Holt, and Q. Xu, 2000: Numerical simulation of a low-level jet over complex terrain in southern Iran. *Mon. Wea. Rev*. **128**, 1309-1327.

Marshall, J., Y. Kushnir, D. Battisti, P. Chang, A. Czaja, R. Dickson, J. Hurrell, M. McCartney, R. Saravanan, and M. Visbeck, 2001: North Atlantic climate variability: phenomena, impacts, and mechanisms. *Int. J. Climatol*., **21**, 1863-1898.

Meehl, G.A., and H. van Loon, 1979: The seesaw in winter temperatures between Greenland and northern Europe. Part III: Teleconnections with lower latitudes. *Mon. Wea. Rev*., **107**, 1095-1106.

Nazemosadat, M. J., 1996: The impact of oceanic and atmospheric indices on rainfall variability. Ph.D. thesis, University of New South Wales, 265pp.

Nazemosadat, M. J., 2000: The impact of ENSO on winter rainfall in Iran. *Proc 26th National and 3rd Int. Hydrology and Water Resources Symp.*, Perth, Australia, Institute of Engineers, 538-543.

Nazemosadat, M. J., 2001: Winter rainfall in Iran: ENSO and aloft wind interactions. *Iranian J. Sci. Technol.*, **25**, 611-624

Nazemosadat, M. J. and A. R. Ghasemi, 2002: The influence of the Caspian Sea SST on the winter and spring rainfalls over northern parts of Iran. *Proc. Int. Conf. on Hydrology and Watershed Management*, Hyderbad, India, Jawaharlal Nehru Technological University, 297-304.

Trenberth, K. E., G. W. Branstator, D. Karoly, and A. Kumar, 1998: Progress during TOGA in understanding and modeling global teleconnections associated with tropical sea surface temperatures. *J. Geophys. Res*., **103**, 14 291-14 324.

Van Loon, H. and R. A. Madden, 1981: The Southern Oscillation. Part I: Global associations with pressure and temperature in northern winter. *Mon. Wea. Rev*., **109**, 1150-1162.

Yang, S., K.-M. Lau, S.-H. Yoo, J.L. Kinter, K. Miyakoda and C.-H. Ho, 2004: Upstream subtropical signals preceding the Asian summer monsoon circulation. *J. Climate*, **17**, 4213-4229.

APPENDIX: FIGURES

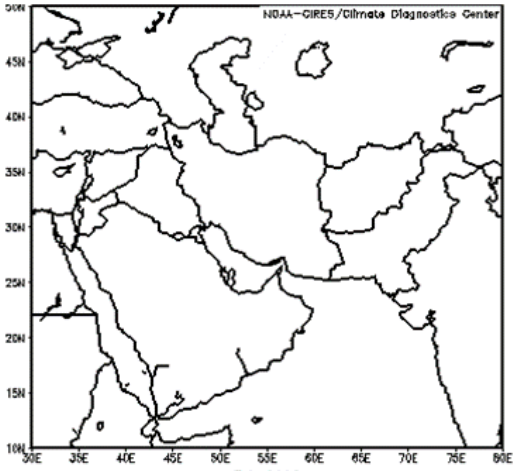

Fig 1. Southwest Asia region that was the focus of our study

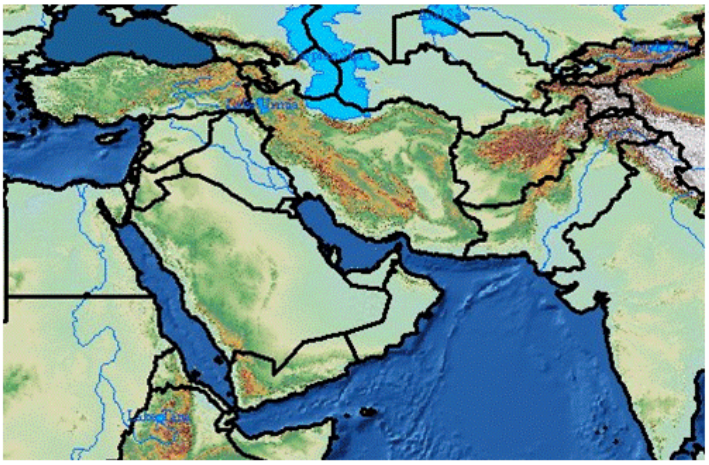

Fig 2. Topography of SWA. Note the complex topography that dominates Iran, Afghanistan, and Pakistan. Figure created at http://www.afccc.af.mil (Accessed 21 March 2006)

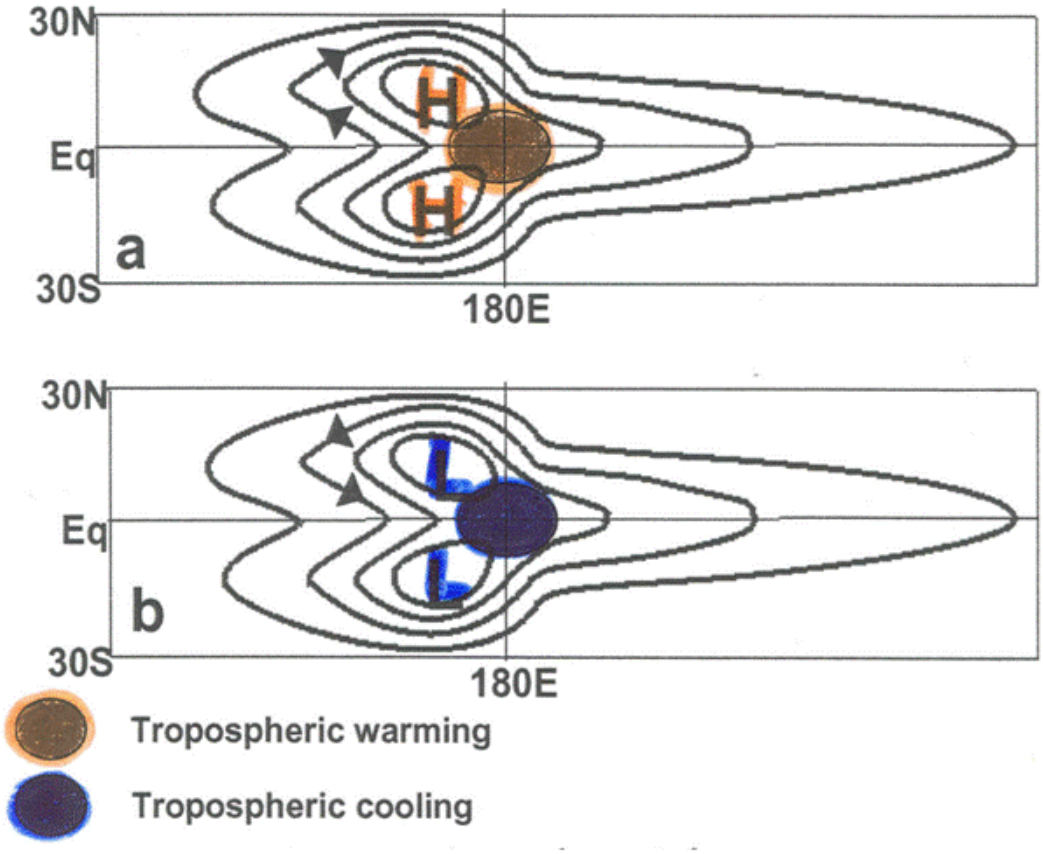

Figure 3: Solution for anomalous warming and cooling about the Equator. (a) and (b) are contours of *perturbation* pressure. There is a ridge in (a) and a trough in (b) at the Equator to the east of the forcing region. On the other hand, the pressure to the west of the forcing region is different relative to its value off the Equator. Two circulations are found on the northwest and southwest flanks of the forcing region. From Ford (2000).

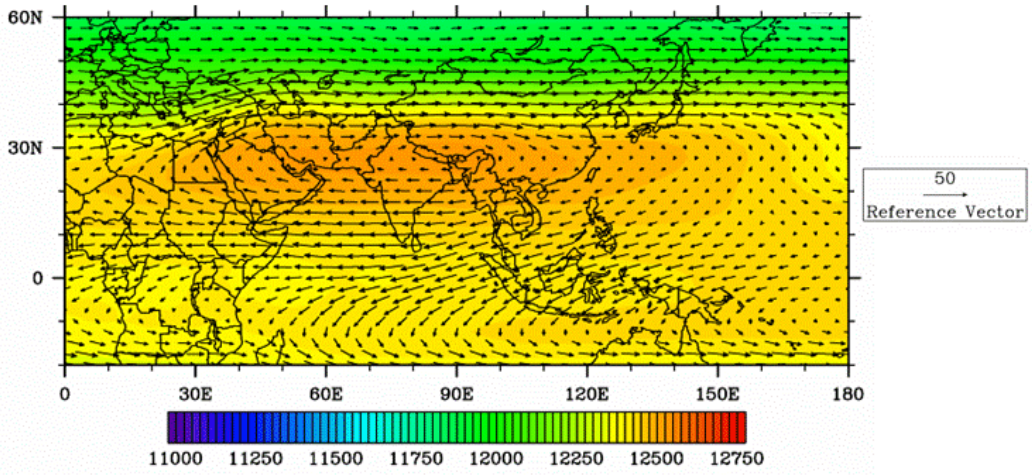

Fig. 4. Long term mean 200-hPa GPH (color shading, m) and vector winds (m s^{-1}) for July-September. Note the Rossby-Kelvin wave pattern in the GPH pattern over the eastern IO, Maritime Continent, and western Pacific.

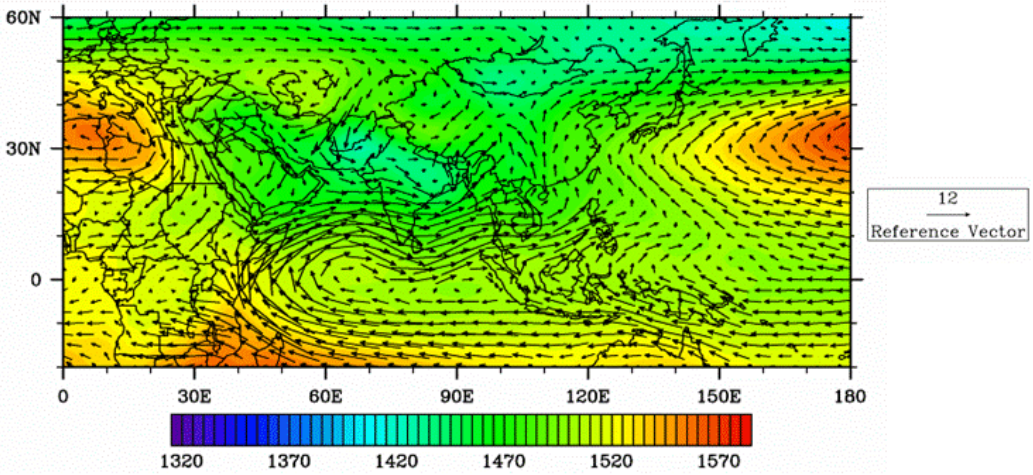

Fig. 5. Long term mean 850-hPa GPH (color shading, m) and vector winds (m s^{-1}) for July-September. Note the strong southwesterly winds over the Arabian Sea and northwestern Indian Ocean in response to the low level troughing over Asia.

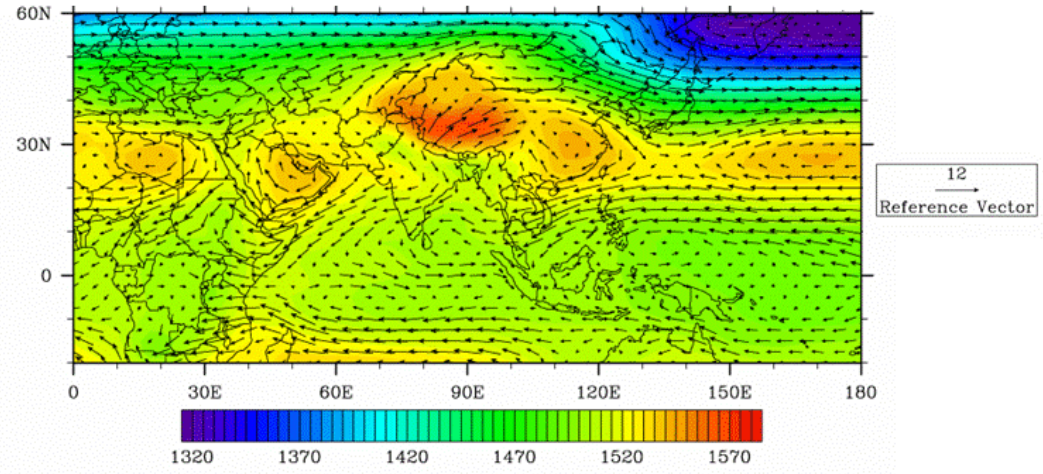

Fig. 6. Long term mean 850-hPa GPH (color shading, m) and vector winds (m s^{-1}) for October-December. Note the winds in the Arabian Sea and northwestern IO are now northeasterly during autumn, as opposed to onshore during the summer.

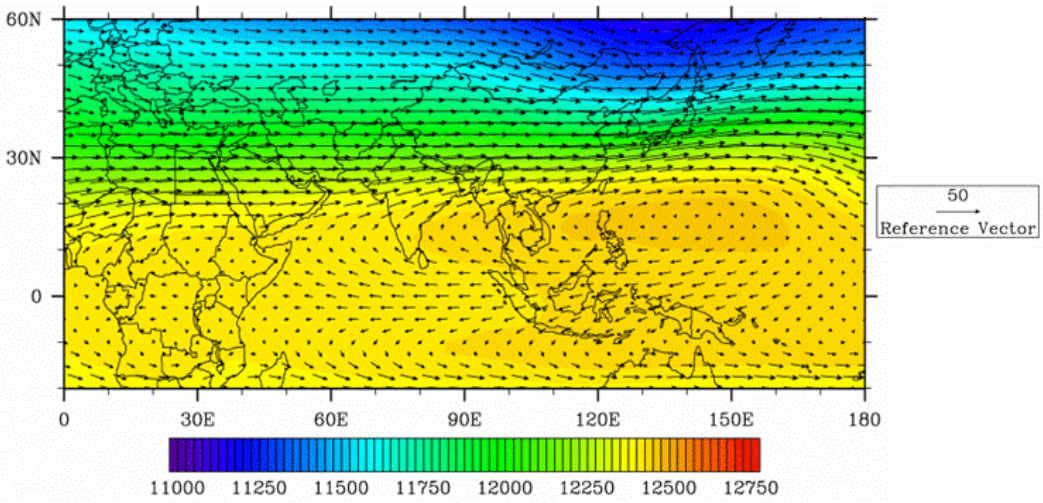

Fig. 7. Long term mean 200-hPa GPH (color shading, m) and vector winds (m s^{-1}) for October-December. Note the Rossby-Kelvin wave response In the upper level GPH-wind field over the Maritime Continent and western Pacific.

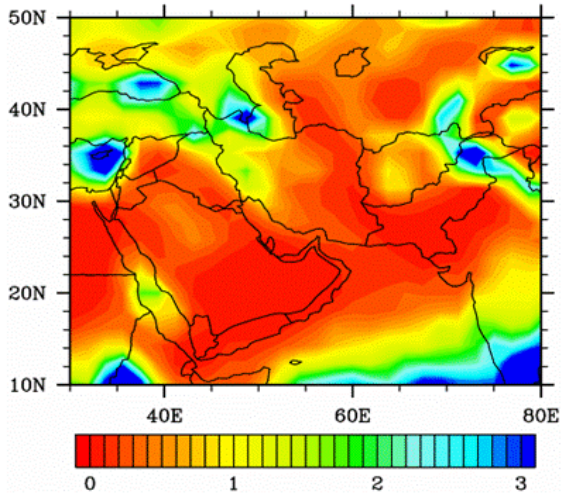

Fig. 8. Long term mean precipitation rate (mm day^{-1}) for October-December. Note the higher precipitation rates found in the areas of higher terrain.

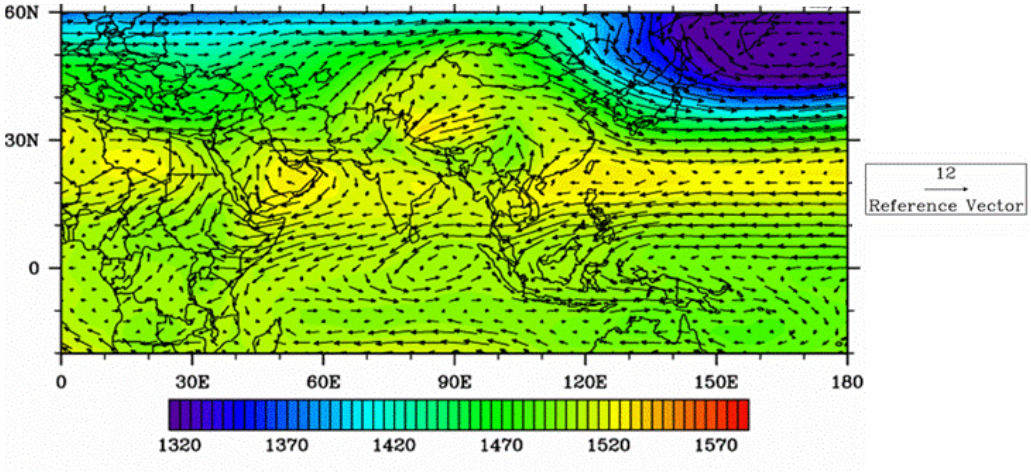

Fig. 9. Long term mean 850-hPa GPH (color shading, m) and vector winds (m s^{-1}) for January-March. The northeasterly winds in the Arabian Sea are strongest during the winter.

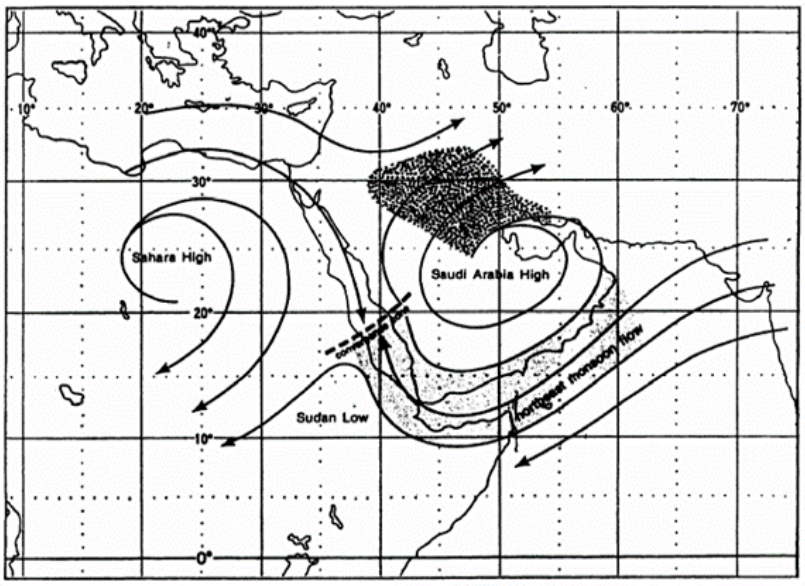

Fig. 10. Schematic showing the long term mean surface streamline pattern associated with the Saudi Arabian High. The shaded region (over the Arabian Sea and the Horn of Africa) denotes outflow support to the northeast monsoon circulation. The stippled area (to the north of the center of the high) represents the westerly outflow component that supports the extratropical low pressure systems that move through. From Walters and Sjoberg (1988).

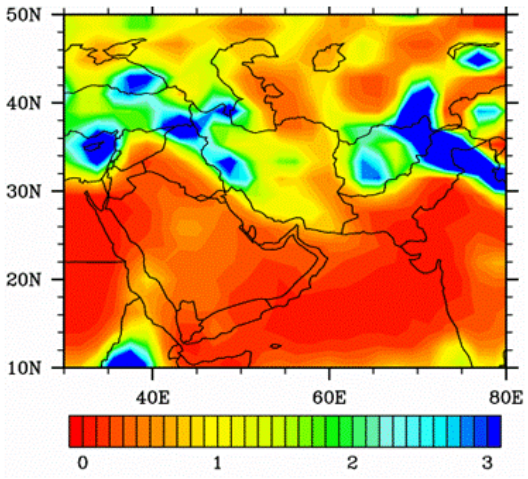

Fig. 11. Long term mean precipitation rate (mm day^{-1}) For January-March. Precipitation rates are highest during the winter in most areas, especially in higher terrain regions.

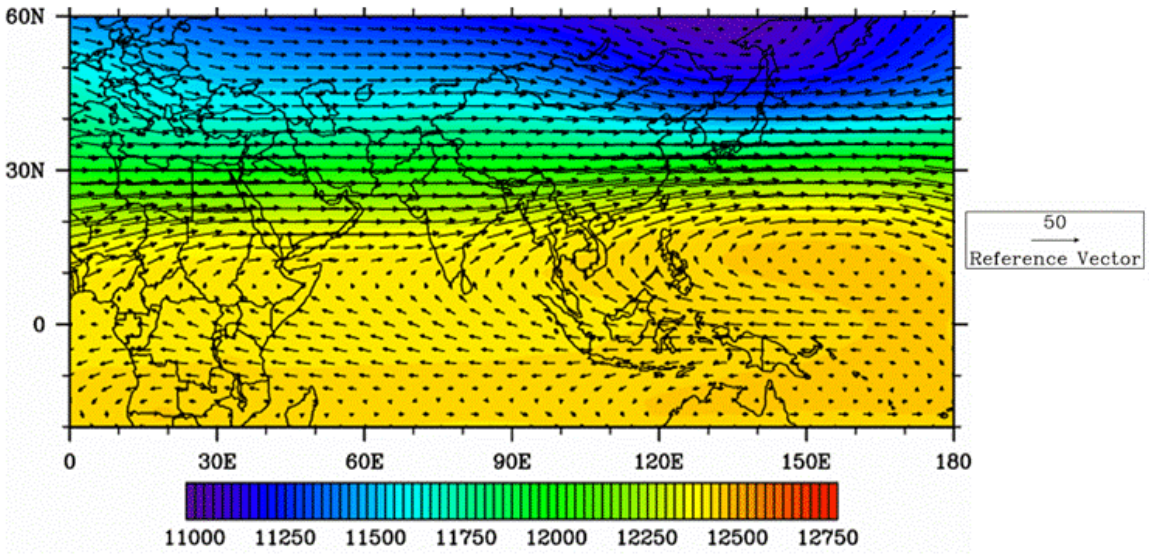

Fig. 12. Long term mean 200-hPa GPH (color shading, m) and vector winds (m s^{-1}) for January-March. Note the axis of the Subtropical Jet is further to the east than in autumn. The Rossby-Kelvin wave response over the Maritime Continent and western Pacific is also further to the east than in autumn.

a.

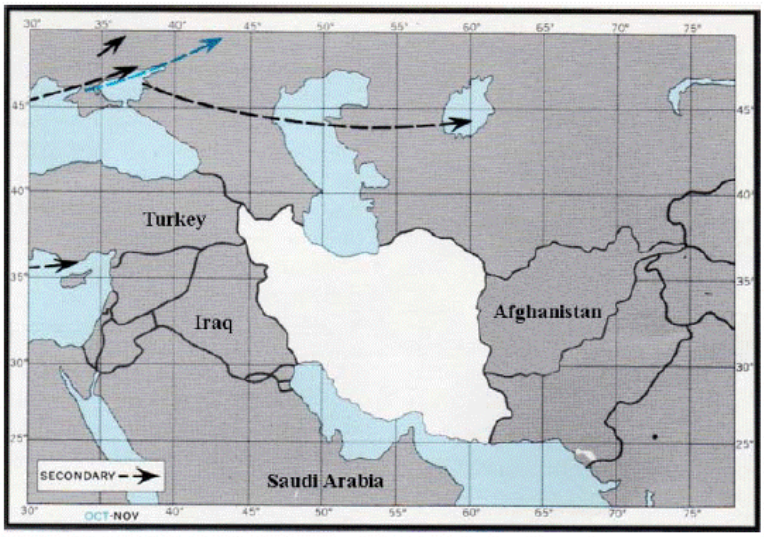

b.

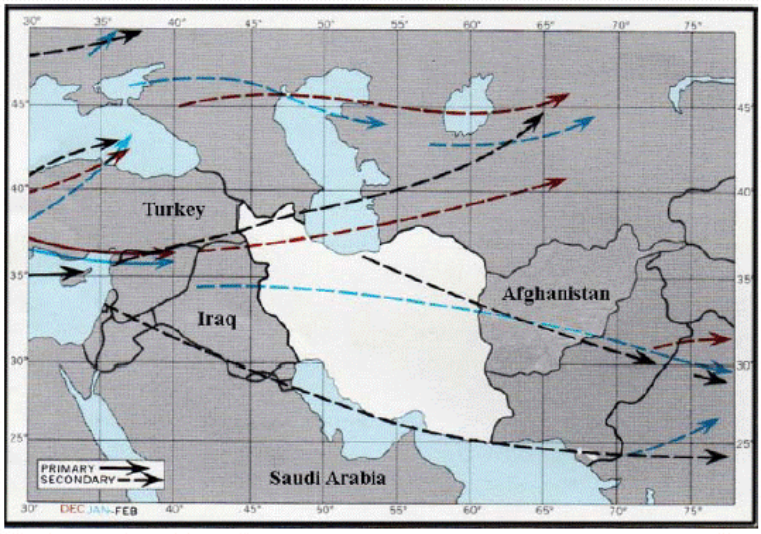

Fig 13. Schematics showing common storm tracks over SWA for (a) October (blue) and November (black), and (b) December (red), January (blue), and February (black). Primary storm tracks are shown in solid arrows, while secondary storm tracks are shown in dashed arrows. From Higdon (2004).

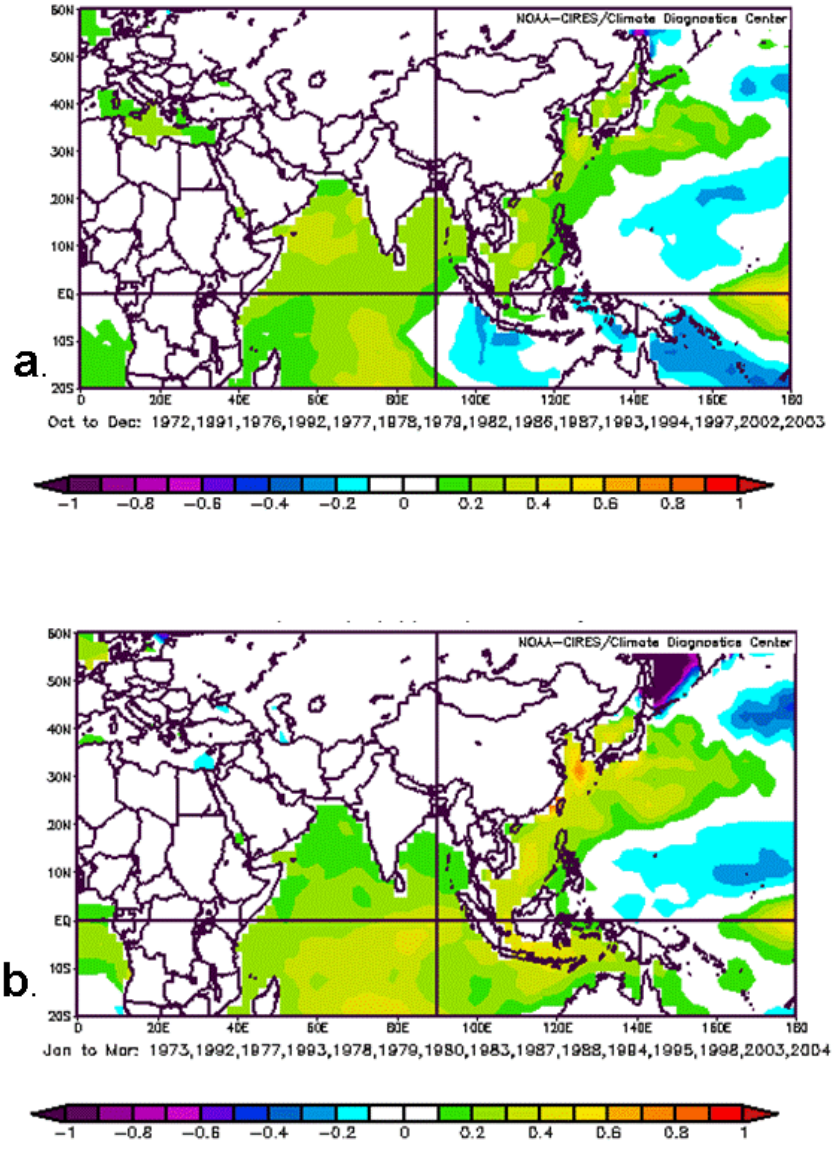

Fig. 14. Composite anomalies of SST (C) for (a) October-December and (b) January-March during El Nino periods. Note the change in sign of the SST anomaly off the coast of western Indonesia from autumn to winter. The composited EN periods are listed just below each figure. Figures created at http://www.cdc.noaa.gov/cgi-bin/Composites/printpage.pl (Accessed 21 March 2006).

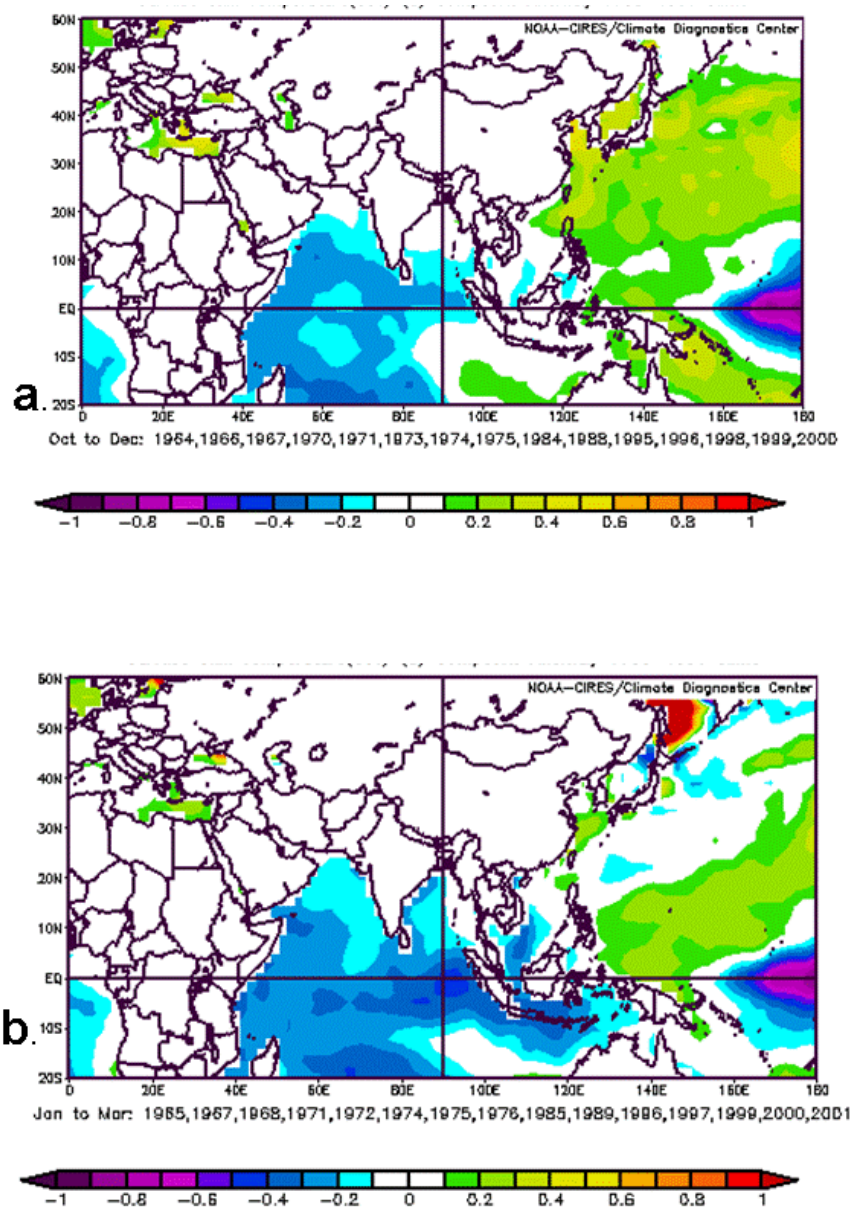

Fig. 15. Composite anomalies of SST (C) for (a) October-December and (b) January-March during La Nina periods. The composited EN periods are listed just below each figure. Figures created at http://www.cdc.noaa.gov/cgi-bin/Composites/printpage.pl (Accessed 21 March 2006).

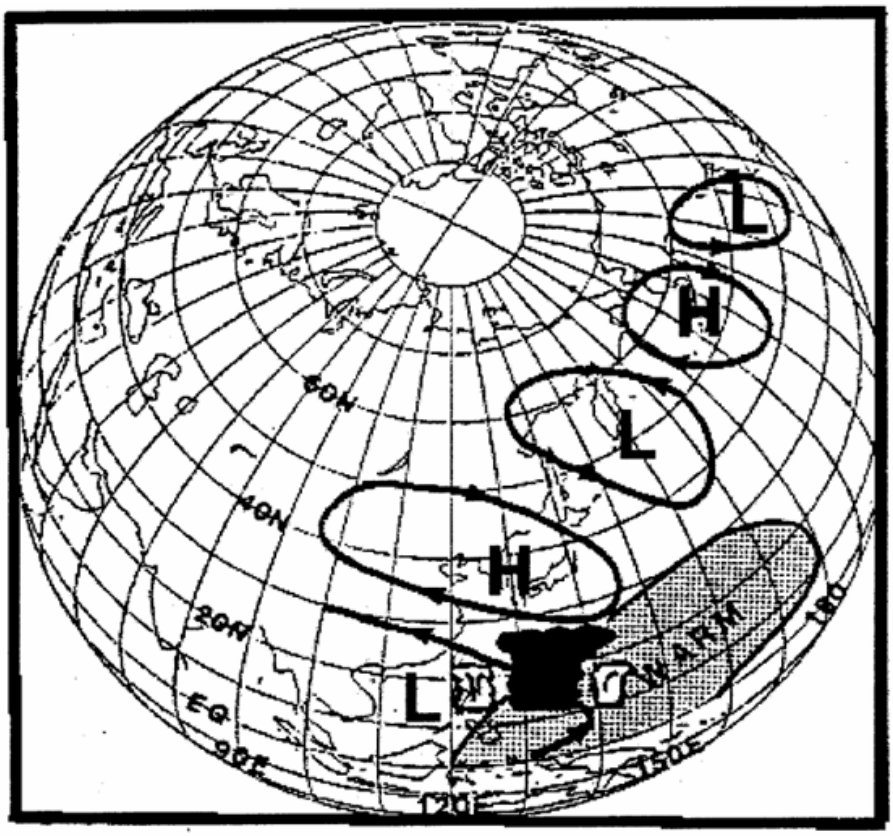

Fig. 16. Schematic showing 500-hPa GPH anomalies associated with increased convection over warmer than normal sea surface temperature (SST) in the tropical western Pacific. H denotes a positive height anomaly, and L denotes a negative height anomaly. From Nitta (1987)

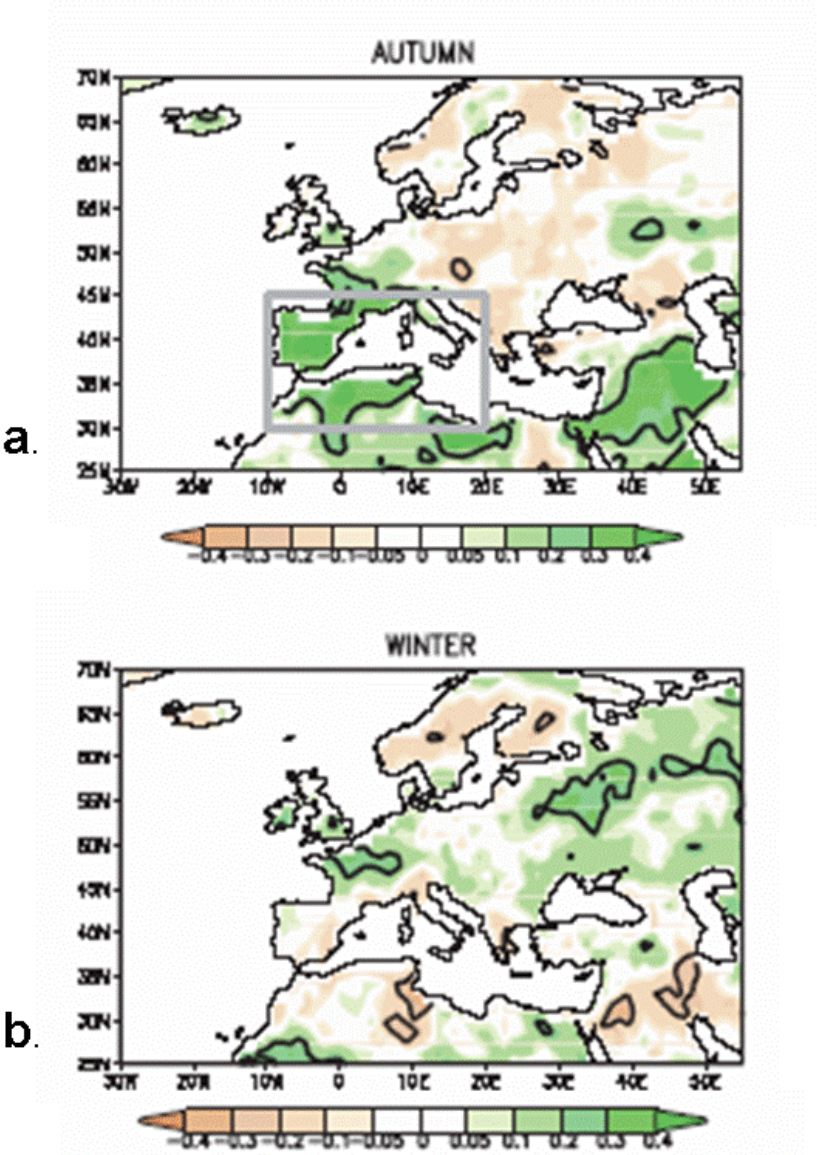

Fig. 17. Seasonal correlations of rainfall in Europe and the Mediterranean and the Nino3.4 index for the period 1948-1996 for (a) autumn and (b) winter. Rainfall data is from the CRU. Correlation coefficients enclosed by contours are statistically significant at the 95% level. Note that there is a positive correlation during autumn over the portions of SWA shown, but a negative correlation over most of SWA during winter. From Mariotti et al. (2002).

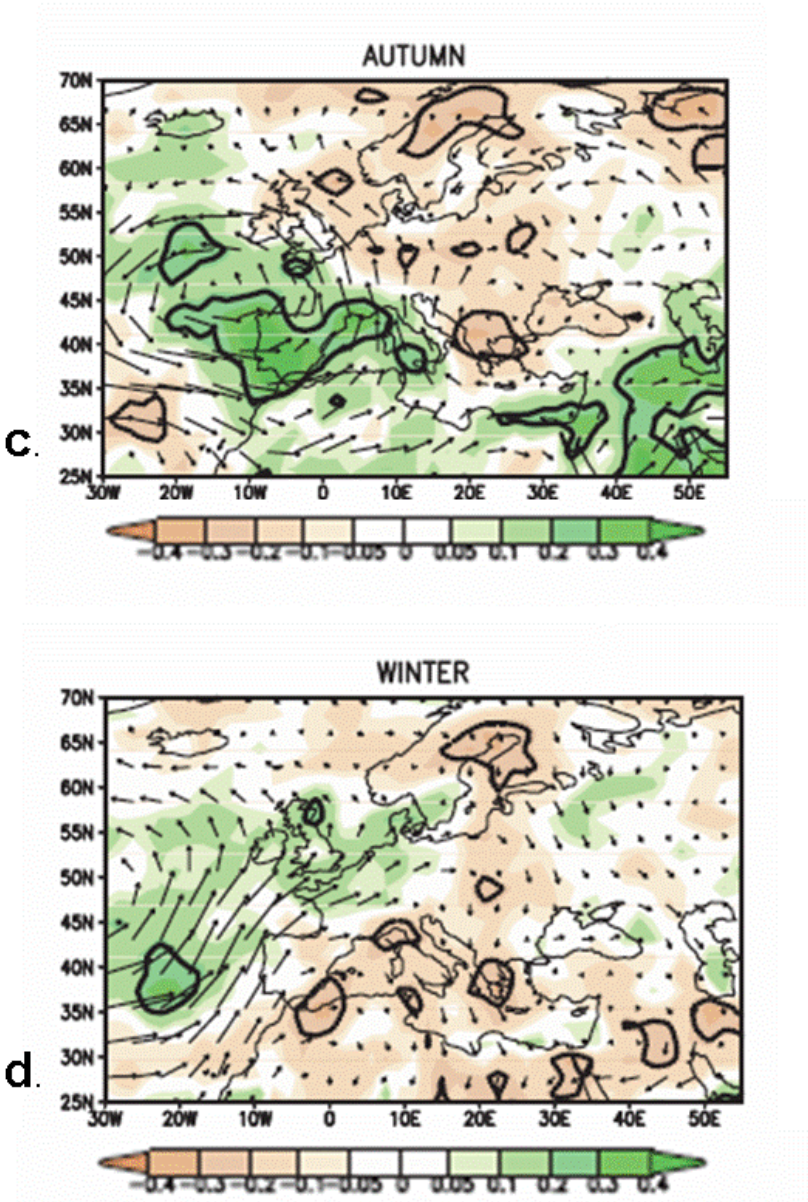

Fig. 17. (cont.) Seasonal regression of vertically integrated moisture flux and the Nino3.4 index (vectors) for (c) autumn and (d) winter. Seasonal correlation of rainfall with the Nino3.4 index is also reported (shaded; values enclosed by contours are statistically significant at the 95% level). from Mariotti et al. (2002). Note the reversal in correlation between autumn and winter over SWA.

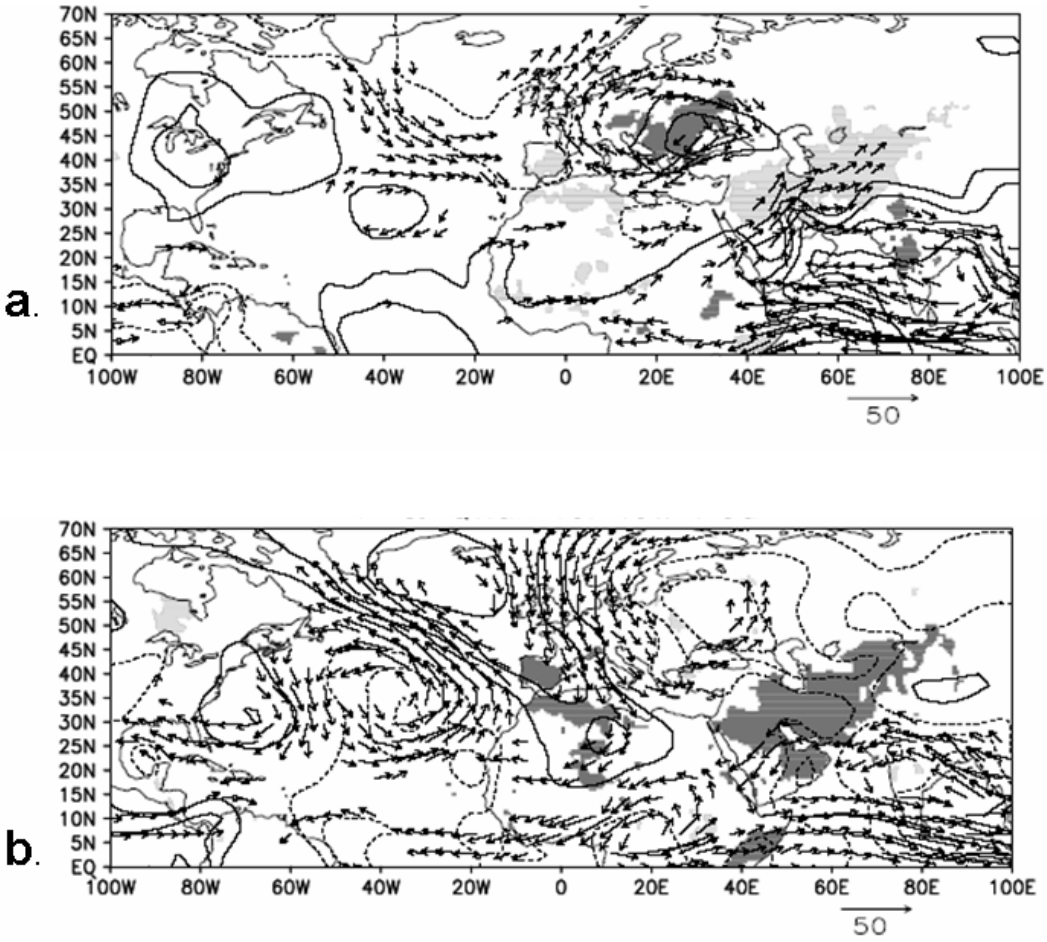

Fig. 18. Composite anomalies of atmospheric circulation and rainfall associated with (a) high and (b) low precipitation anomalies during the period 1948-2000. significant rainfall anomalies (light and dark shades are for positive and negative values respectively), SLP anomalies (solid and dashed contours are for positive and negative values respectively starting at absolute values greater than 0.2 Std, with intervals of 0.2), anomalous moisture flux (vectors, in kg $m^{-1}s^{-1}$; only vectors with an amplitude greater than 10kg $m^{-1}s^{-1}$ are plotted). Note the onshore moisture flux into SWA during periods of anomalously high precipitation and the offshore moisture flux out of SWA during periods of anomalously low precipitation. From Mariotti et al. (2005).

a.

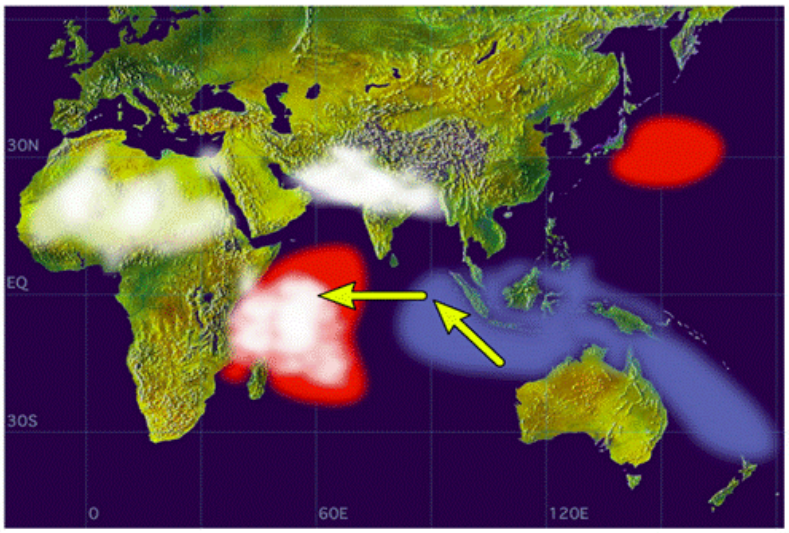

b.

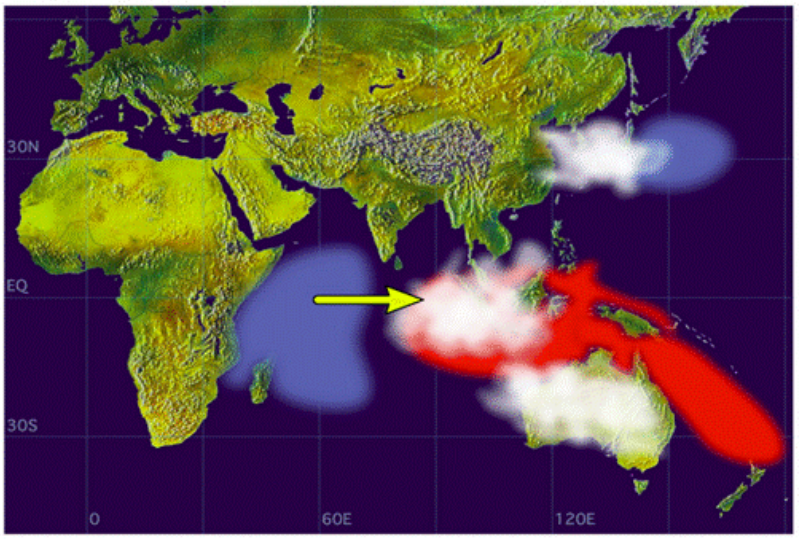

Fig 20. Schematics showing the SST anomaly patterns associated with the (a) positive and (b) negative phases of the IOZM. Red shading denotes positive SST anomalies, and blue shading denotes negative SST anomalies. Clouds are drawn in areas that experience above normal convection during the two phases.
From http://www.jamstec.go.jp/frsgc/research/d1/iod/IOD1.html
(Accessed 21 March 2006)

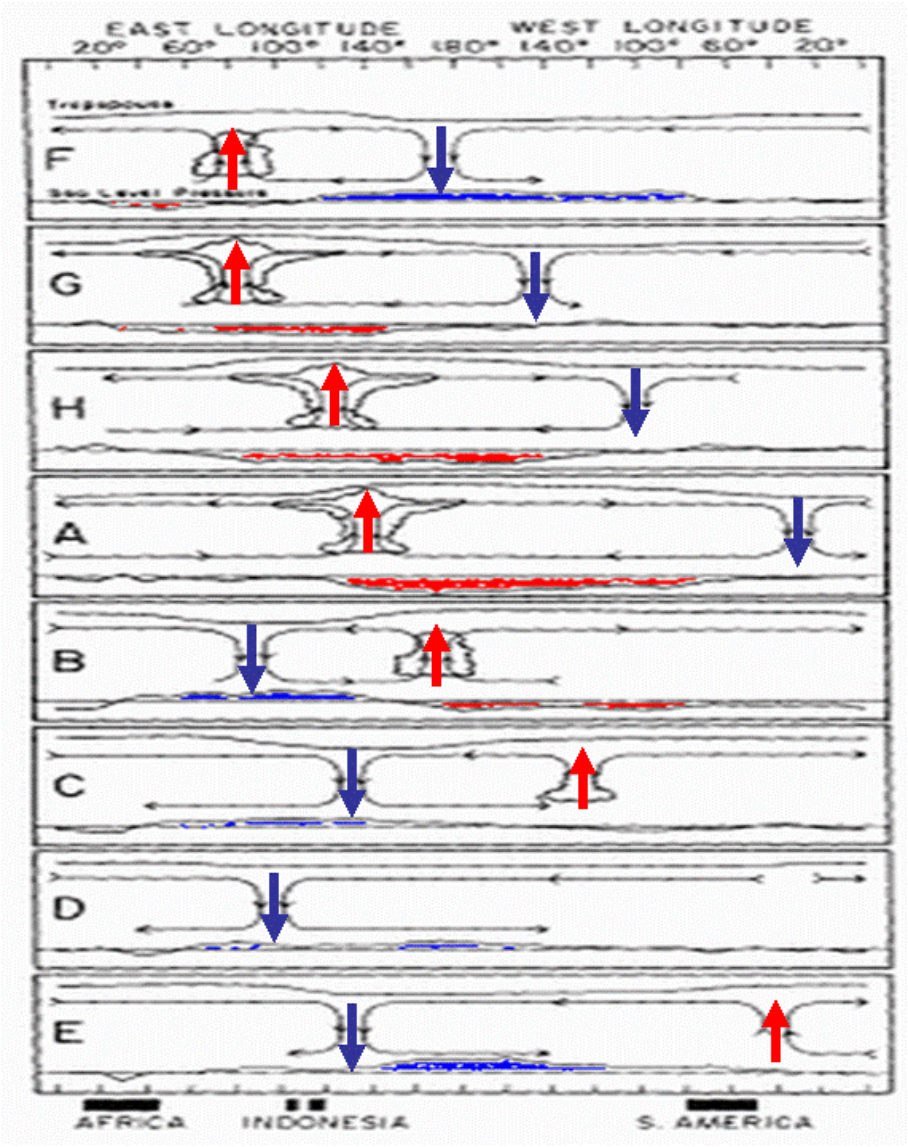

Fig. 21. Schematic showing the eastward progression of the convective (clouds, upward red arrows) and subsidence (downward blue arrows) components of the MJO across the Indian and Pacific Ocean. The red and blue arrows are indicative of the anomalous vertical circulation. The red and blue shading are indicate negative and positive SLP anomalies respectively. Adapted from Madden and Julian (1994).

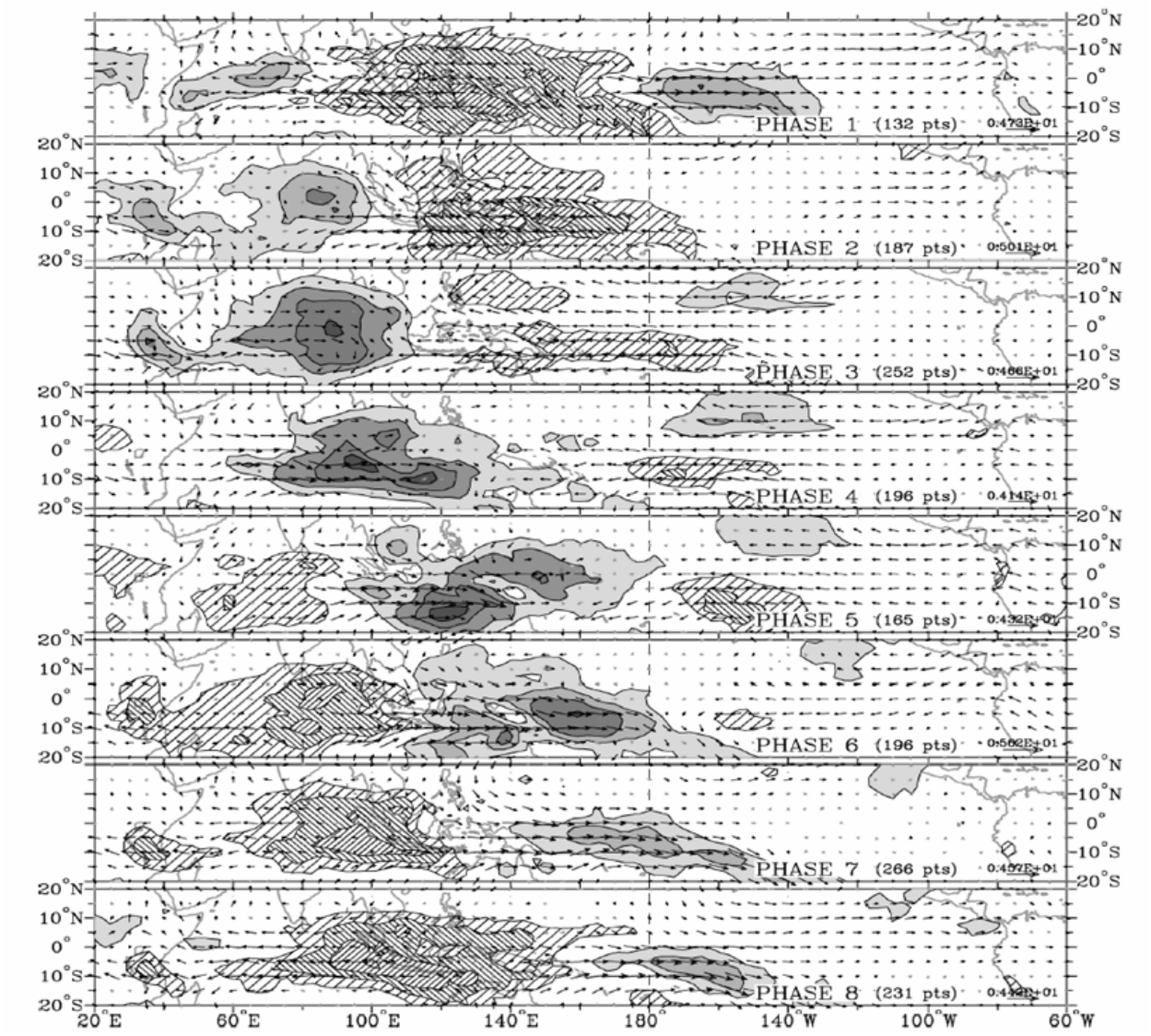

Fig. 22. Composite anomalies of OLR and 850-hPa vector winds for the eight MJO phases defined by Wheeler and Hendon (2004). Shading levels denote OLR anomalies less than -7.5, -15, -22.5, and -30 W m^{-2} respectively and hatching levels denote OLR anomalies greater than 7.5, 15, 22.5, and 30 W m^{-2} respectively. Arrows indicate wind anomalies statistically significant at the 99% level. The magnitude of the largest vector (m s-1) is shown on the bottom right and the number of days (points) falling within each phase category is given. From Wheeler and Hendon (2004).

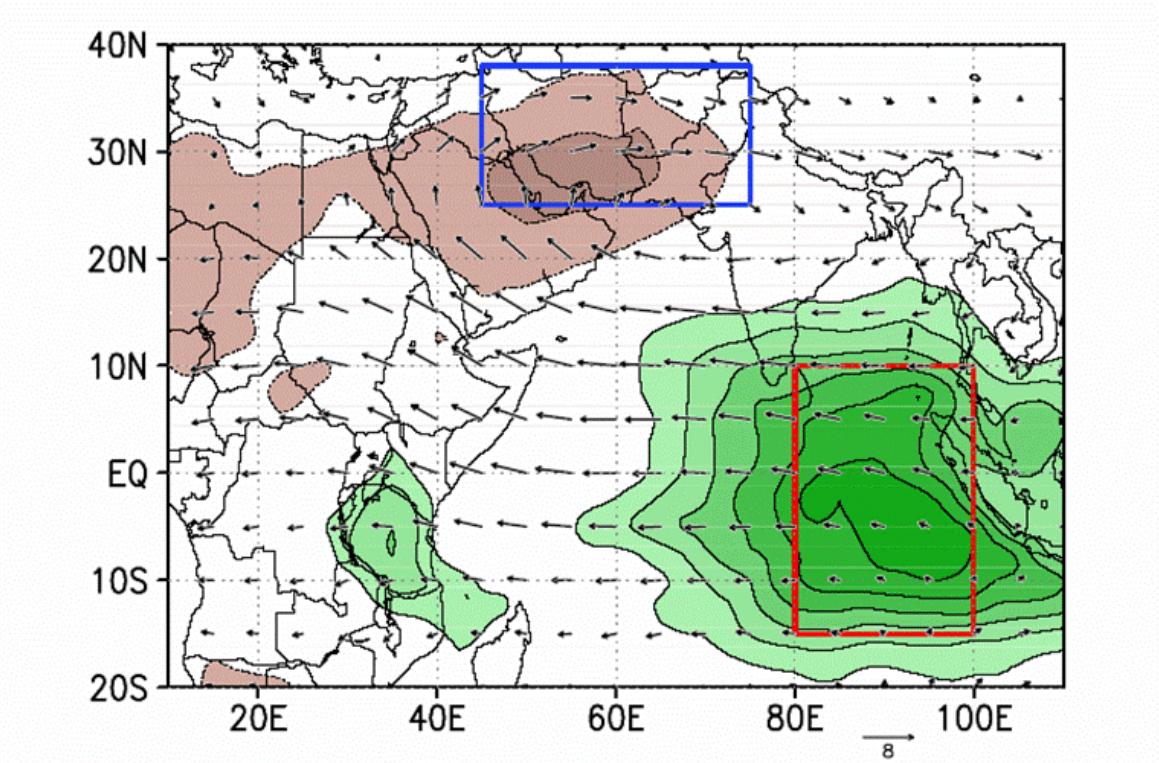

Fig. 23. Difference in daily OLR and 200-hPa wind anomalies (m s^{-1}) between the convective and subsidence components of the MJO in the eastern Indian Ocean (red box), for November-April, 1979-2001. The OLR anomalies are contoured at intervals of 4 W m^{-2}). Negative OLR anomalies are shaded green, while positive anomalies are shaded brown. Note the trend for there to be oppositely-signed OLR anomalies between the eastern IO and SWA. From Barlow et al. (2005)

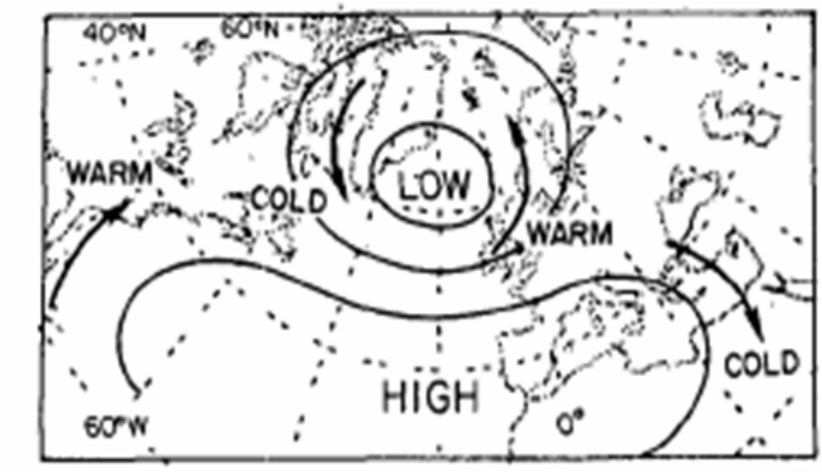

Fig. 24. Schematic showing idealized relationships between pressure and temperature anomalies associated with the positive phase of the North Atlantic Oscillation. The opposite anomalies are associated with the negative phase. From Wallace and Gutzler (1981).

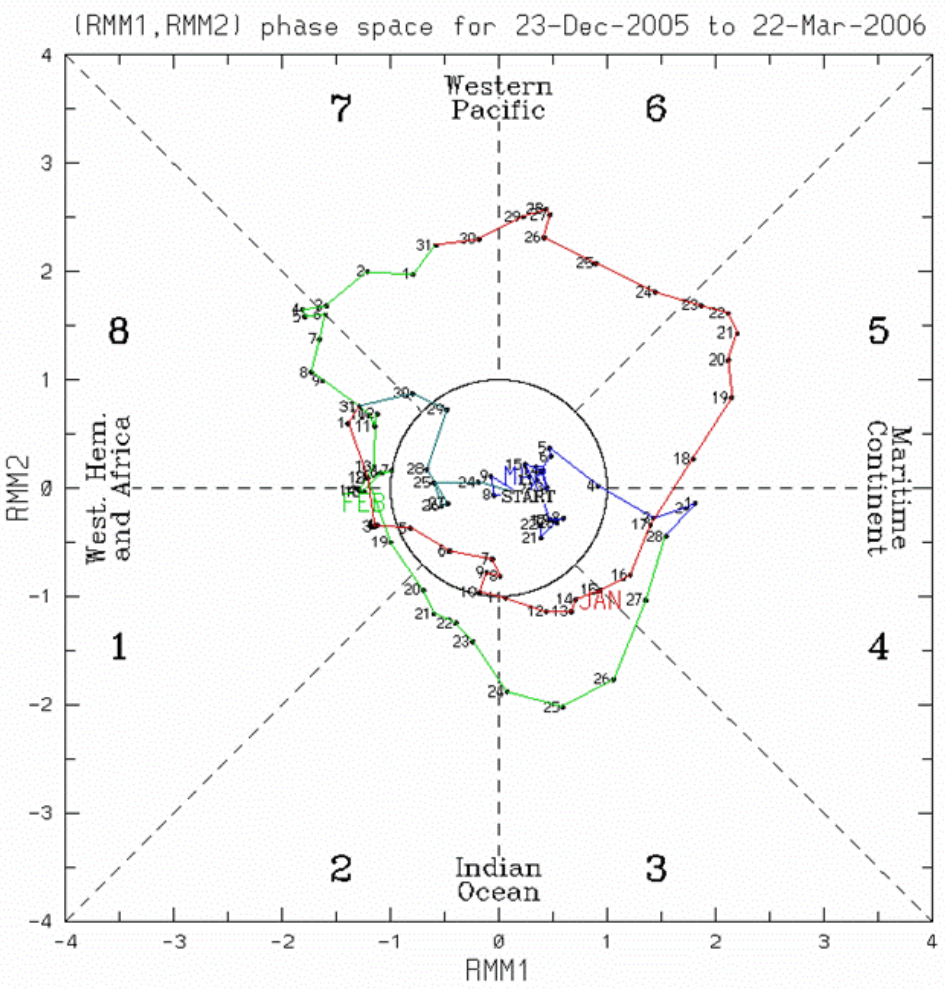

Fig. 25. The RMM phase space as defined by Wheeler and Hendon (2004) for January 1, 2006 through March 21, 2006. The red line corresponds to January, the green to February, and the blue to March. Points represent individual days, and the phase numbers correspond to the approximate locations of the convective component of the MJO as defined in Fig. 22. The counter-clockwise path traced out by the lines represents the eastward progression of the MJO. The further the point is from the origin, the stronger the MJO, and all points in the center circle represent a weak MJO. Figure from http://www.bom.gov.au/bmrc/clfor/cfstaff/matw/maproom/RMM/

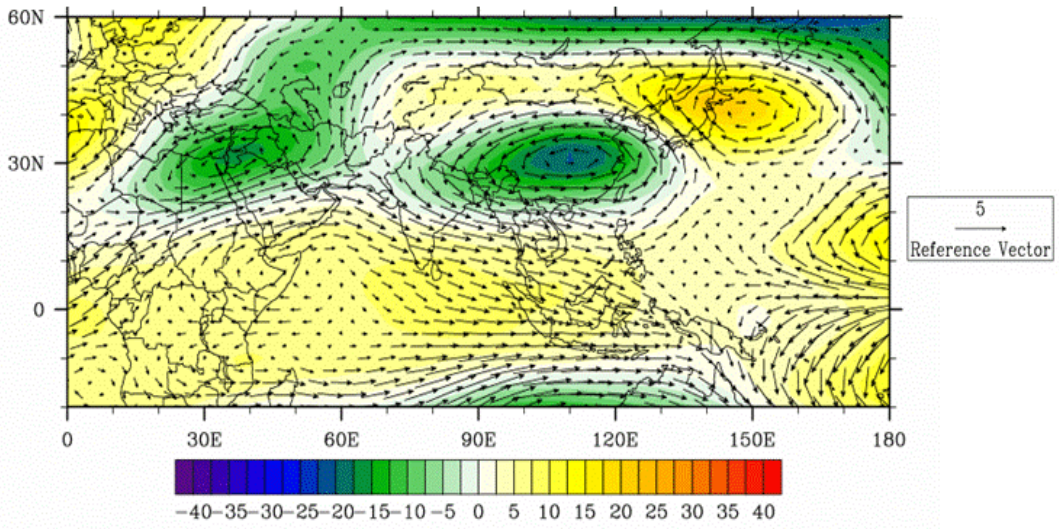

Fig. 26. Composite anomalies of 200-hPa GPH (color shading, m) and vector winds (m s^{-1}) for October-December during El Nino periods. The Rossby-Kelvin wave response to the decreased convection in the vicinity of the Maritime Continent is evident in the troughing and cyclonic wind anomalies over southern Asia and Australia.

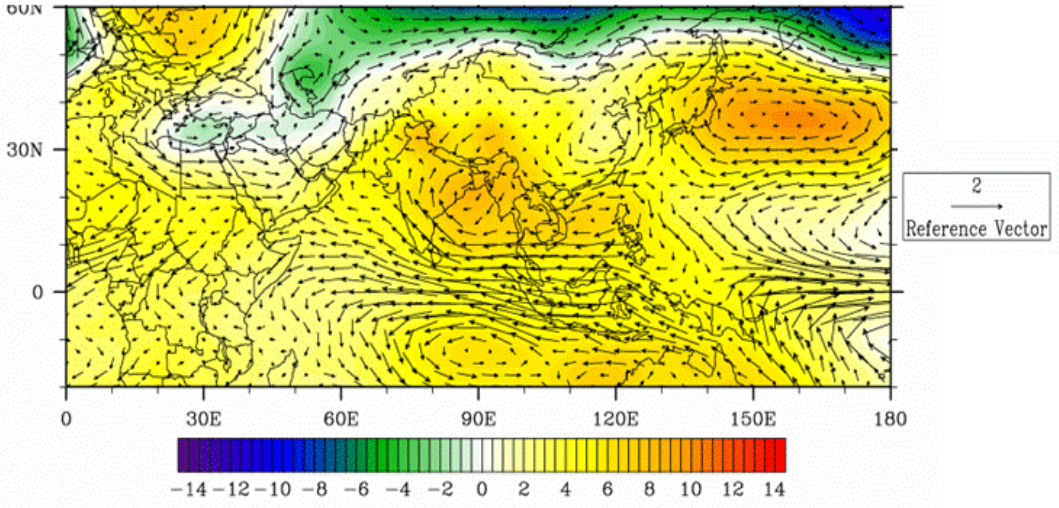

Fig. 27. Composite anomalies of 850-hPa GPH (color shading, m) and vector winds (m s^{-1}) for October-December during EN periods. Note the broad anticyclonic wind anomaly over southern Asia that directs the low level flow onshore into SWA from a region of low level divergence in the vicinity of the Maritime Continent associated with subsidence in that region.

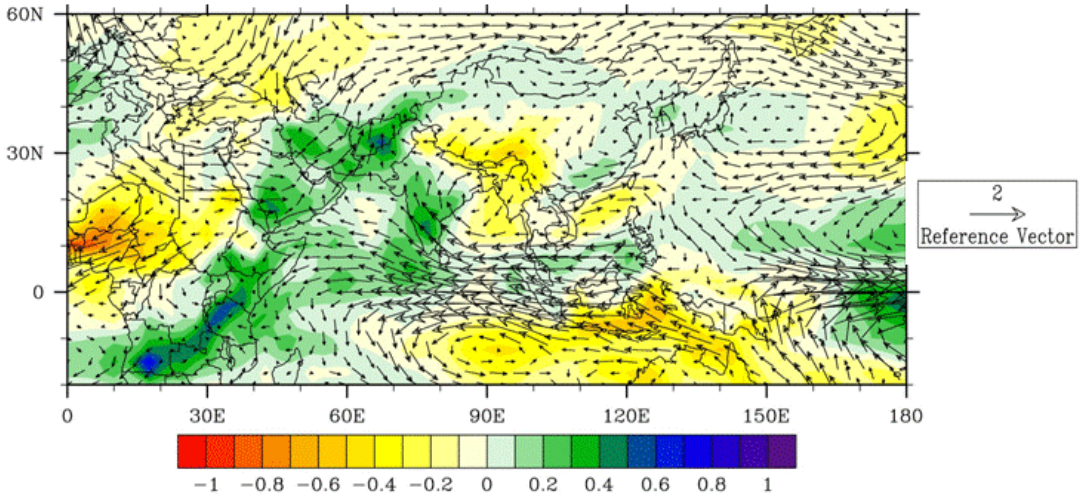

Fig. 28. Composite anomalies of 850-hPa GPH (color shading, m) and vector winds (m s^{-1}) for October-December during El Nino periods. The anomalous onshore flow results in above normal low level moisture over SWA.

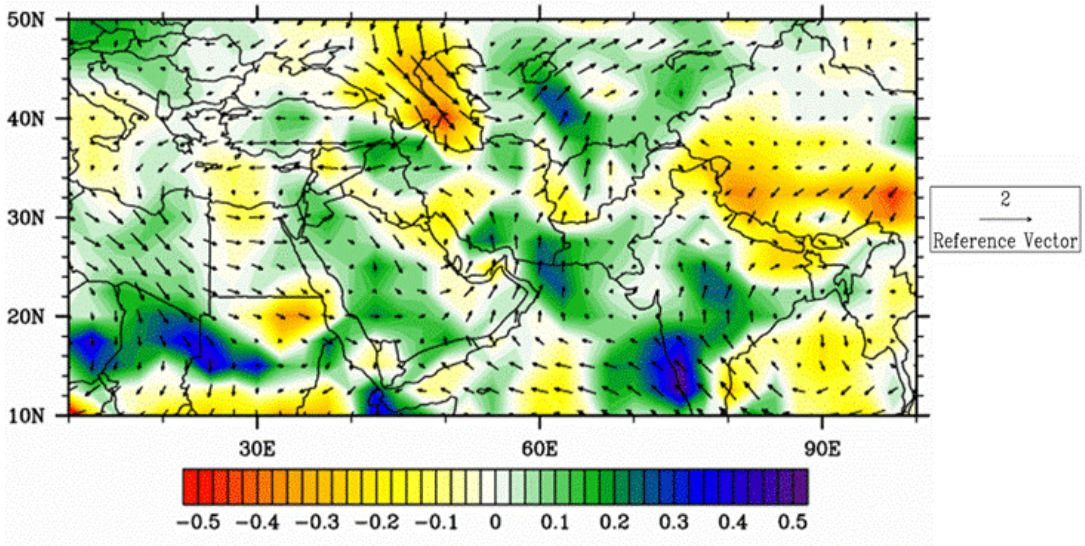

Fig. 29. Composite anomalies of 850-hPa moisture advection (shading, g $kg^{-1}s^{-1}$) and vector winds (m s^{-1}) for October-December during El Nino periods. Moisture advection have been multiplied by 10^8. The onshore flow from the Arabian Sea into SWA results in positive moisture advection anomalies.

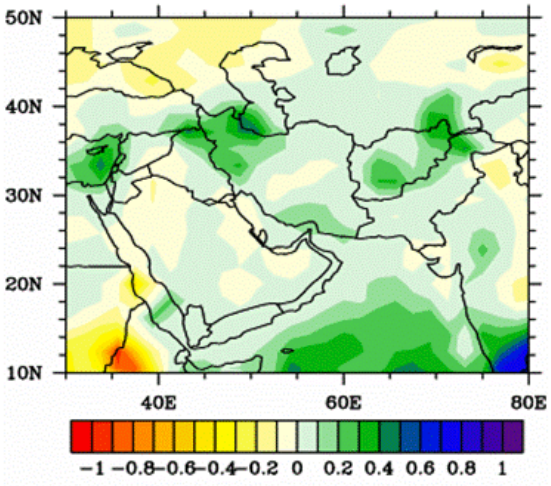

Fig. 30. Composite anomaly of precipitation rate (mm day^{-1}) for October-December during El Nino periods. SWA, in general, receives above-normal precipitation during the autumn of El Nino periods.

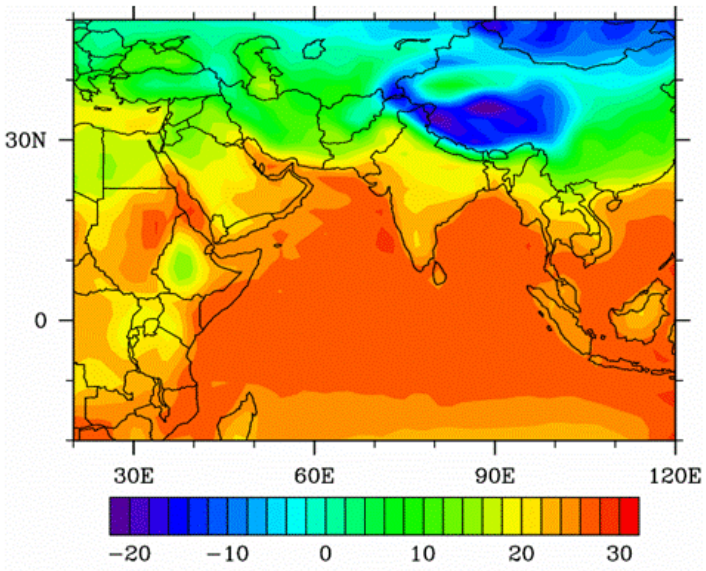

Fig. 31. Long term mean temperature (2 m, °C) for October-December. Note the significantly higher temperatures over the northwestern IO and Arabian Sea compared to SWA during autumn.

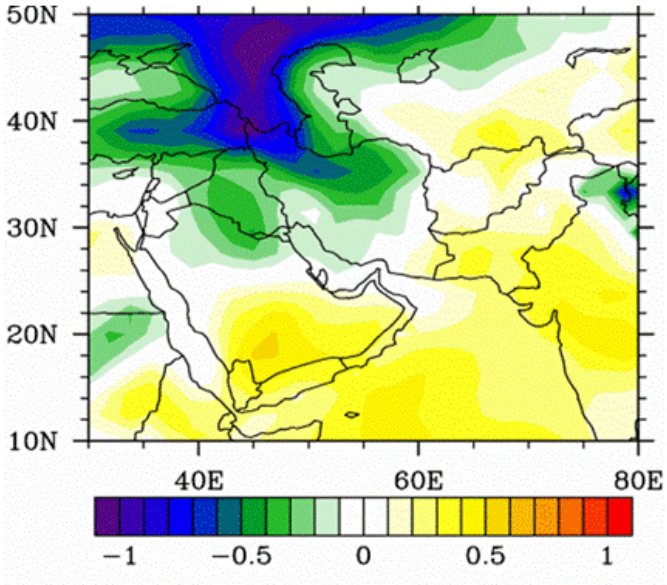

Fig. 32. Composite anomaly of temperature (2 m, °C) during El Nino periods. The southerly wind anomalies over southern and eastern SWA have led to anomalously warm conditions, while near the Caspian Sea northerly wind anomalies lead to cooler conditions.

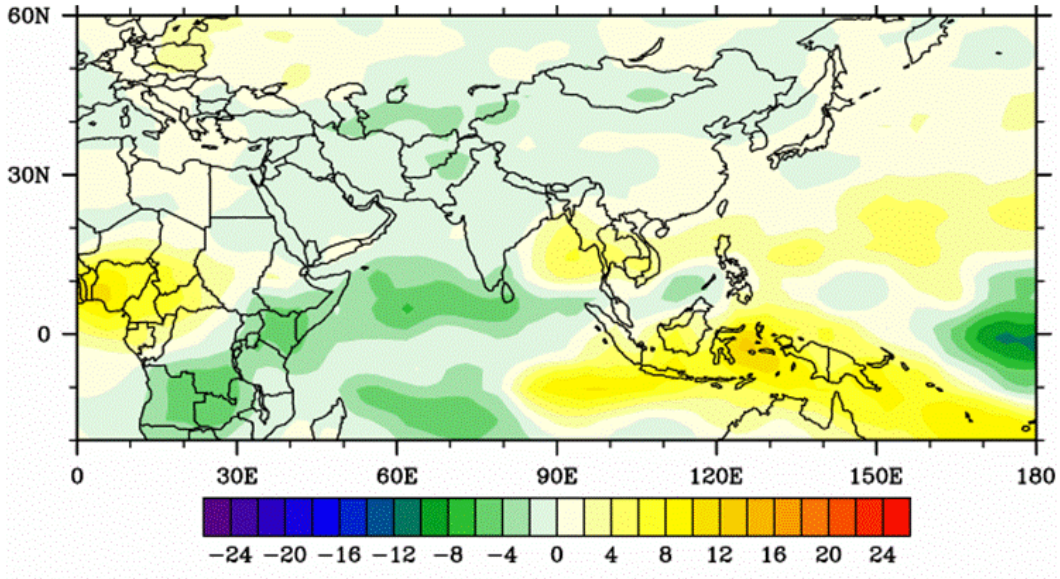

Fig. 33. Composite anomaly of OLR (W m^{-2}) for October-December during El Nino periods. The dipole in OLR anomalies between SWA and the Maritime Continent is visible. This is representative of the decrease in convection in the vicinity of the Maritime Continent that leads to an increase in cloud cover and precipitation in SWA.

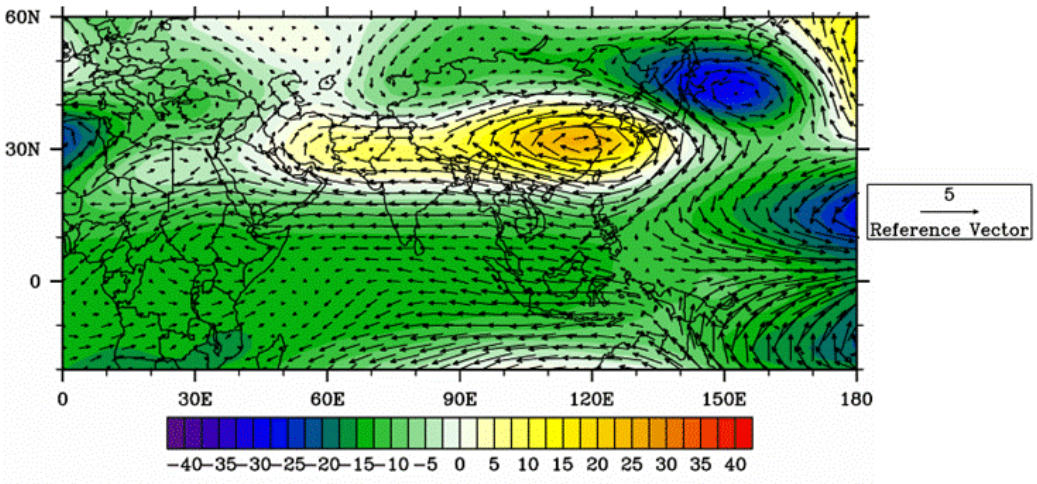

Fig. 34. Composite anomalies of 200-hPa GPH (color shading, m) and vector winds (m s^{-1}) for October-December during La Nina periods. The upper level Rossby-Kelvin wave response to the increase in convection in the vicinity of the Maritime Continent is evident in the anomalous ridging.

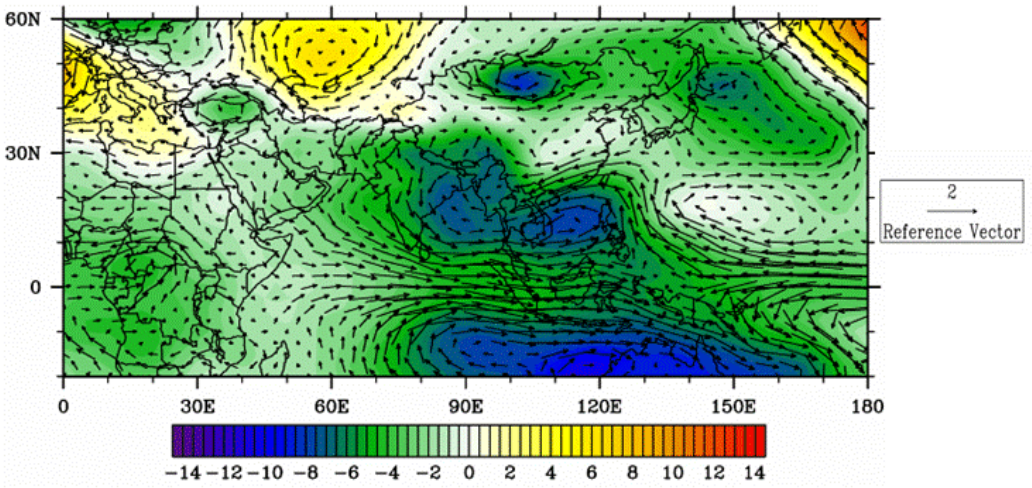

Fig. 35. Composite anomalies of 850-hPa GPH (color shading, m) and vector winds (ms^{-1}) for October-December during La Nina periods. Note the reversal in low level flow from autumn that now leads to offshore wind anomalies. Anomalous low level convergence is also evident over the Maritime Continent.

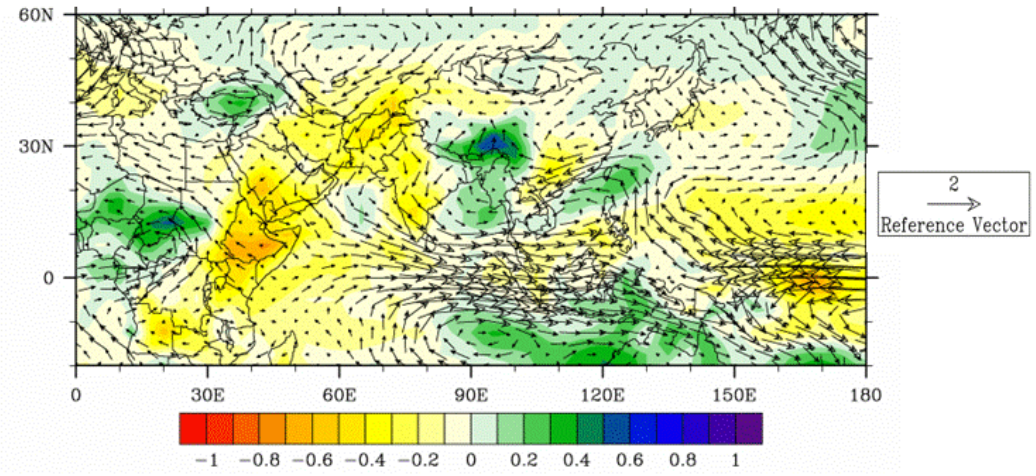

Fig. 36. Composite anomalies of 850-hPa specific humidity (color shading, g kg^{-1}) and vector winds (m s^{-1}) for October-December during La Nina periods. The offshore wind anomalies lead to drier conditions over SWA in autumn during La Nina periods.

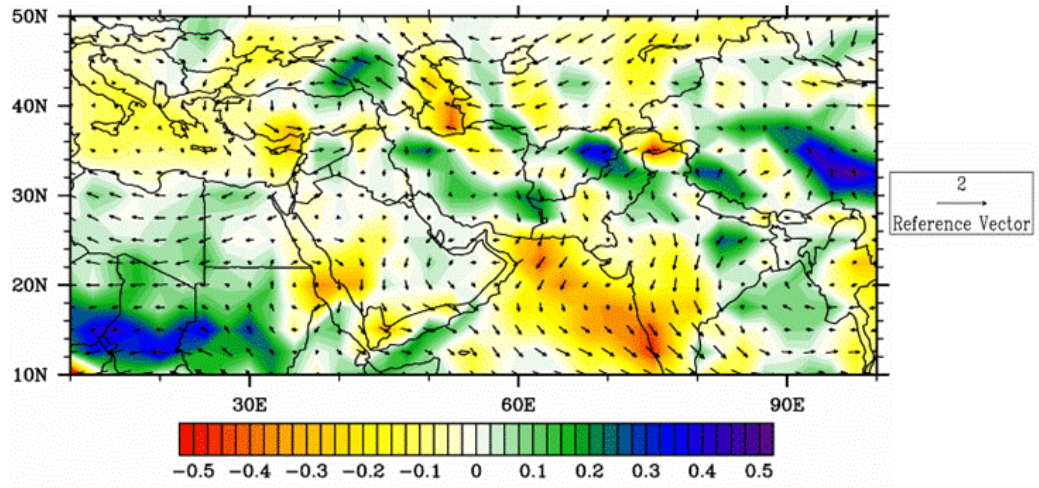

Fig. 37. Composite anomalies of 850-hPa moisture advection (color shading, g $kg^{-1}s^{-1}$) and vector winds (ms^{-1}) for October-December during La Nina periods. Moisture advection values have been multiplied by 10^8. The offshore wind anomalies over the Arabian Sea lead to negative moisture advection anomalies in autumn during La Nina periods.

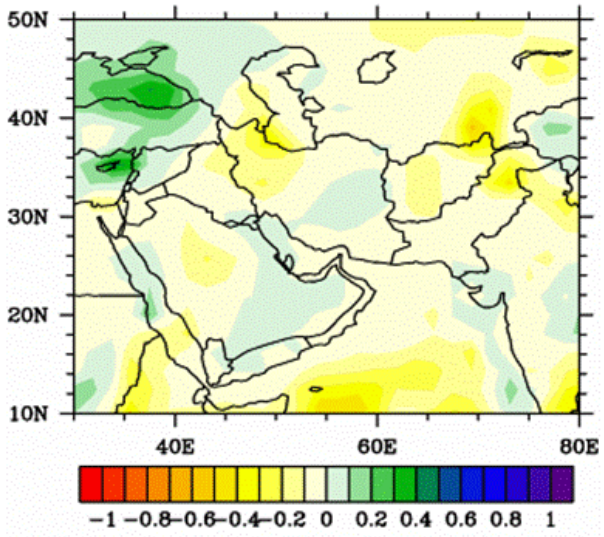

Fig. 38. Composite anomaly of precipitation rate (mm day^{-1}) for October-December during La Nina periods.

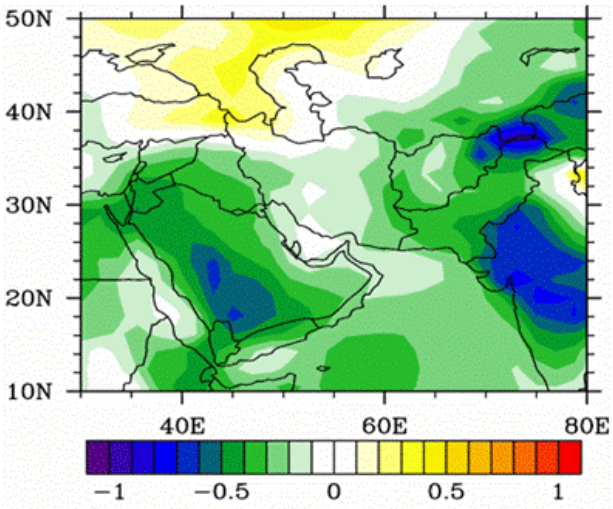

Fig. 39. Composite anomaly of temperature (2 m, °C) for October-December during La Nina periods.

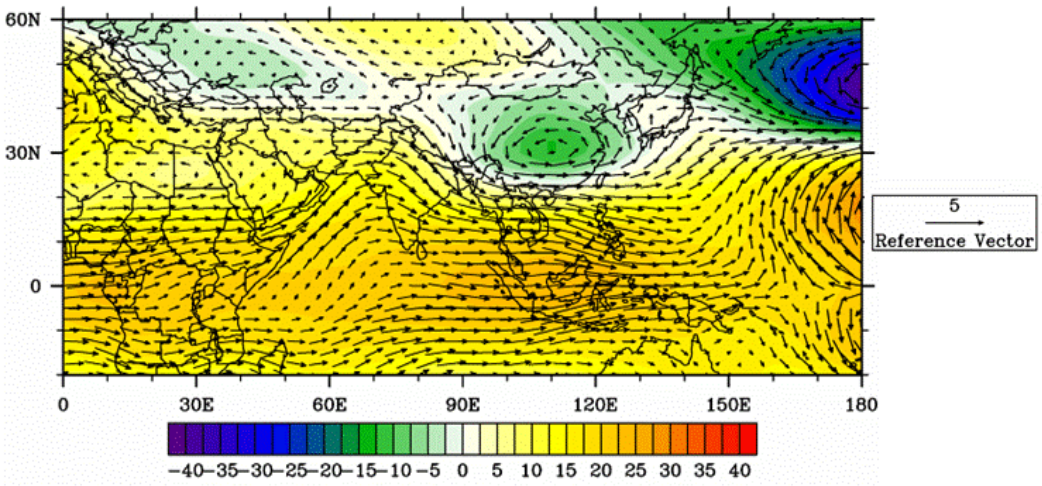

Fig. 41. Composite anomalies of 200-hPa GPH (color shading, m) and vector winds (m s^{-1}) for January-March during El Nino periods. Note the change in anomaly patterns from autumn (Fig. 26). The upper level anomaly pattern has changed significantly compared to winter, especially the Rossby-Kelvin wave response over southern Asia.

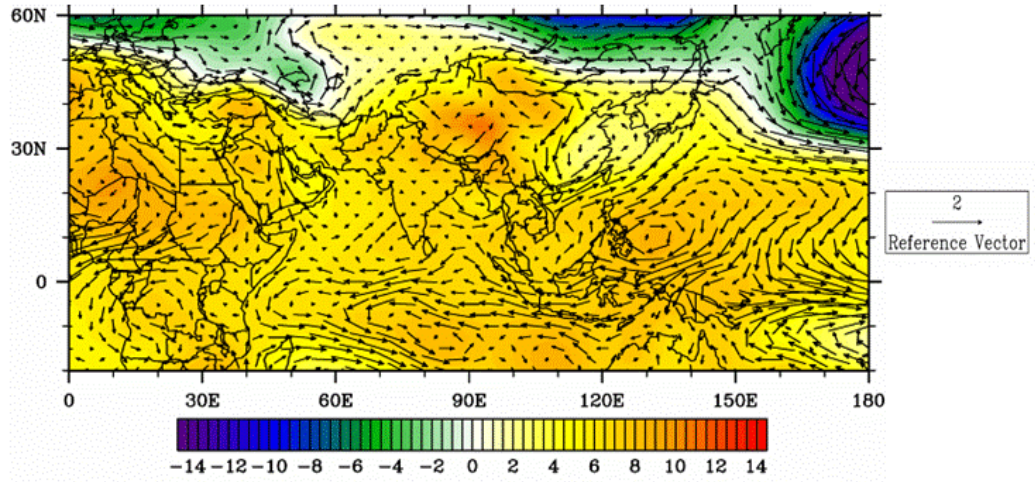

Fig. 42. Composite anomalies of 850-hPa GPH (color shading, m) and vector winds (m s^{-1}) for January-March of El Nino periods. The low level anomalous winds over SWA are offshore in winter, as opposed to onshore during the autumn. This is associated with the corresponding change in the upper level circulation (Fig. 41).

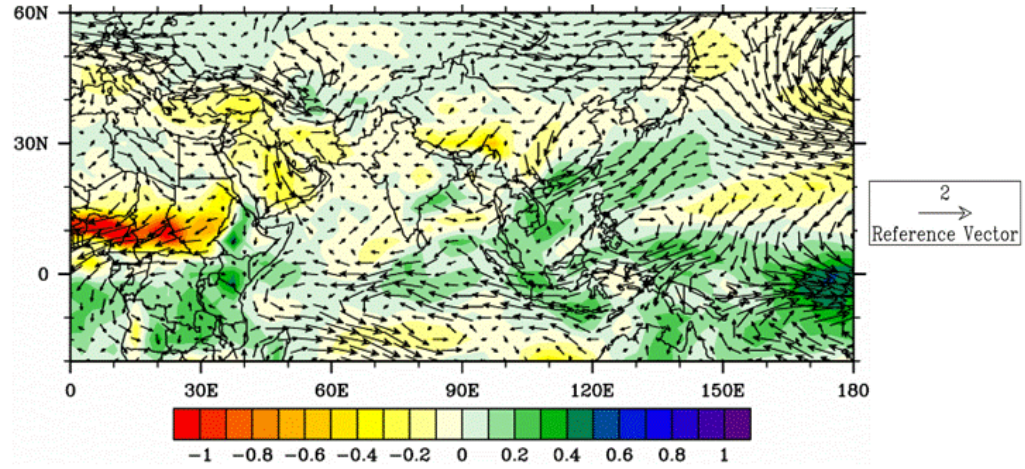

Fig. 43. Composite anomalies of 850-hPa specific humidity (color shading, g kg^{-1}) and vector winds (m s^{-1}) for January-March during El Nino periods. The anomalously offshore winds during the winter El Nino case lead to drier conditions over most of SWA.

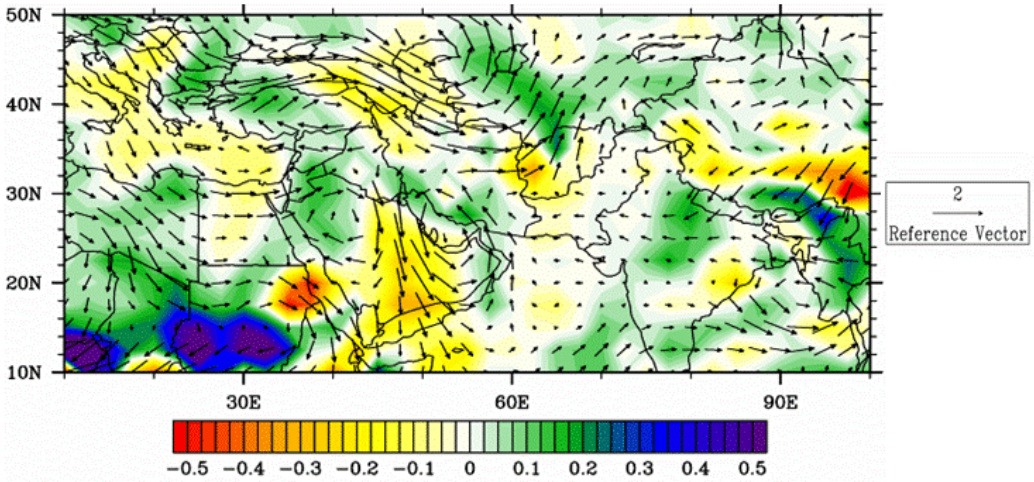

Fig. 44. Composite anomalies of 850-hPa moisture advection (color shading, g $kg^{-1}s^{-1}$) and vector winds (m s^{-1}) for January-March during El Nino periods. Moisture advection values have been multiplied by 10^8. Note the strong offshore wind anomalies over the Arabian Peninsula lead to significant negative moisture advection over this region. The weakening of the Saudi Arabian High is clear in the anomaly wind pattern.

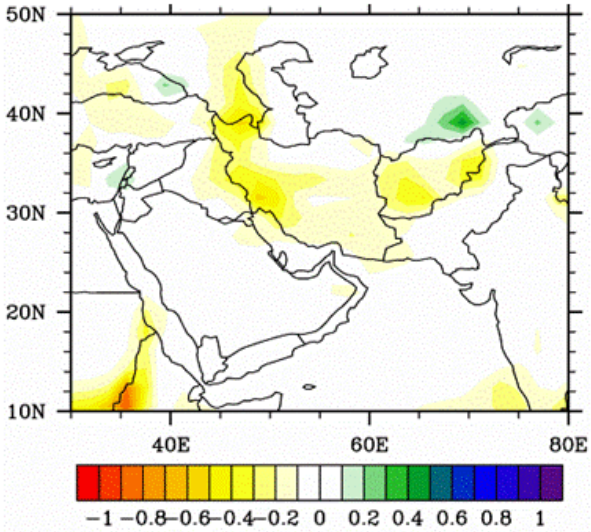

Fig. 45. Composite anomaly of precipitation rate (mm day^{-1}) for January-March during El Nino periods.

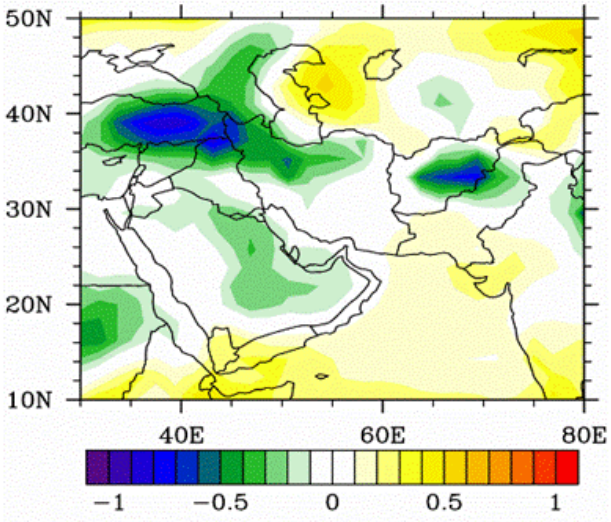

Fig. 46. Composite anomaly of temperature (2 m,° C) for January-March during El Nino periods.

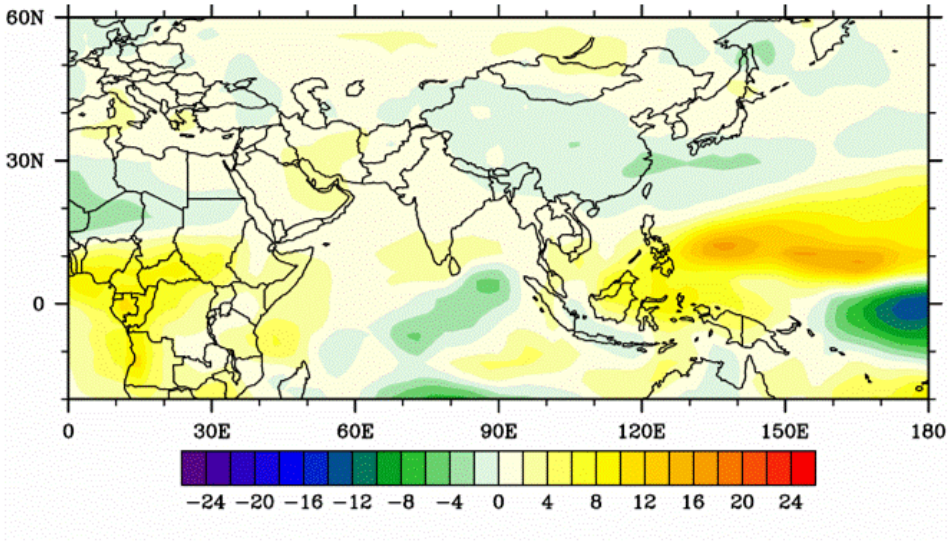

Fig. 47. Composite anomaly of OLR (W m^{-2}) for January-March during El Nino periods. The dipole pattern that was present during the autumn El Nino case is not clear in the winter case. The OLR anomaly pattern shows more small-scale variation, but there is a weak tendency over SWA is for positive OLR anomalies and less cloudy conditions. This fits with the below normal precipitation anomalies.

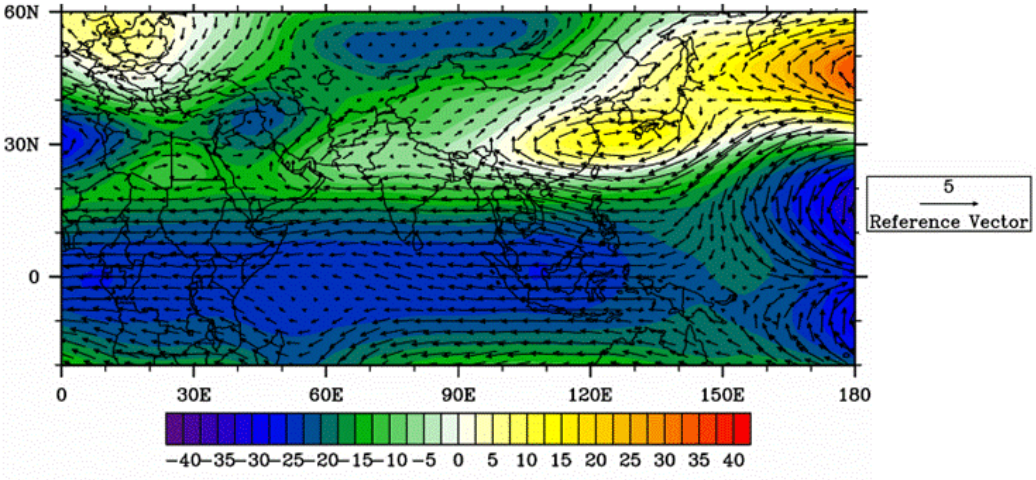

Fig. 48. Composite anomalies of 200-hPa GPH (color shading, m) and vector winds (m s^{-1}) for January-March during La Nina periods. The upper level anomaly field changes significantly between autumn and winter, as it does during El Nino.

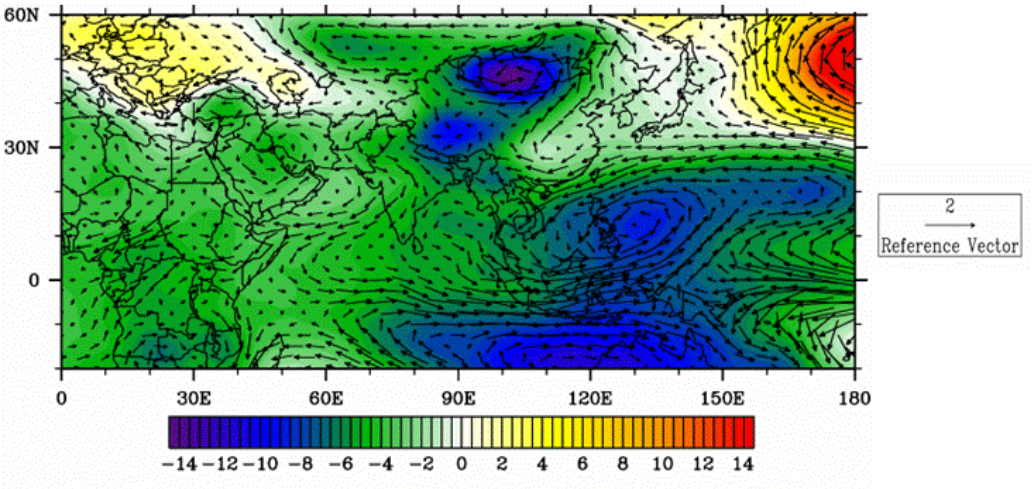

Fig. 49. Composite anomalies of 850-hPa GPH (color shading, m) and vector winds (m s^{-1}) for January-March during La Nina periods.

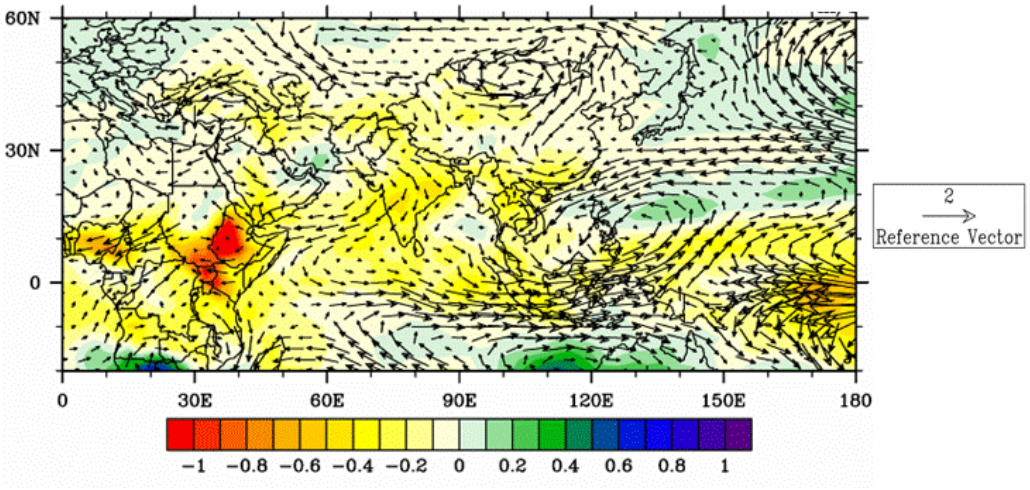

Fig. 50. Composite anomalies of 850-hPa specific humidity (color Shading, g kg^{-1}) and vector winds (m s^{-1}) for January-March during La Nina periods.

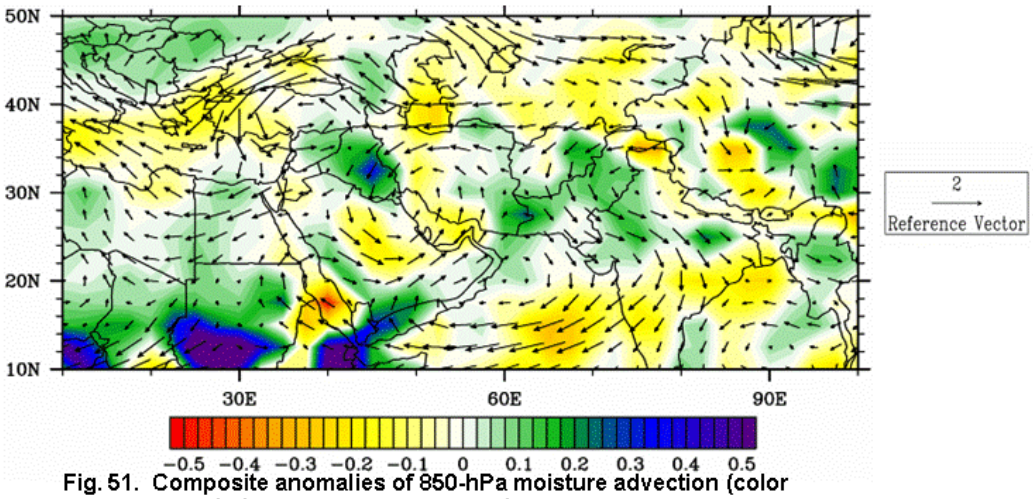

Fig. 51. Composite anomalies of 850-hPa moisture advection (color shading, g $kg^{-1}s^{-1}$) and vector winds (m s^{-1}) for January-March during La Nina periods. Moisture advection has been muliplied by 10^8. Note the more complicated moisture advection anomaly pattern in winter than in autumn.

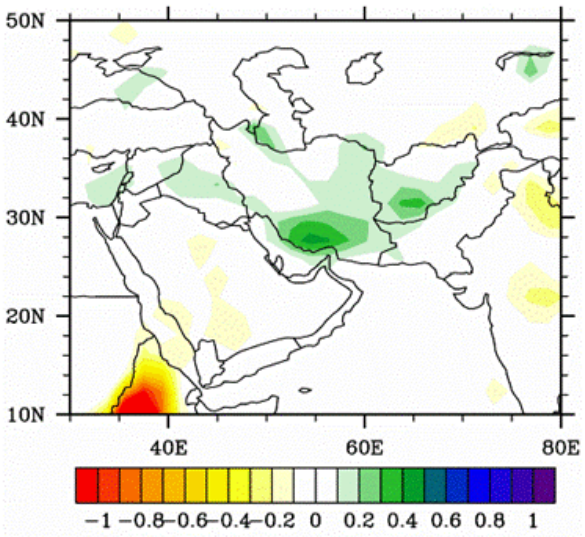

Fig. 52. Composite anomaly of precipitation rate (mm day^{-1}) for January-March during La Nina periods. The increase in precipitation in southern Iran is representative of the increase in onshore flow that accompanies the weakening of the Saudi Arabian High.

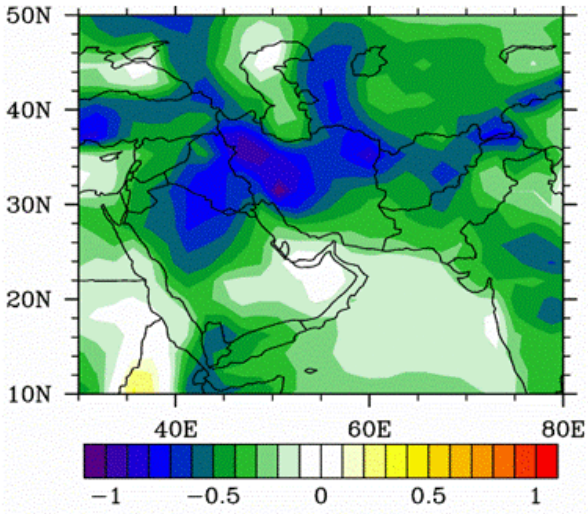

Fig. 53. Composite anomaly of temperature (2 m, °C) for January-March during La Nina periods.

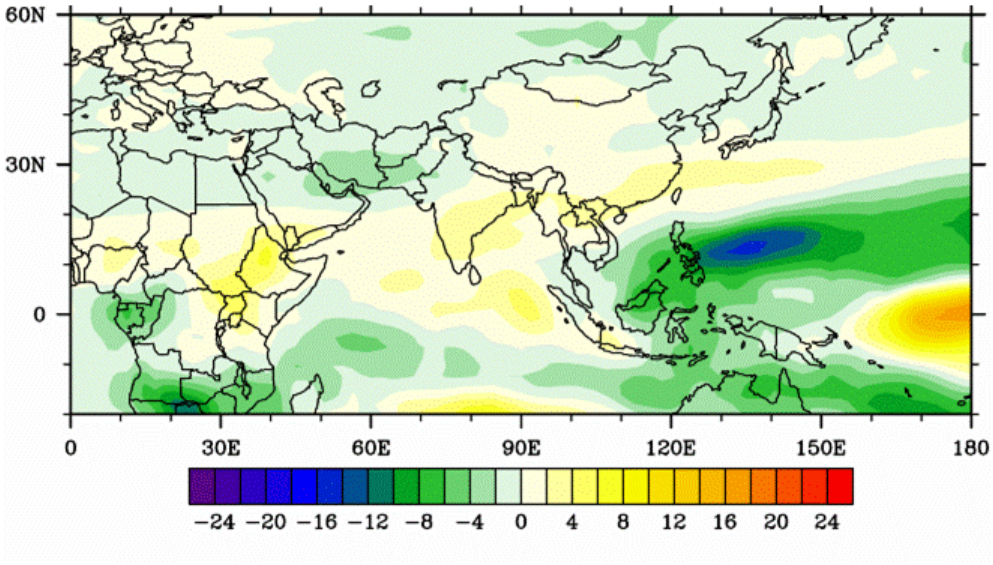

Fig. 54. Composite anomaly of OLR (W m^{-2}) for January-March during La Nina periods.

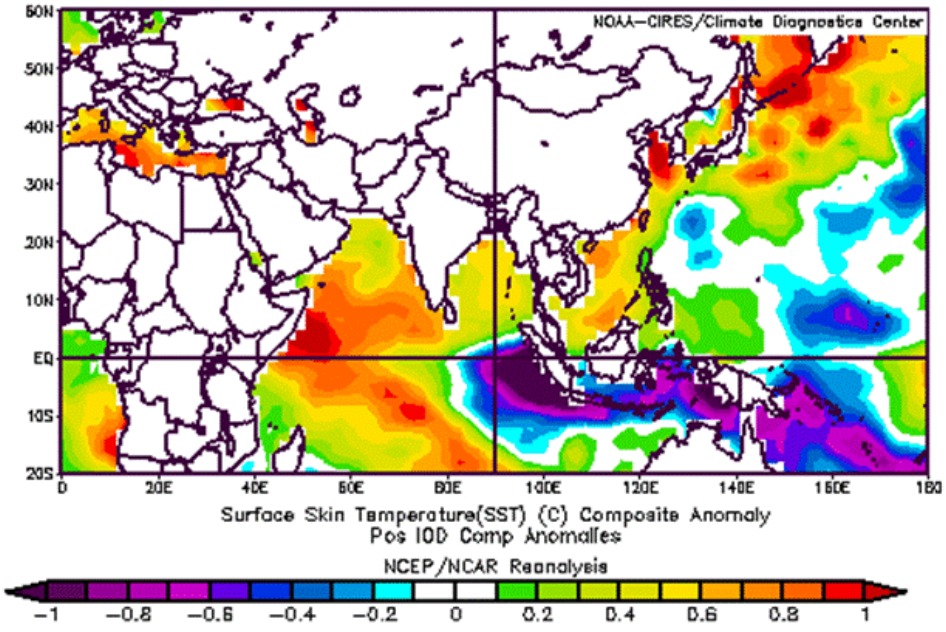

Fig. 55. Composite anomaly of SST (°C) for October-December during Positive IOZM periods. Note the strong cool anomaly in the eastern IO, off the coast of Sumatra, and the strong warm anomaly off the coast of the Horn of Africa that is the signature of the positive phase of the IOZM. During the negative phase of the IOZM the opposite pattern is observed. Figures created at http://www.cdc.noaa.gov/cgi-bin/Composites/printpage.pl (Accessed 21 March 2006).

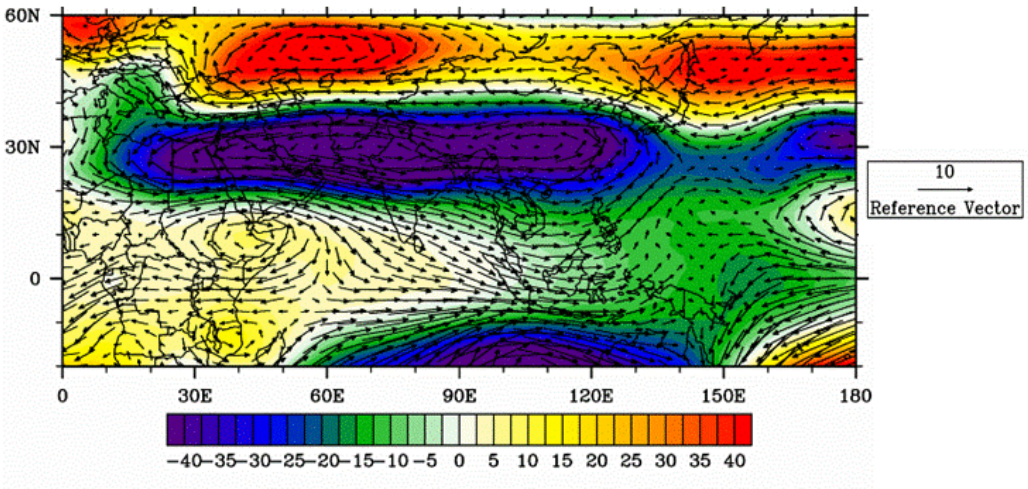

Fig. 56. Composite anomalies of 200-hPa GPH (color shading, m) and vector winds (m s^{-1}) for October-December during positive IOZM periods. The upper level GPH anomaly pattern over southern Asia shows a clear Rossby-Kelvin wave response in the troughing associated with the decrease in convection near the Maritime Continent. Compare with Fig. 3.

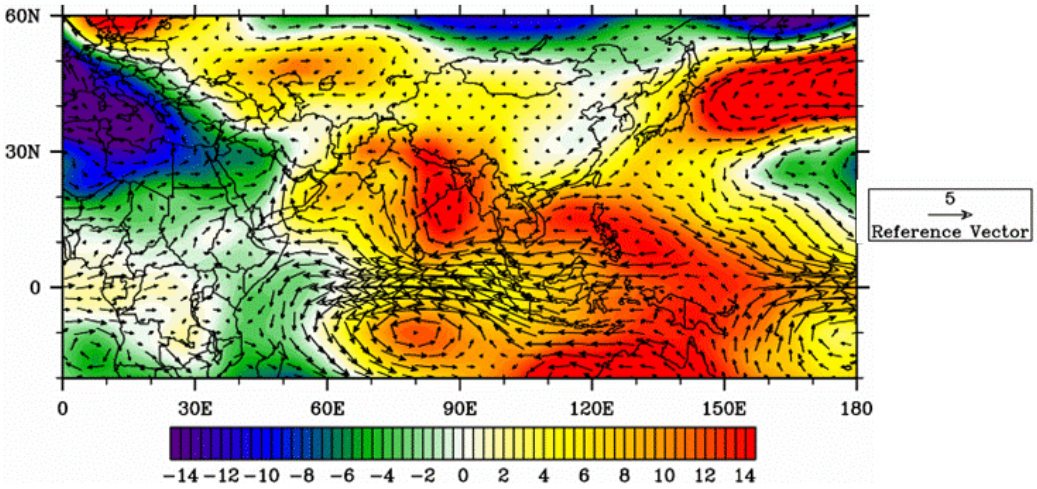

Fig. 57. Composite anomalies of 850-hPa GPH (color shading, m) and vector winds (m s^{-1}) for October-December during positive IOZM periods. The anomaly patterns are similar to those for the autumn EN case (Fig. 27), but the anomalous onshore flow over SWA is much stronger in this case.

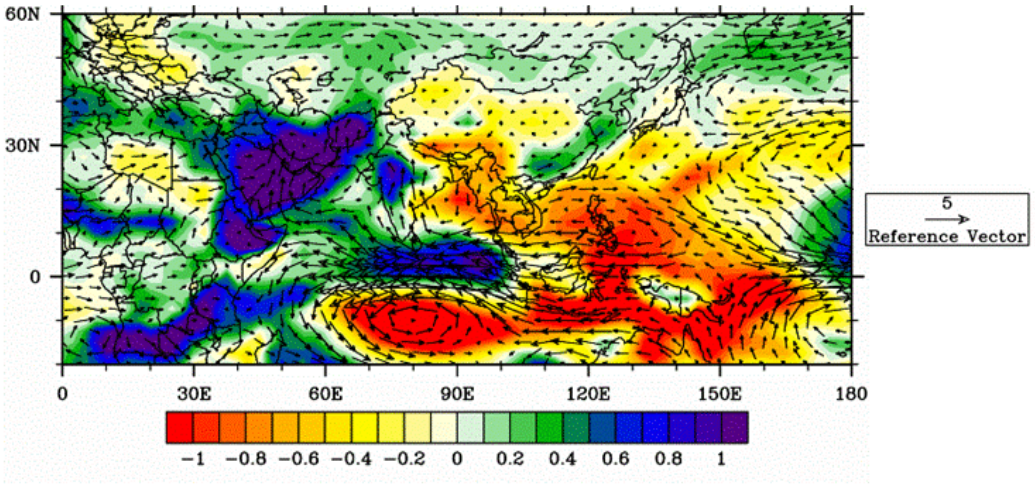

Fig. 58. Composite anomalies of 850-hPa specific humidity (SH, color shading, g kg^{-1}) and vector winds (m s^{-1}) for October-December during positive IOZM periods. The increase in SH associated with the onshore flow anomaly is striking.

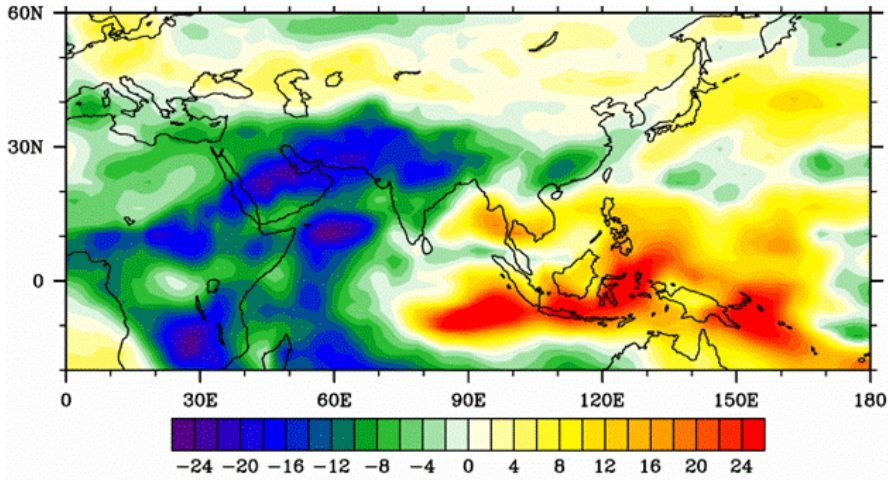

Fig. 59. Composite anomaly of OLR (W m^{-2}) for October-December during positive IOZM periods. Note the clear OLR dipole, with negative OLR anomalies over SWA and the western IO – east Africa region and positive OLR anomalies over the Maritime Continent. This indicates an anomalous increase (decrease) in precipitation and clouds in the western (eastern) part of the dipole.

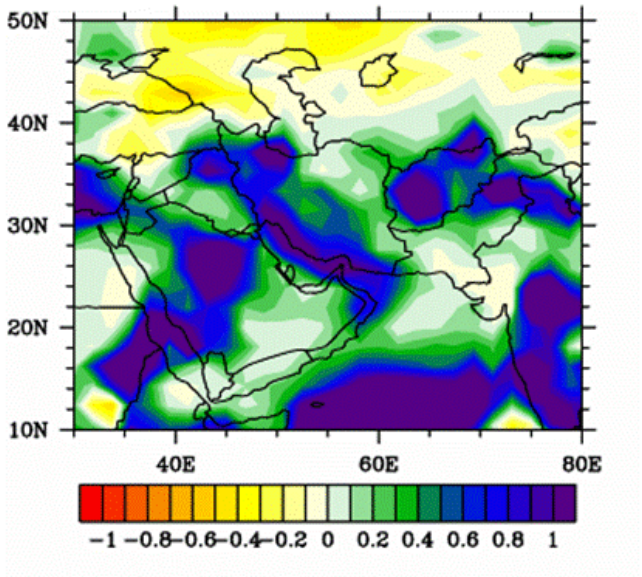

Fig. 60. Composite anomaly of precipitation rate (mm day^{-1}) for October-December during positive IOZM periods. Strong positive IOZM events clearly tend to lead to an increase in precipitation over SWA.

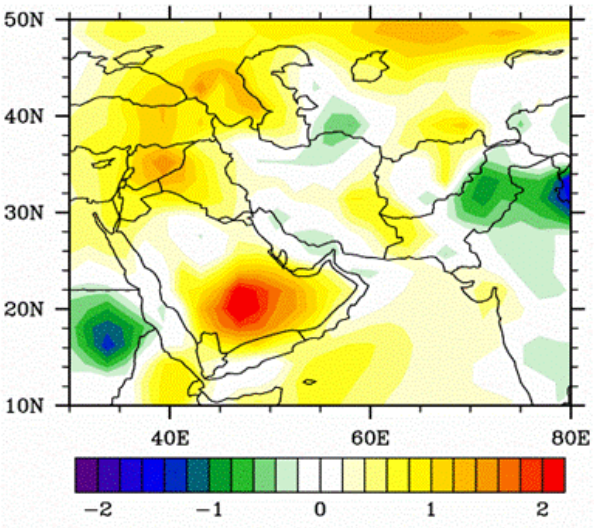

Fig. 61. Composite anomaly of temperature (2 m, °C) for October-December during positive IOZM periods. Note the increase in the temperature scale compared to the previously shown cases.

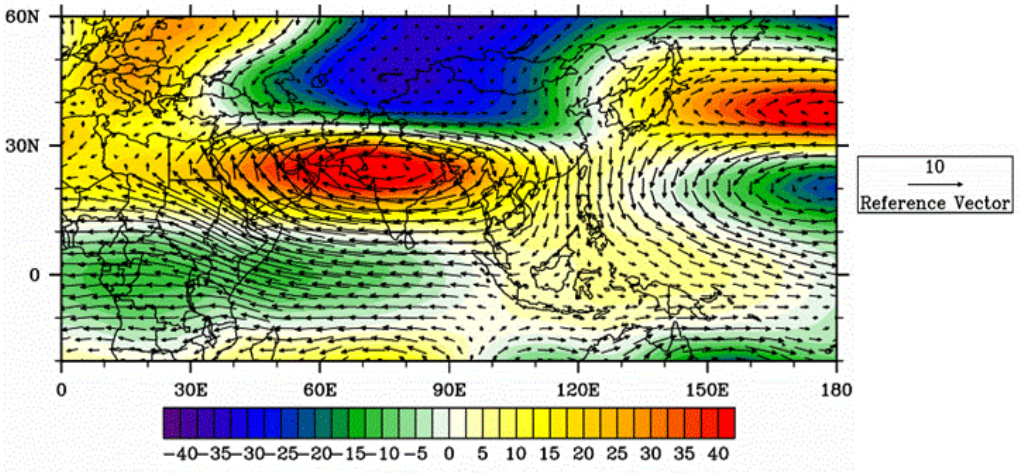

Fig 62. Composite anomalies of 200-hPa GPH (color shading, m) and vector winds (m s^{-1}) for October-March when the convective component of the MJO is in the eastern IO. The Rossby-Kelvin wave pattern in the anomalous upper level ridging over southern Asia is quite striking for this case.

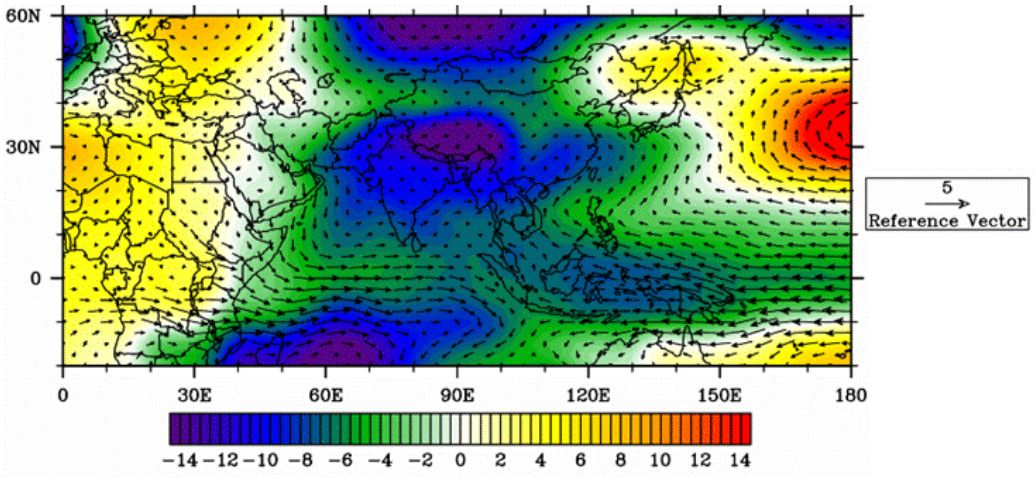

Fig. 63. Composite anomalies of 850-hPa GPH (color shading, m) and Vector winds (m s^{-1}) for October-March when the convective component of the MJO is in the eastern IO. As can be seen, when the convective component of the MJO is in the eastern IO, SWA is in a favorable location to receive offshore wind anomalies.

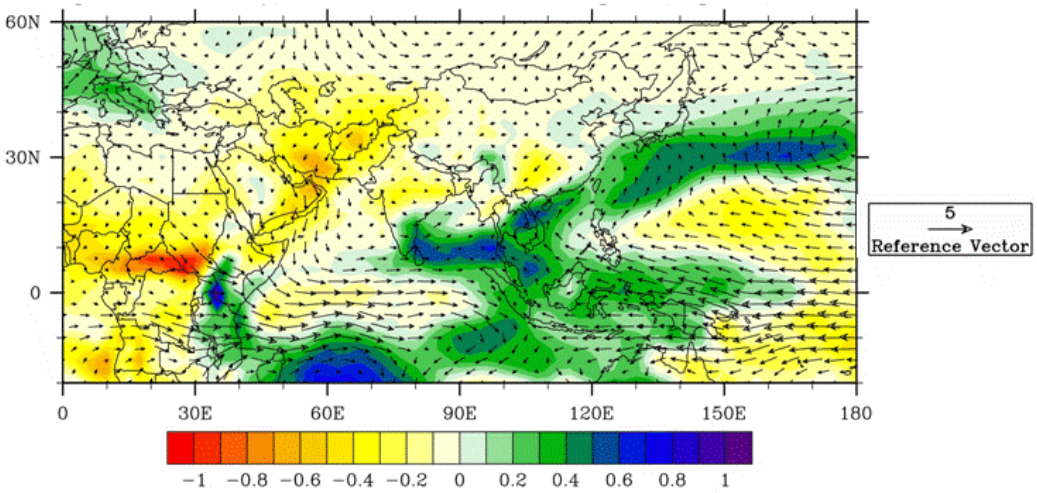

Fig. 64. Composite anomalies of 850-hPa specific humidity (color shading, g kg^{-1}) and vector winds (m s^{-1}) for October-March when the convective component of the MJO is in the eastern IO. The offshore wind anomalies clearly lead to drier conditions over SWA.

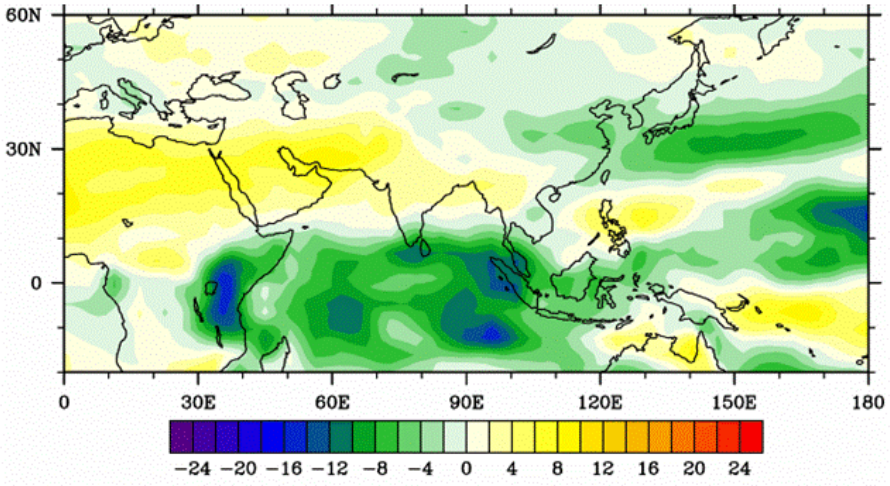

Fig. 65. Composite anomaly of OLR (W m^{-2}) for October-March when the convective component of the MJO is in the eastern IO. The anomalous offshore low level winds (Fig. 64) and resulting decrease in available low level moisture leads to a decrease in cloud cover over SWA. The increase in convection over the Io, especially the eastern IO, is also evident.

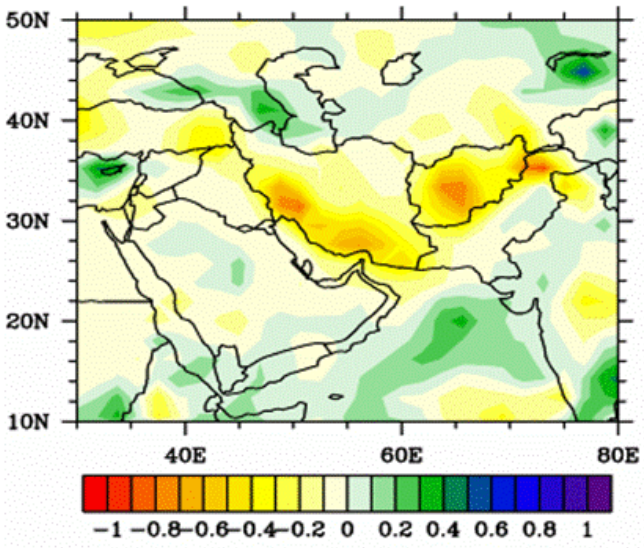

Fig. 66. Composite anomaly of precipitation rate (mm day^{-1}) for October-March when the convective component of the MJO is in the eastern IO.

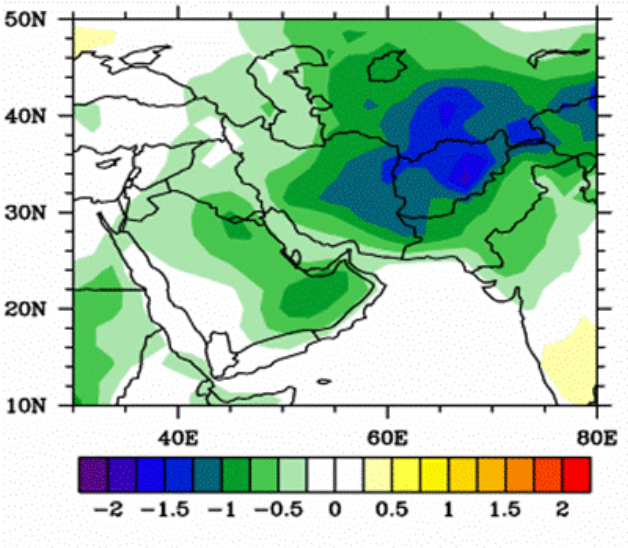

Fig. 67. Composite anomaly of temperature (2 m, °C) for October-March when the convective component of the MJO is in the eastern IO.

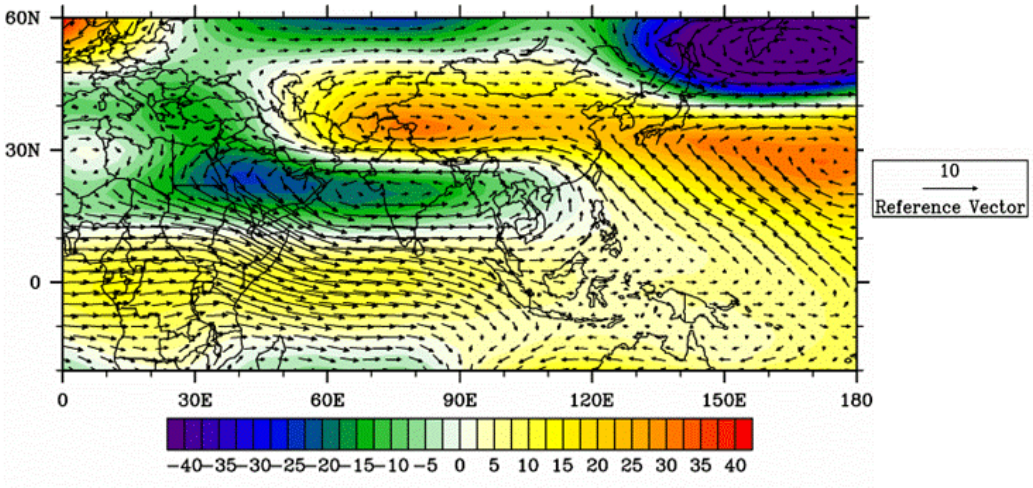

Fig. 68. Composite anomalies of 200-hPa GPH (color shading, m) and vector winds (m s^{-1}) for October-March when the subsidence component of the MJO is in the eastern IO.

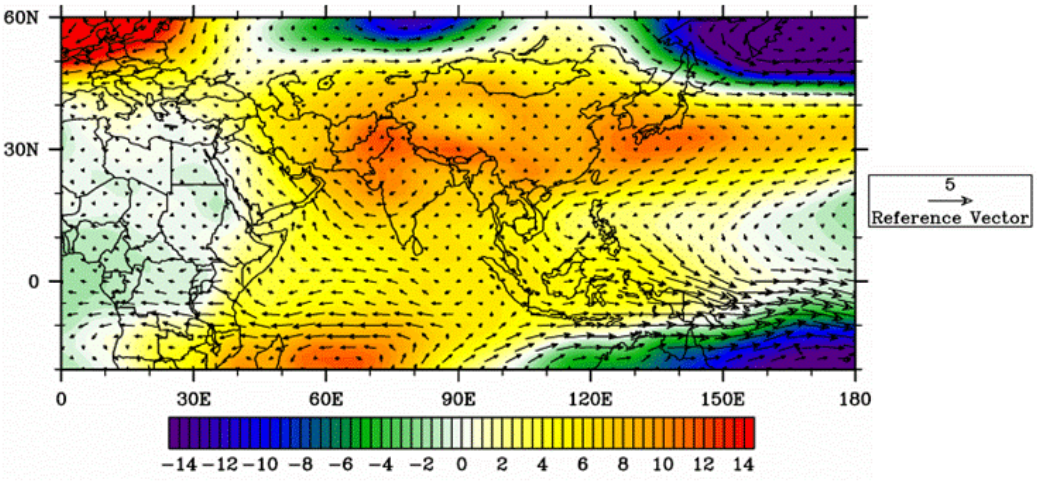

Fig. 69. Composite anomalies of 850-hPa GPH (color shading, m) and vector winds (m s^{-1}) for October-March when the subsidence component of the MJO is in the eastern IO.

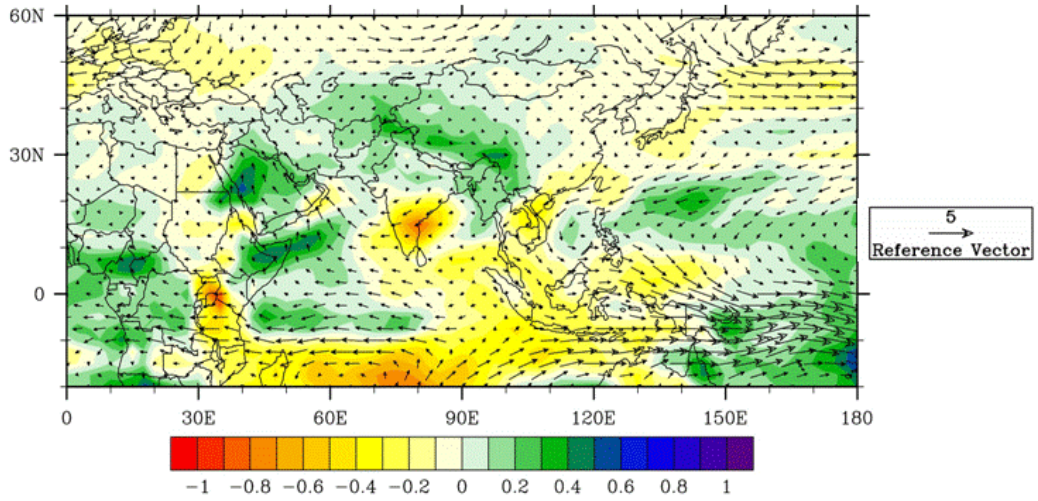

Fig. 70. Composite anomalies of 850-hPa specific humidity (color shading, g kg^{-1}) and vector winds (m s^{-1}) for October-March when the subsidence component of MJO is in the eastern IO. With the reversal in the low level wind anomalies over the northwestern IO (compared to the case when the convective component was in the eastern IO) there is an increase in low level moisture.

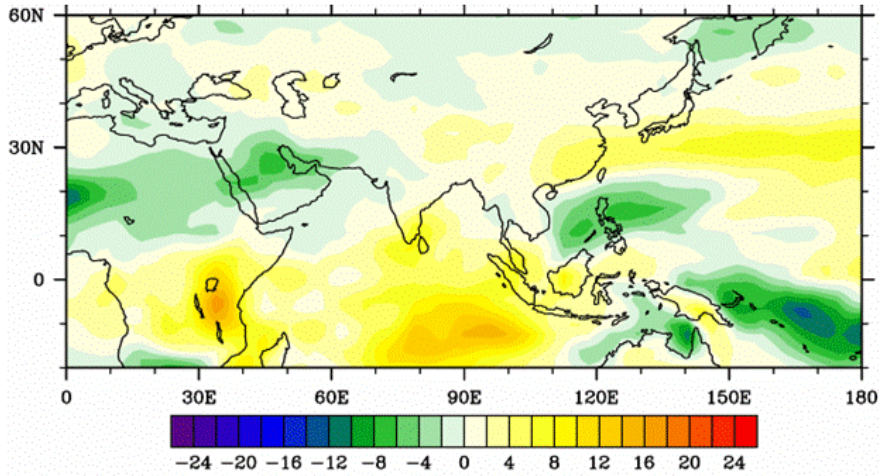

Fig. 71. Composite anomaly of OLR (W m^{-2}) for October-March when the subsidence component of the MJO is in the eastern IO. The increase in low level moisture leads to an increase in cloud cover over SWA. The decrease in convection over the eastern IO is apparent in the negative OLR anomalies observed over the eastern IO.

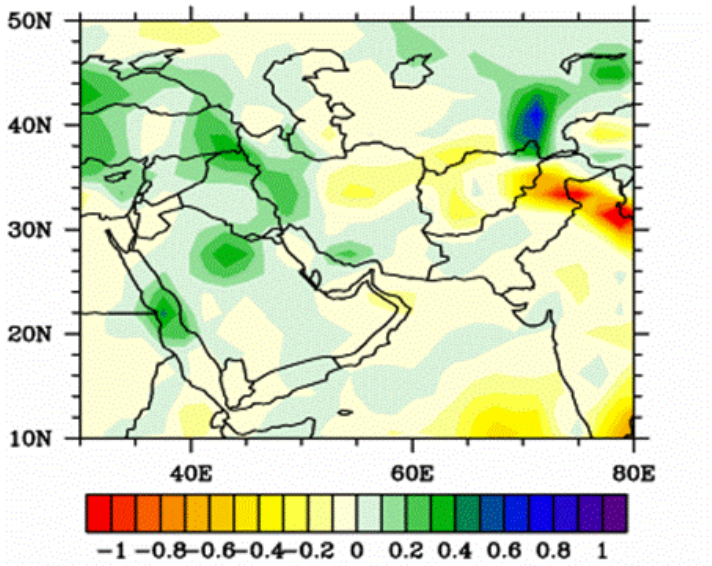

Fig. 72. Composite anomaly of precipitation rate (mm day-1) for October-March when the subsidence component of the MJO is in the eastern IO.

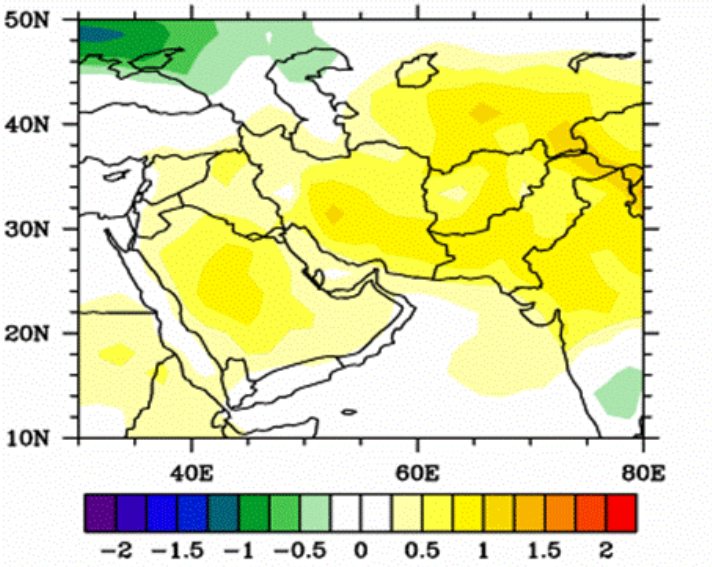

Fig. 73. Composite anomaly of temperature (2 m , °C) for October-March when the subsidence component of the MJO is in the eastern IO.

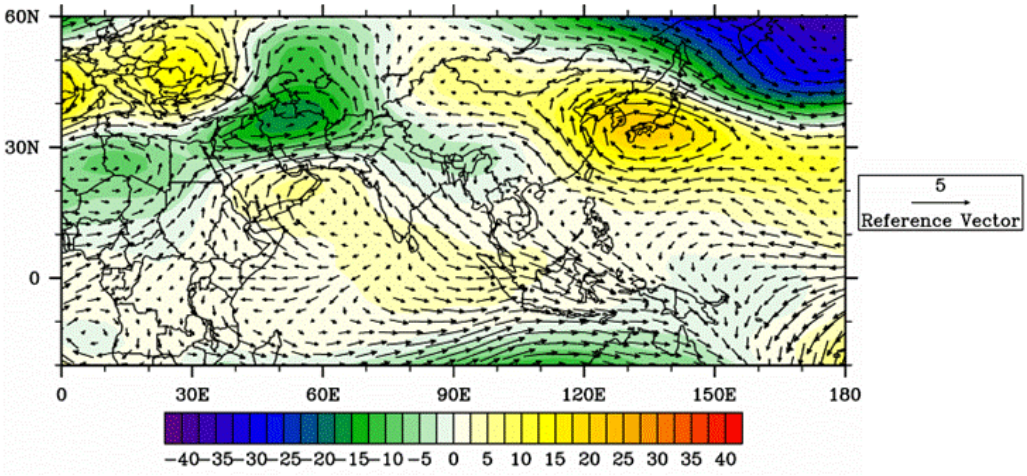

Fig. 74. Composite anomalies of 200-hPa GPH (color shading, m) and vector winds (m s^{-1}) for October-December during the positive phase of the NAO.

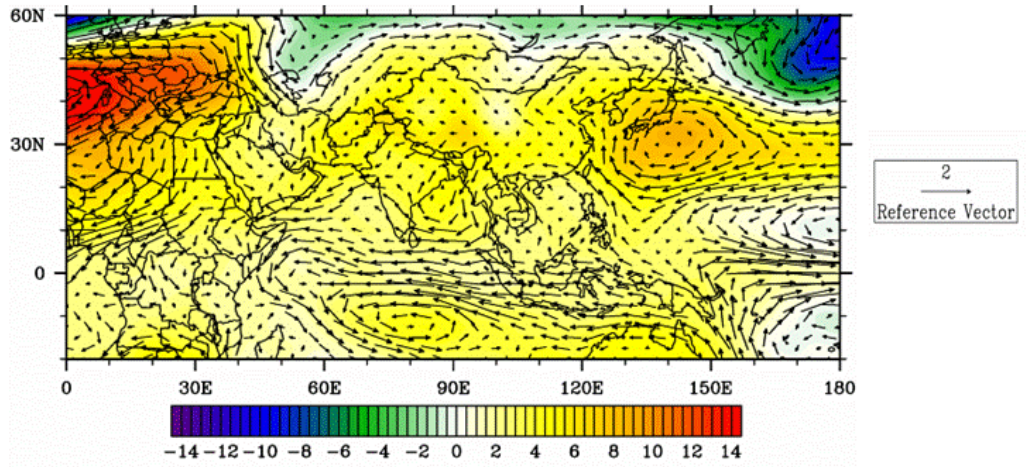

Fig. 75. Composite anomalies of 850-hPa GPH (color shading, m) and vector winds (m s^{-1}) for October-December during the positive phase of the NAO. Figs. 74-75 show an equivalent barotropic structure in the upper and lower level extratropical circulation anomalies.

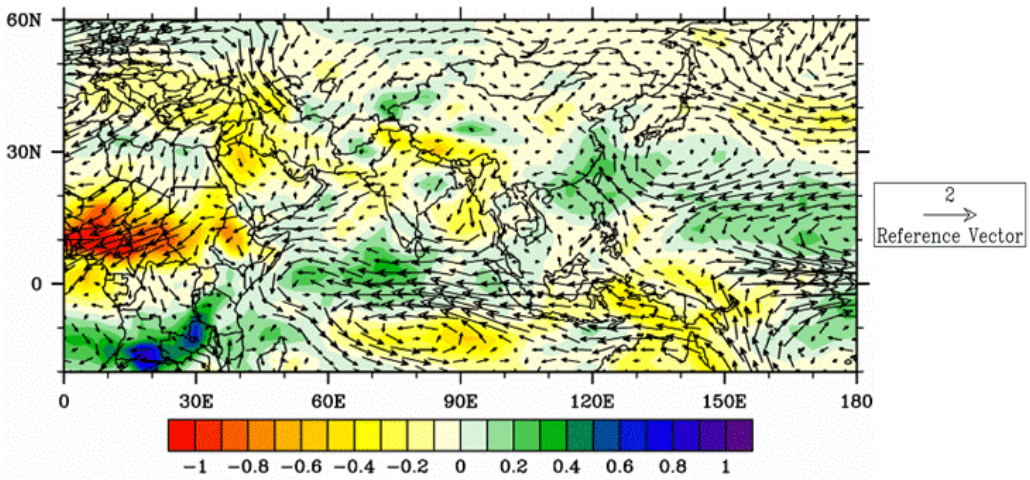

Fig 76. Composite anomalies of 850-hPa specific humidity (color shading, g kg-1) and vector winds (m s-1) for October-December during the positive phase of the NAO. The low level wind and SH anomalies show a relatively large amount of small-scale variation during the autumn.

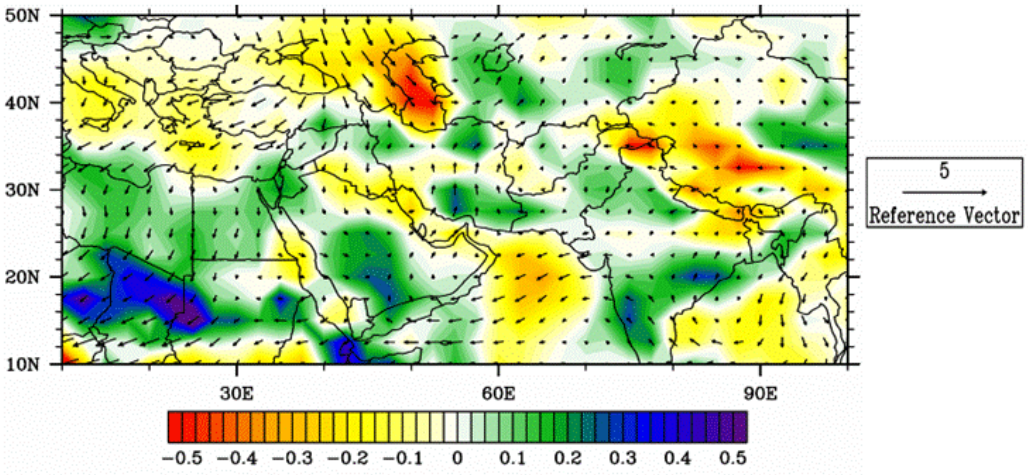

Fig. 77. Composite anomalies of 850-hPa moisture advection (color shading, g $kg^{-1}s^{-1}$) and vector winds (m s^{-1}) for October-December during the positive phase of the NAO. Moisture advection has been multiplied by 10^8.

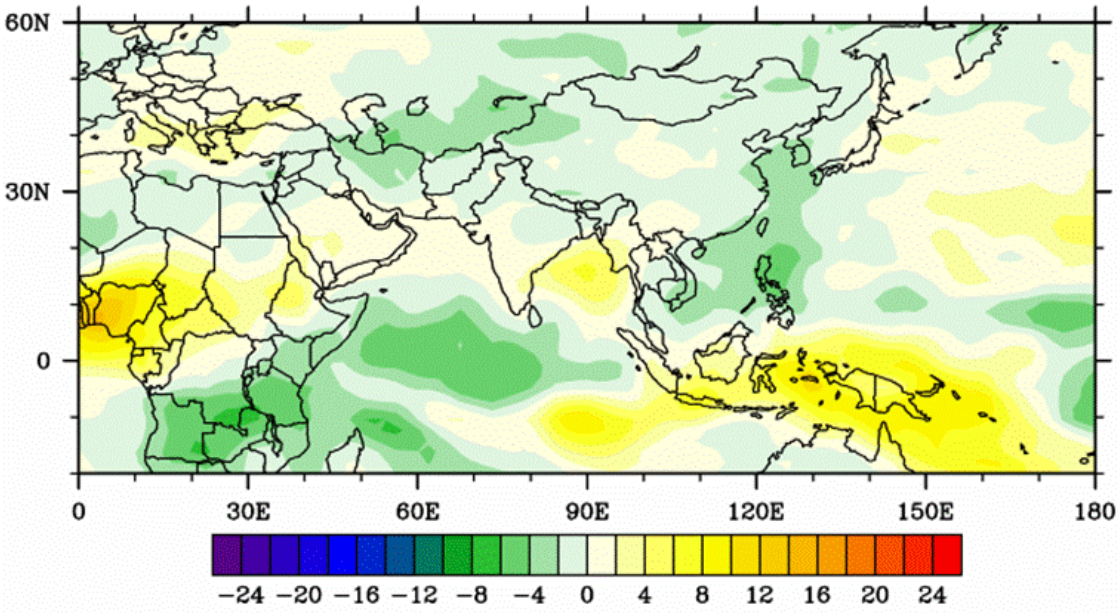

Fig. 78. Composite anomaly of OLR (W m^{-2}) for October-December during the positive phase of the NAO.

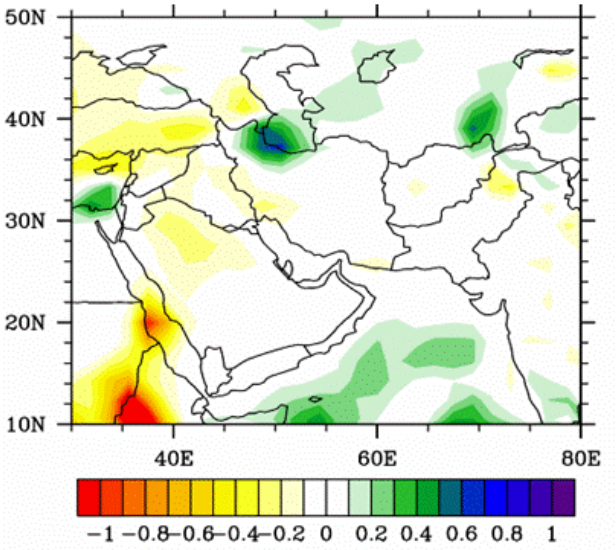

Fig. 79. Composite anomaly of precipitation rate (mm day^{-1}) for October-December during the positive phase of the NAO.

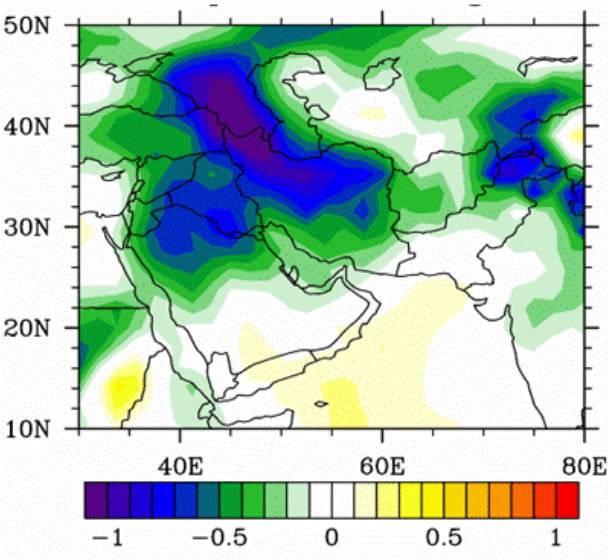

Fig. 80. Composite anomaly of temperature (2 m, °C) for October-December during the positive phase of the NAO.

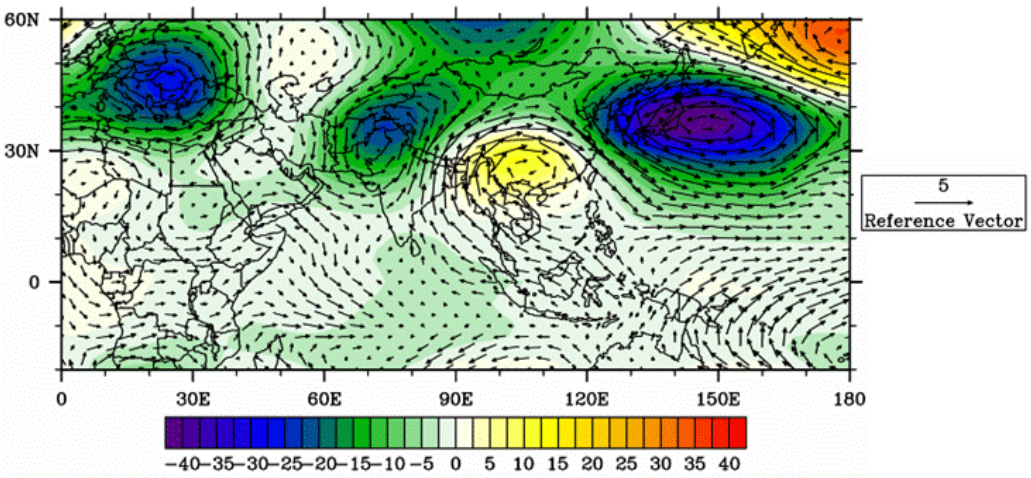

Fig. 81. Composite anomalies of 200-hPa GPH (color shading, m) and vector winds (m s^{-1}) for October-December during the negative phase of the NAO.

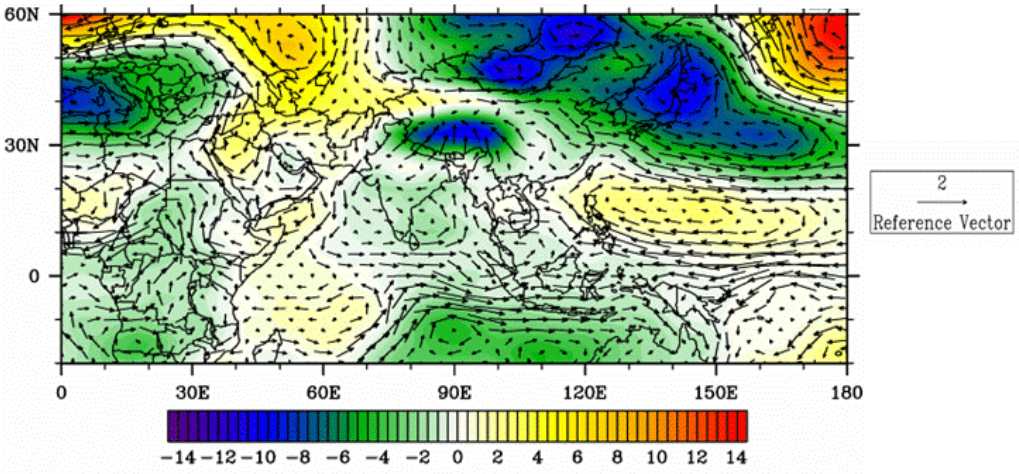

Fig. 82. Composite anomalies of 850-hPa GPH (color shading, m) and vector winds (m s^{-1}) for October-December during the negative phase of the NAO.

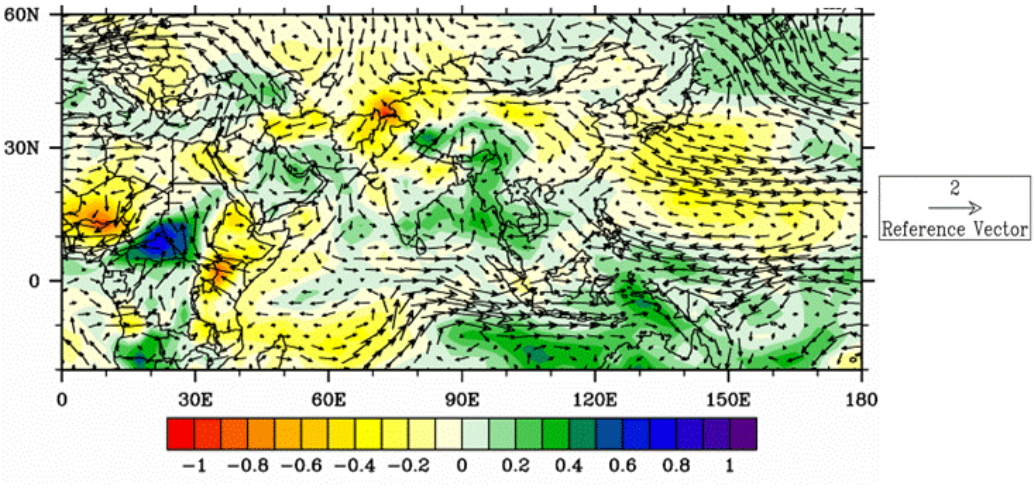

Fig. 83. Composite anomalies of 850-hPa specific humidity (color shading, g kg^{-1}) and vector winds (m s^{-1}) for October-December during the negative phase of the NAO.

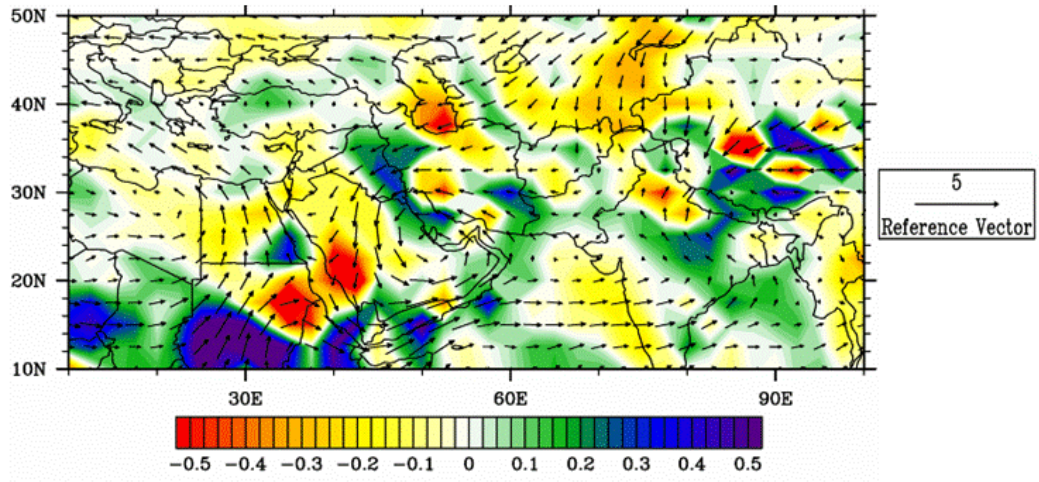

Fig. 84. Composite anomalies of 850-hPa moisture advection (color shading, g $kg^{-1}s^{-1}$) and vector winds (m s^{-1}) for October-December during the negative phase of the NAO. Moisture advection has been multiplied by 10^8.

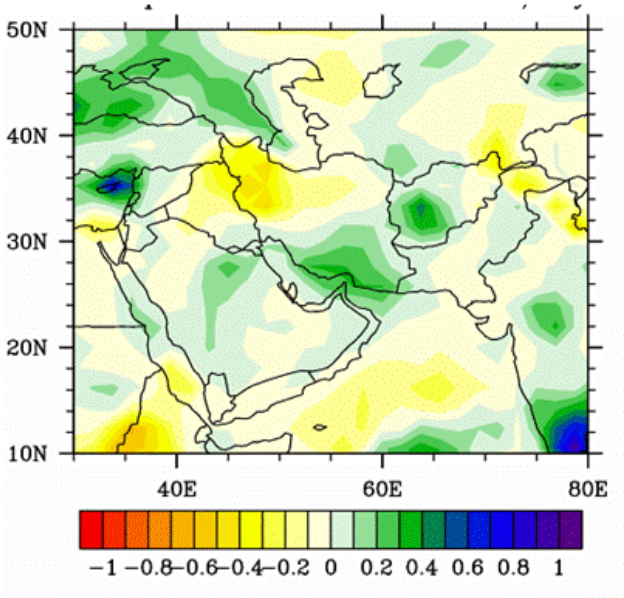

Fig. 85. Composite anomaly of precipitation rate (mm day^{-1}) for October-December during the negative phase of the NAO.

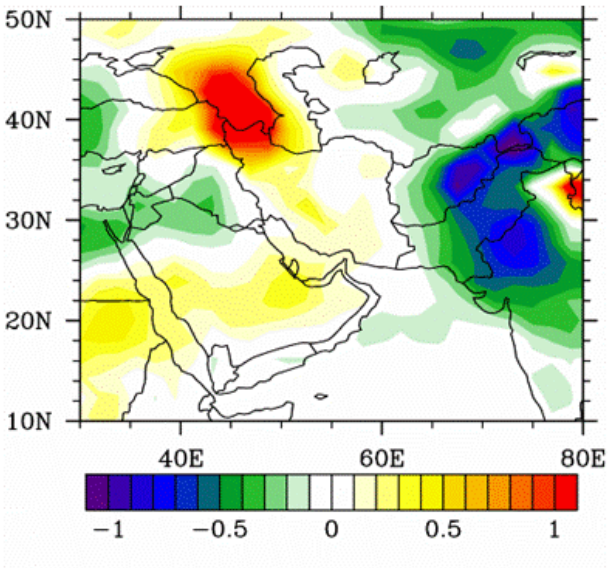

Fig. 86. Composite anomaly of temperature (2 m, °C) for October-December during the negative phase of the NAO.

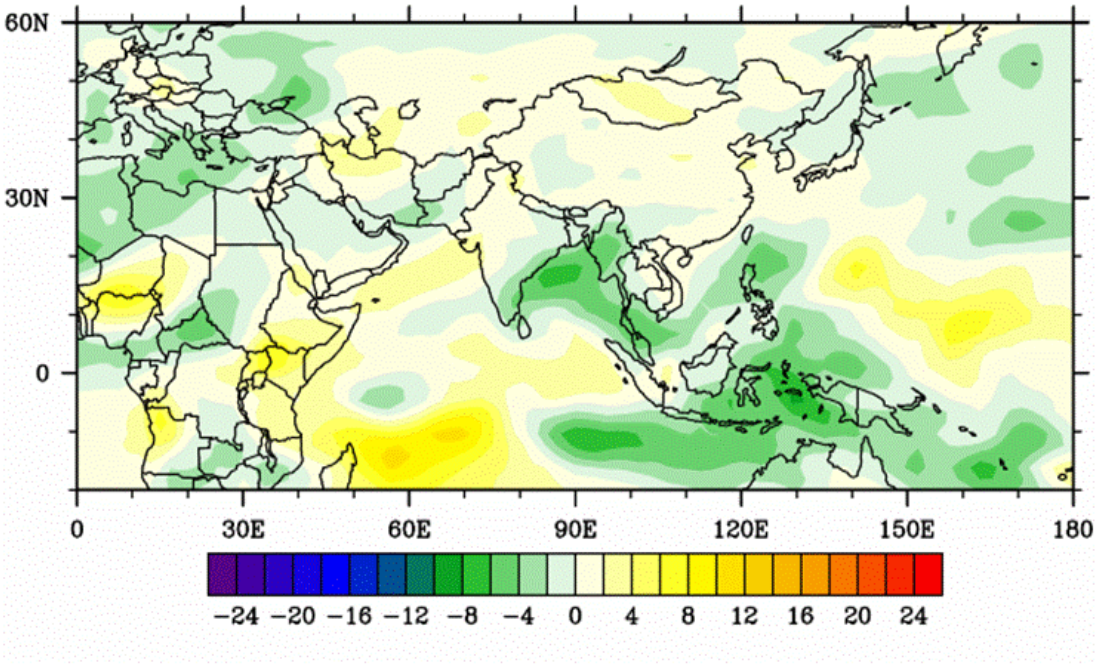

Fig 87. Composite anomaly of OLR (W m^{-2}) for October-December during the negative phase of the NAO.

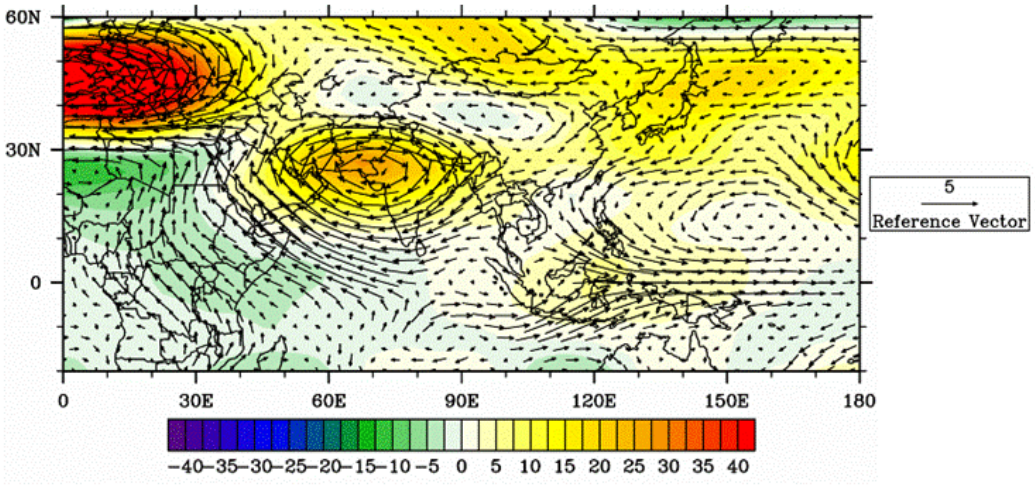

Fig. 88. Composite anomalies of 200-hPa GPH (color shading, m) and vector winds (m s^{-1}) for January-March during the positive phase of the NAO.

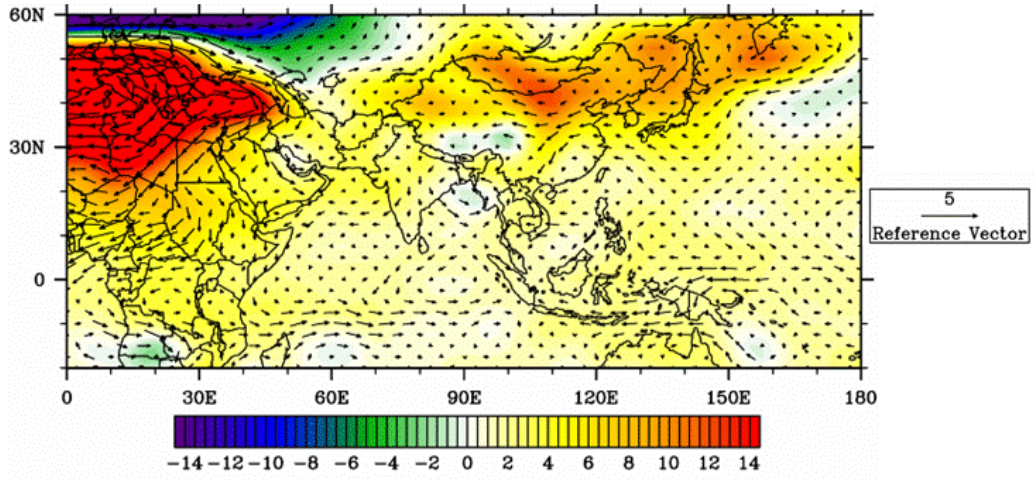

Fig. 89. Composite anomalies of 850-hPa GPH (color shading, m) and vector winds (m s^{-1}) for January-March during the positive phase of the NAO. Note the much larger anomalies in upper and lower level GPH and winds in winter than in autumn (compare Figs. 88-89 to Figs. 81-82).

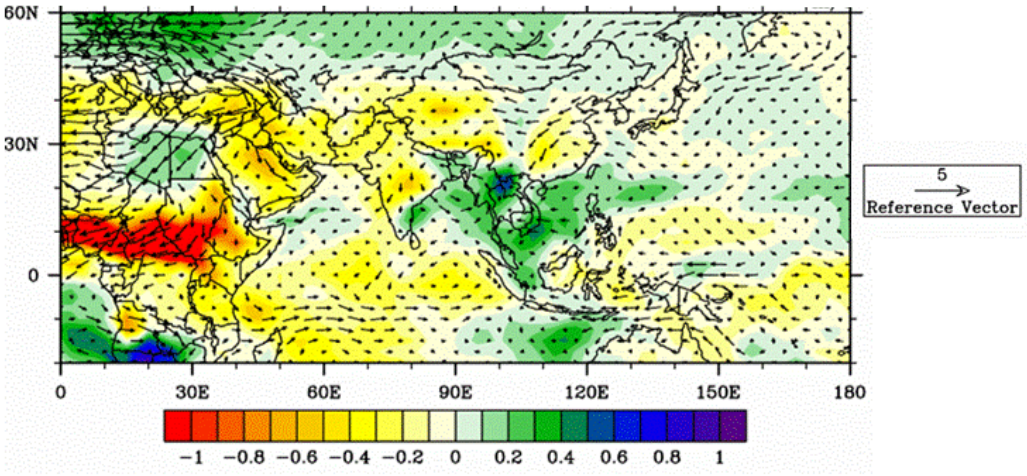

Fig. 90. Composite anomalies of 850-hPa specific humidity (color shading, g kg^{-1}) and vector winds (m s^{-1}) for January-March during the positive phase of the NAO. The low level wind and SH anomalies are much more spatially coherent in winter than in autumn (compare Fig. 90 to Fig. 76). As a result of the increase in northerly flow associated with the strengthening of the Azores High, SWA is drier than normal.

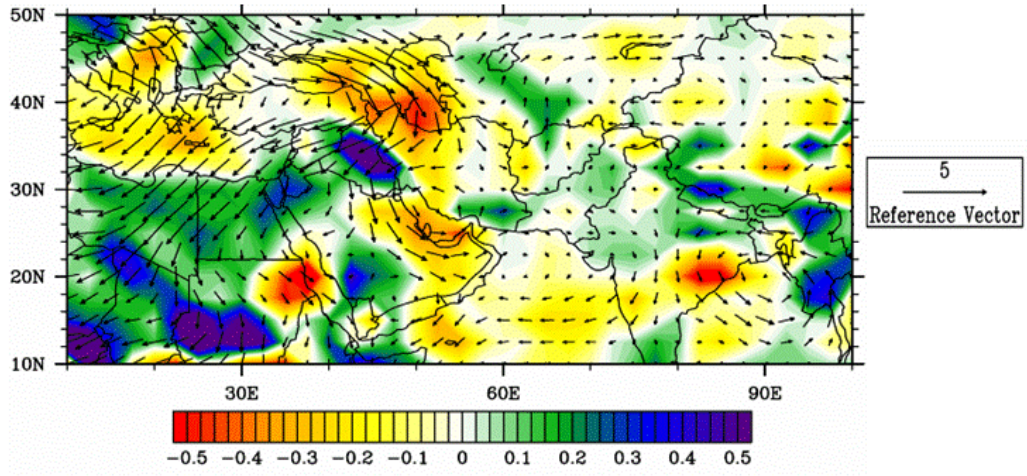

Fig. 91. Composite anomalies of 850-hPa moisture advection (color shading, g kg^{-1}s^{-1}) and vector winds (m s^{-1}) for January-March during the positive phase of the NAO. Moisture advection has been multiplied by 10^8. Note the negative moisture advection anomalies associated with the northerly wind anomalies over northern Iran and the Caspian Sea.

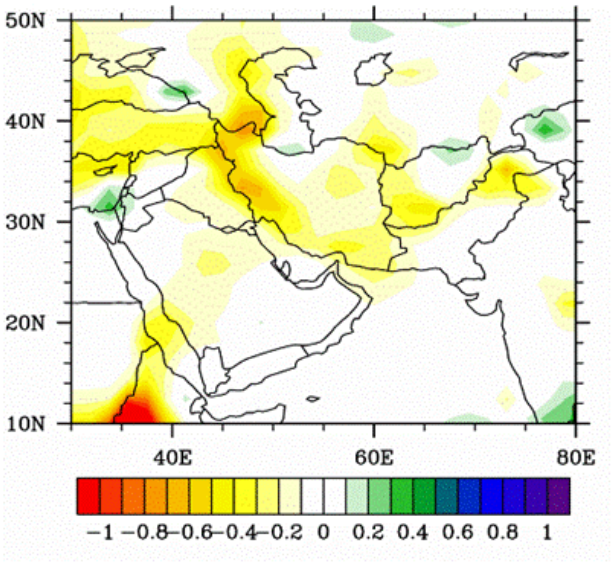

Fig. 92. Composite anomaly of precipitation rate (mm day^{-1}) for January-March during the positive phase of the NAO.

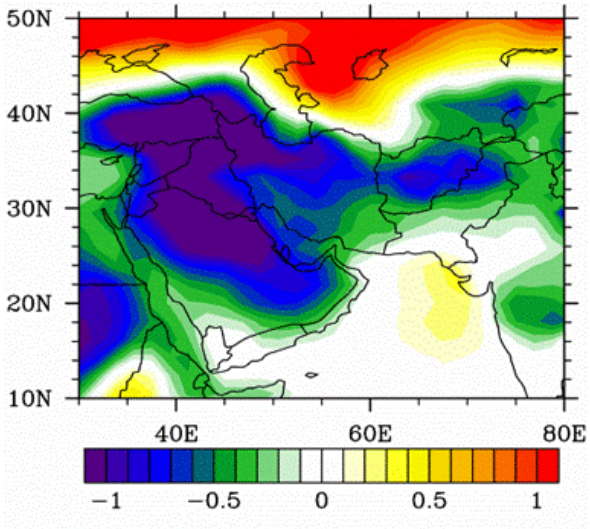

Fig. 93. Composite anomaly of temperature (2 m, °C) for January-March during the positive phase of the NAO. The strong negative temperature anomalies over SWA during the winter are striking for the NAO case.

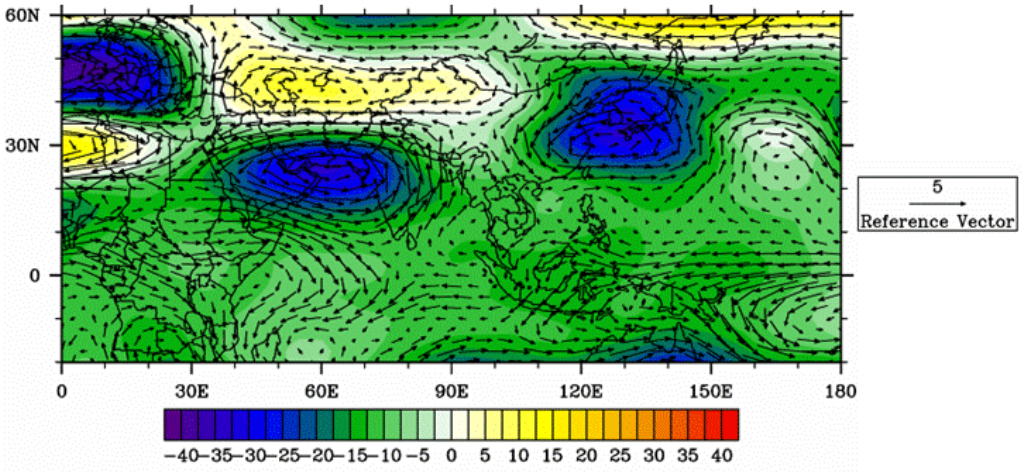

Fig. 94. Composite anomalies of 200-hPa GPH (color shading, m) and vector winds (m s^{-1}) for January-March during the negative phase of the NAO.

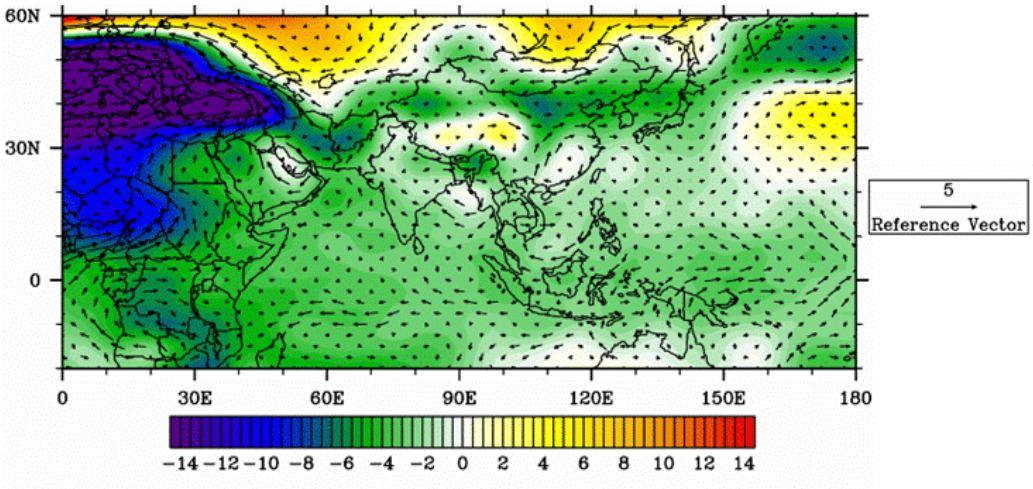

Fig. 95. Composite anomalies of 850-hPa GPH (color shading, m) and vector winds (m s^{-1}) for January-March during the negative phase of the NAO. Note the reversal in GPH-wind anomaly fields over the Mediterranean between the positive NAO and negative NAO cases.

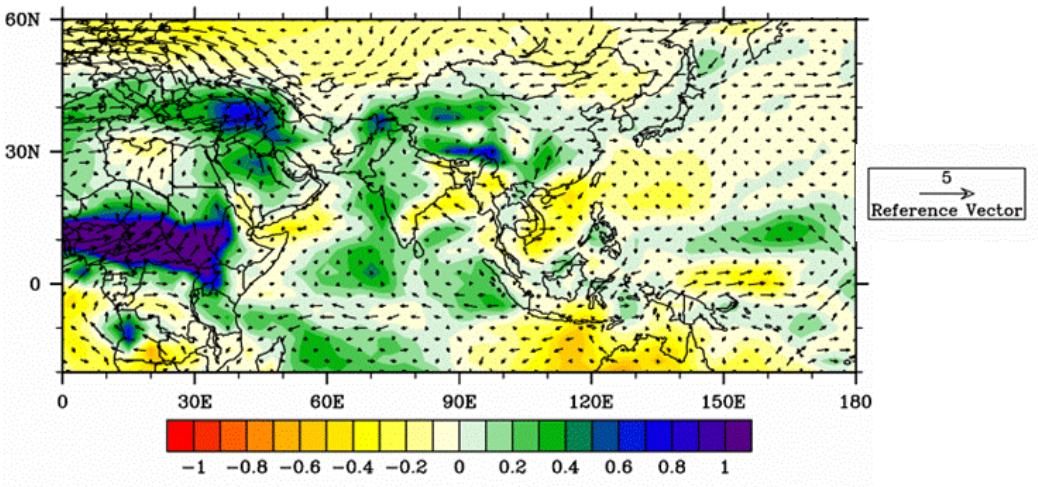

Fig. 96. Composite anomalies of 850-hPa specific humidity (color shading, g kg^{-1}) and vector winds (m s^{-1}) for January-March during the negative phase of the NAO. During the negative phase of the NAO, the weakening of the Azores High and the increased frequency of southerly winds, tends to produce an increase in low level moisture over SWA.

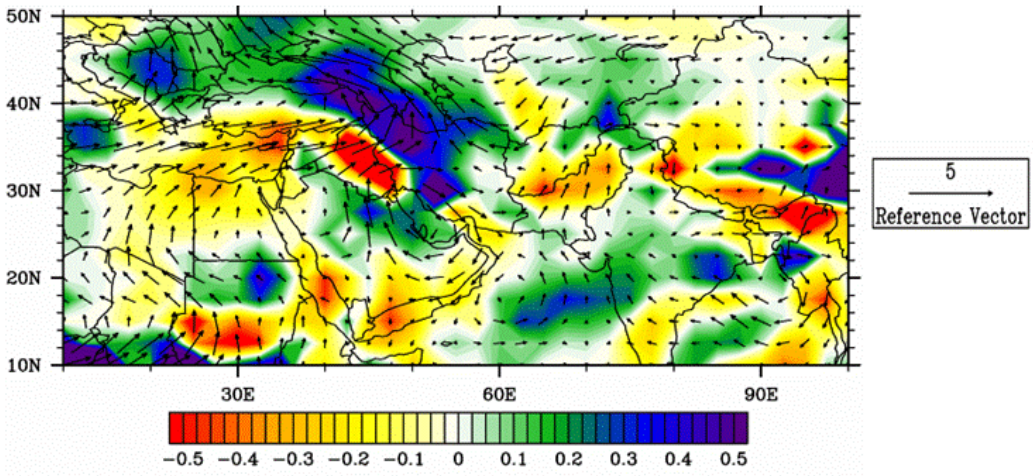

Fig. 97. Composite anomalies of 850-hPa moisture advection (color shading, g $kg^{-1}s^{-1}$) and vector winds (m s^{-1}) for January-March during the negative phase of the NAO. Moisture advection has been multiplied by 10^8. Note the striking positive moisture advection anomalies over Iran and the Caucasus region. The anomalous southerly winds lead to anomalous flows of low level moisture into the eastern Mediterranean and northern SWA.

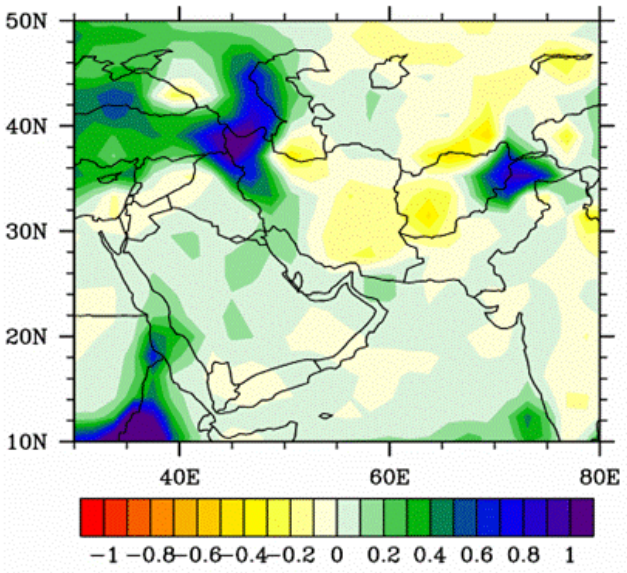

Fig. 98. Composite anomaly of precipitation (mm day^{-1}) for January-March during the negative phase of the NAO.

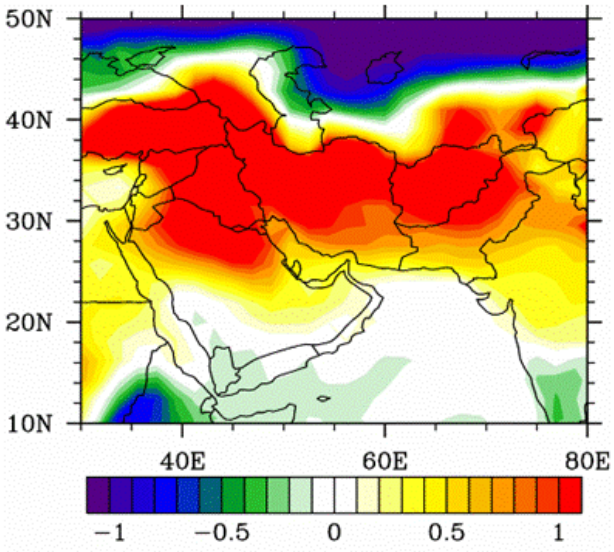

Fig. 99. Composite anomaly of temperature (2 m, °C) for January-March during the negative phase of the NAO. The low level southerly wind anomalies associated with the negative NAO tend to cause significant warming throughout SWA.

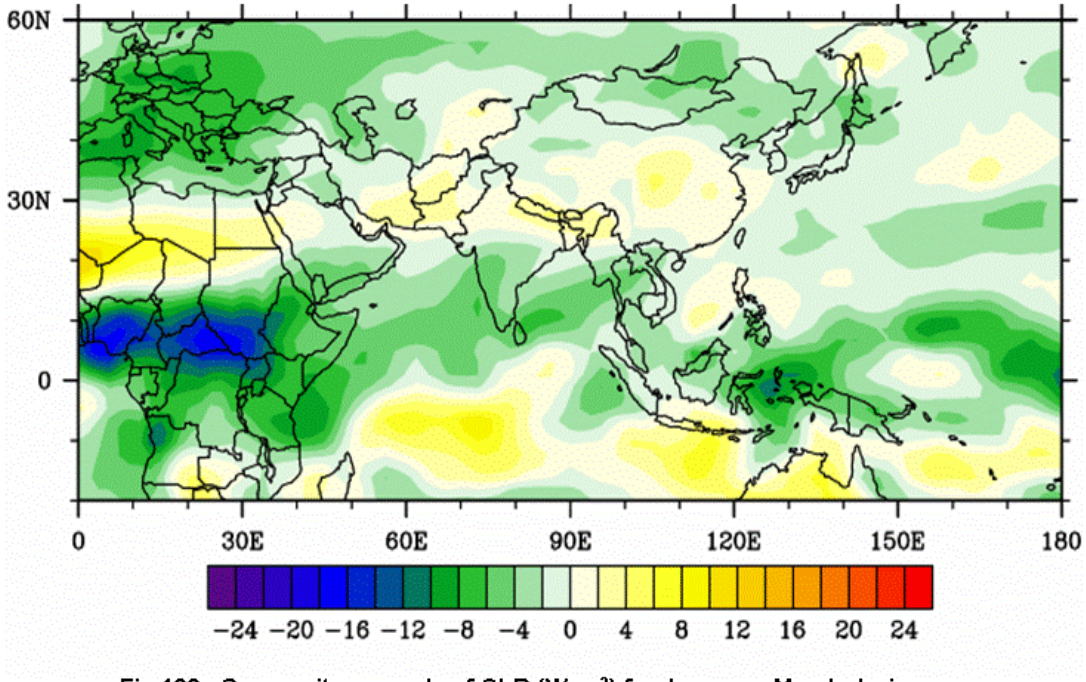

Fig 100. Composite anomaly of OLR (W m^{-2}) for January - March during the negative phase of the NAO.

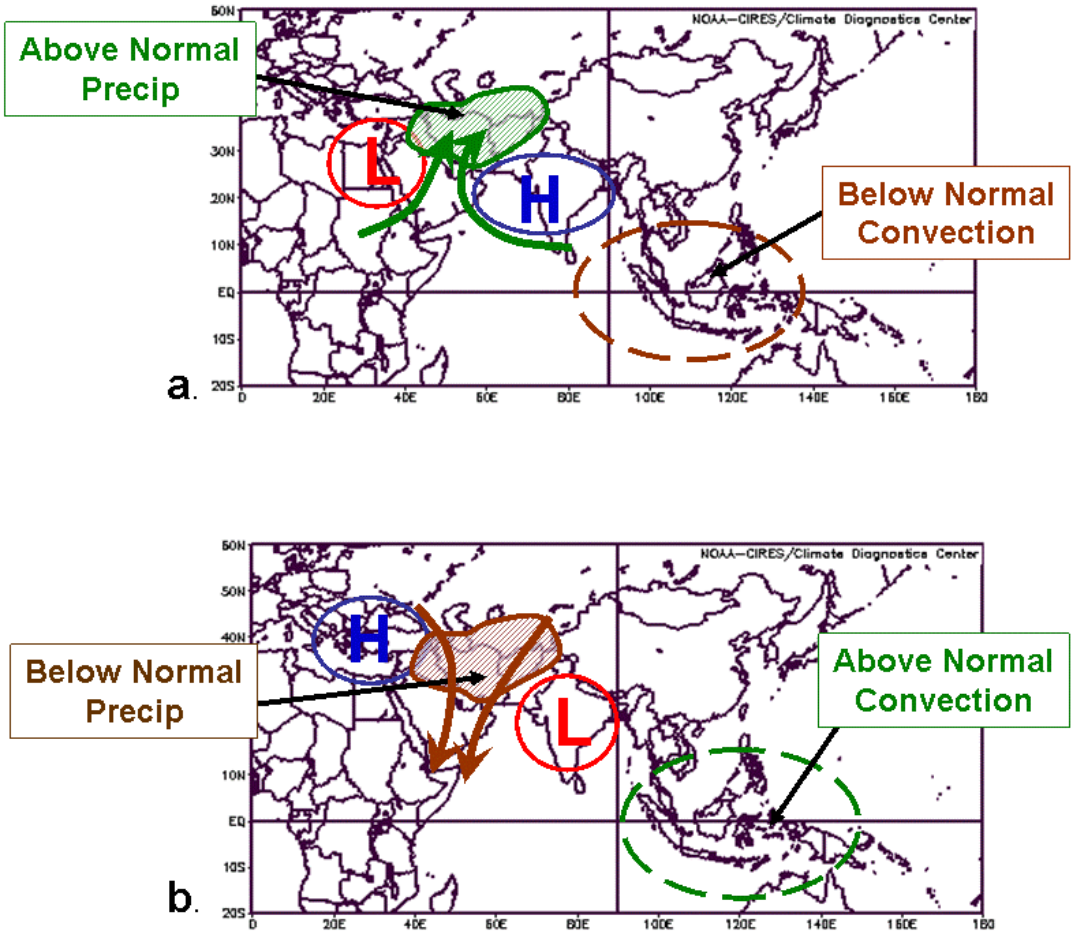

Fig. 101. Simplified schematics depicting the low level GPH-wind anomalies associated with (a) above normal and (b) below normal precipitation over SWA.

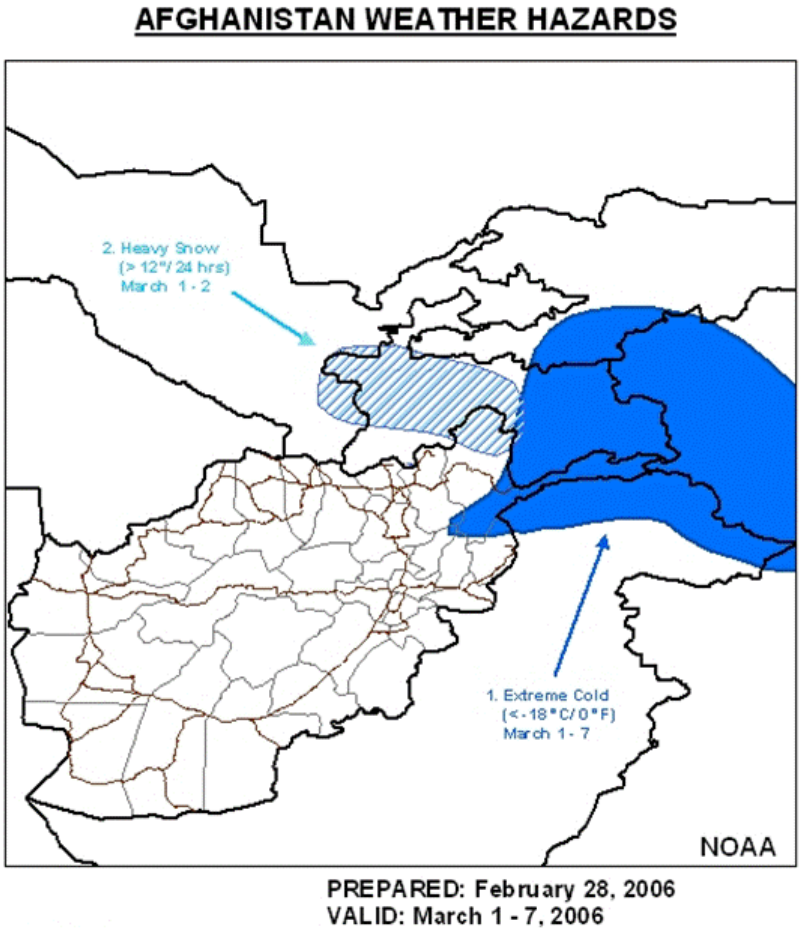

Fig. 102. Prototype product created by NOAA. This product shows possible weather hazards in Afghanistan and Pakistan. Product provided by the AFCCC Seasonal Prediction Working Group.

Climo Impacts Forecasts for Operational Planning

Operation	Impacts for Periods With Normal (LTM) Conditions					Impact Anomalies for Heavy Precip Periods (e.g., MJO Sub Comp in E IO)				
EO (Electro-optics) Over Target Area	CIG CLR-SCT	Abs Hum	Moon N/A			CIG	Abs Hum	Moon N/A		
ISR (Intelligence, Surveillance, Reconnaissance) Predator – Bagram	CIG >2000'	Vis >3sm	X-winds <10kt	Icing MDT	Turb MDT	CIG	Vis	X-winds	Icing	Turb

Impact anomalies: red = worse than normal; white = no change; green = better than normal

Fig. 103. Prototype of stoplight chart type product that incorporates climate variations into planning

THIS PAGE INTENTIONALLY LEFT BLANK

INITIAL DISTRIBUTION LIST

1. Defense Technical Information Center
   Ft. Belvoir, Virginia

2. Dudley Knox Library
   Naval Postgraduate School
   Monterey, California

3. Meteorology Department
   Code MR/WA
   Naval Postgraduate School
   Monterey, California

4. Dr. Tom Murphree
   Code MR/ME
   Naval Postgraduate School
   Monterey, California